Straightening out the mechanisms of axial elongation using mouse mutant analysis

by

Deborah R Farkas

Bachelor of Science, Carnegie Mellon University, 1999

Submitted to the Graduate Faculty of

The College of Arts and Sciences in partial fulfillment

of the requirements for the degree of

Doctor of Philosophy

University of Pittsburgh

2010

UNIVERSITY OF PITTSBURGH

COLLEGE OF ARTS AND SCIENCES

This dissertation was presented

by

Deborah R Farkas

It was defended on

June 28, 2010

and approved by

Jeff Brodsky, Ph.D. Professor

Jeff Hildebrand, Ph.D. Associate Professor

Beth Roman, Ph.D. Assistant Professor

Neil Hukriede, Ph.D. Associate Professor

Dissertation Advisor: Deborah Chapman, Ph.D. Associate Professor

Straightening out the mechanisms of axial elongation using mouse mutant analysis

Deborah R Farkas Ph.D.

University of Pittsburgh, 2010

Understanding the mechanisms that lead to axial elongation in the mouse has direct relevance to elucidating the etiology of vertebral defects in humans. Through the characterization of a spontaneous mouse mutant, *kinked tail*, and the analysis of Tbx6 protein modulation *in vivo*, I uncovered two distinct mechanisms affecting axial elongation in the mouse. The *kinked tail* mutation is a spontaneous mutation, inherited dominantly, that results in a kinky tail phenotype in heterozygotes and early embryonic lethality in homozygotes. Defective axial elongation in *kinked tail* heterozygotes is displayed as shortened tails and multiple tail kinks resulting from wedge, hemi- and fused vertebrae, similar to those observed in scoliosis patients. These vertebral defects are likely due to a primary notochord defect that is thickened and branched. *Kinked tail* homozygotes fail to undergo gastrulation due to defective distal visceral endoderm cell migration, ultimately resulting in lethality by embryonic day 8.5. The defective cell migration is further compounded by basement membrane defects and gross dysmorphology of the mutant embryo.

Tbx6, a T-box transcription factor, is essential for posterior somite formation, patterning and viability of the mouse embryo. I sought to understand Tbx6 protein regulation and the phenotypic consequences of modulating Tbx6 protein levels *in vivo*. *In vitro* analyses revealed that Tbx6 is a relatively stable protein that appears to be regulated in part by the proteasome in addition to other mechanisms. *In vivo*, less than heterozygous levels of Tbx6 protein results in

rib and vertebral defects, enlarged tailbuds and axial shortening while greater than wildtype levels of Tbx6 protein results in small embryonic tailbuds, axial shortening, and lethality. I further examined the consequences of Tbx6 misexpression using a 3-component transgenic system. The primitive streak and presomitic mesoderm are affected in those embryos that misexpress Tbx6.

Altogether, my analysis of the spontaneous mutation, *kinked tail*, demonstrated a possible role of the notochord in proper axial elongation, and the analysis of Tbx6 protein modulation further clarified the importance of maintaining proper levels of Tbx6 for normal axis elongation and embryonic development.

TABLE OF CONTENTS

LIST OF TABLES

LIST OF FIGURES

PREFACE

I would like to begin by thanking my advisor, Debbie Chapman. There are not enough words (or space) to describe the impact you have had on my life both personally and professionally. We have been together for almost a decade! Through the years, you have provided a tremendous amount of support. You have guided me academically, scientifically, and personally and you were always there when I needed you, in any capacity. Your enthusiasm and perseverance continues to inspire, amaze and motivate me. I will look back at this part of my life fondly and will draw upon your advice and what you have taught me as I embark on the next phase of my career. I have learned an incredible amount about the right way to do science, thinking critically and how to take pride in what I do. I have enjoyed being a part of your family life, watching Dominic and Gregory grow up, having dinner with your parents and of course eating all of the amazing food you make. I will be the first customer at Chapmanini's if it opens, I am sure Dom is already working on a business plan. I am beginning to ramble so I will end this with a very sincere thank you.

I also have a lot of gratitude for my committee, Dr. Jeff Hildebrand, Dr. Beth Roman, Dr. Jeff Brodsky and Dr. Neil Hukriede. Throughout the years you have really pushed me to examine my data critically and provided invaluable advice about how to approach problems both technically and analytically. It is truly a humbling experience to meet with you, I always walk

away knowing what I don't know (which is usually a lot) and it propels me to learn more. You have all individually provided me with support and advice throughout the years and I am grateful for how you have shaped me as a budding research scientist.

I would like to give a general thanks to the Biological Sciences department. Between the other graduate students, undergraduates, ladies of the fiscal and main office, it truly feels like a family. I have enjoyed my time with the department. I also need to thank all of the labs and people that have helped me through the years including the Hildebrand, Stronach, Brodsky, and Roman labs. I would also like to thank all of the amazing instructors that I have taught under or with. It has been an invaluable experience.

Moving down the line, I have to thank Amy Wehn. I don't even know where to begin. I do know that there is no way grad school would have been as much fun without you. We have been through a lot together and I could always rely on you for emotional and scientific support. I am always amazed by you, your knowledge, your science smarts, your ability to jumble words… I wish you luck at UNC, you will do great!! I also need to thank Phillip White, though you left the lab many years ago, you helped me tremendously when I was just beginning my graduate career. Our neighbor lab, the Hildebrand lab, is full of past and present members who have impacted my experience greatly. Mick Yoder, it still feels as if you are here. I really appreciate all of your help scientifically and personally. Your straight-shooting manner has always kept everything in perspective. I am very happy that you found Colleen and you are experiencing fatherhood with Max. Matt Farber, you are incredibly smart and will be successful with whatever you do. I could always depend on you for science help and for the most part, you kept me laughing! Megan Dietz, I thoroughly enjoyed the time I spent with you and miss you.

Becky Gonda. Where to begin with you…As I always tell the story, I remember walking down the hall to introduce myself to you. Who knew then that it would turn into the best friendship I have ever had. Your endless support through everything is a constant in my life. I could not ask for a better Aunt for Dahlia and a better friend for me. I am truly excited for the next phase of both of our lives. I am looking forward to sharing all of the future moments, good and bad, serious and silly, fun and not-so-fun (as if that could ever happen) with you. Thank you for everything and I mean everything!

Last but certainly not least, my family. My parents have provided an incredible amount of support and advice throughout all of my years. Mom, you have shown me that it is more than possible to balance work and family life, and I appreciate all of your help (especially with reading my thesis!). Dad, you have always amazed and inspired me with your work ethic, it provided the much needed motivation to keep pushing through. I suppose I should also thank you for cultivating my love of puns, they continue to play an important role in my everyday life (and to all the poor people that I subject them to). Joel, thank you for all of your support throughout the years. I continually brag about your accomplishments and admire the way you are doing what you love. Roy, I don't know what I would do without you. You are my best friend, my sounding board, my crazy receptacle; you keep me laughing and keep everything in perspective. You are a loving, supportive, fun-loving person who I continue to appreciate more and more everyday. I am very excited for the next phase in our lives. Finally, to my Dahlia Bea…you have changed my life in every way. You make me appreciate things I never thought I would. You make everything worthwhile and your laugh alone can fix anything. I look forward to watching you grow and laugh at the amazing things that you say. Thank you for being the center of my life.

1.0 INTRODUCTION

Understanding the molecular mechanisms that underlie the development of an embryo from a single fertilized egg to a fully functioning organism is the main driving force in the field of developmental biology. Traditionally, characterization of mutant phenotypes has offered a wealth of information regarding the function of genes during development and the adverse effects that are caused by their loss. The mouse is an excellent model system for investigating defective development as it provides information that directly relates to human beings. Our laboratory uses the mouse as a model system to understand the molecular basis of axial elongation and rib and vertebrae formation. Specifically, we are interested in the role of T-box transcription factors in the specification and patterning of paraxial mesoderm that will later generate the ribs and vertebrae of the adult organism.

1.1 CELL FATE DECISIONS

A major question of developmental biology is how does a single fertilized egg develop into a multi-cellular adult organism? The answer lies within the particular gene expression profile of each cell, in part due to the activity of transcription factors. These transcription factors and their downstream targets allow the cell to become fated to a particular cell type and function. The temporal and spatial control of gene expression is a key component to the proper development of

the embryo. Additional mechanisms including post-translational modifications further give cells their unique identity leading to cell fate decisions concomitant with growth and morphogenesis ultimately leading to the formation of viable offspring. Investigation into these mechanisms will reveal how the single-cell embryo can generate all of the essential tissues and organ systems necessary to form a viable adult.

1.2 EARLY DEVELOPMENT OF THE MOUSE EMBRYO

Following fertilization, the egg undergoes cell divisions and the resulting embryo begins a series of highly complex and coordinated changes in gene expression, growth and morphogenesis. The one-cell embryo undergoes several cleavage events prior to implantation in the uterus. At the 16-cell stage, two cell lineages become apparent: the outer layer, the trophectoderm, which is an extraembryonic tissue and the inner cell mass (ICM), which will go on to form the embryo proper. By embryonic day (e) 4.5, the embryo, termed an egg cylinder, implants into the uterus and is characterized by three distinct tissues, the ICM, the primitive endoderm that separates the ICM from the blastocoelic cavity, and the trophectoderm that surrounds these cell types (Fig. 1). Cells from the ICM will form the embryonic ectoderm or epiblast and the primitive endoderm, which will later differentiate into the visceral endoderm (Wolpert, 2002). Epiblast cells will then rapidly proliferate and continue to do so throughout development generating both the embryonic and extraembryonic tissues of the embryo. Later stages of development, including axis establishment and gastrulation, are discussed below.

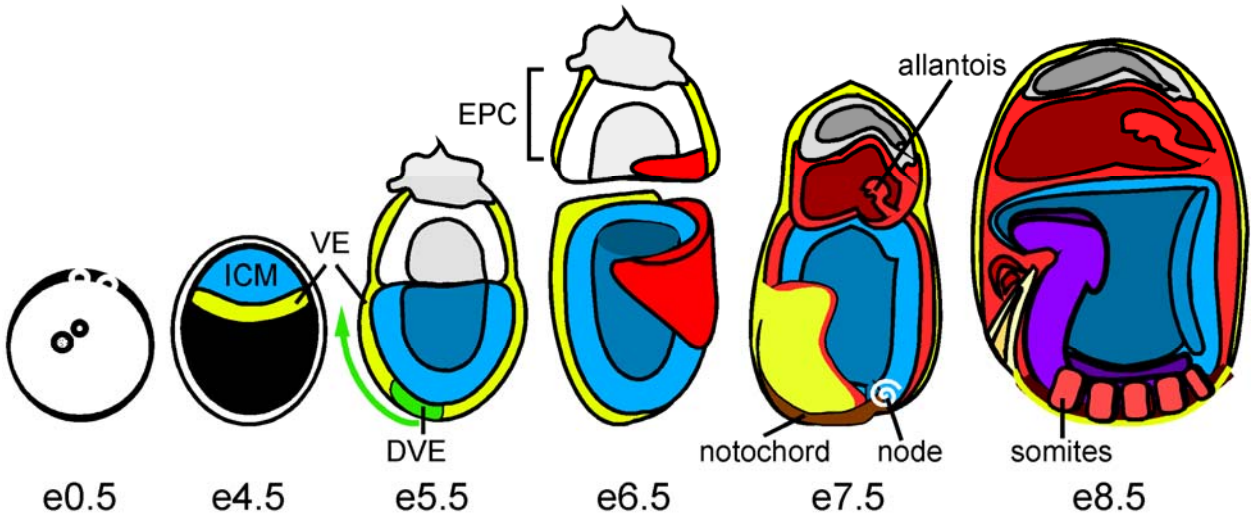

Figure 1: Landmarks of mouse development. At e0.5, the fertilized egg is recognized by a male and female pronucleus. Four days later (e4.5), the embryo consists of an inner cell mass (blue) and visceral endoderm (VE, yellow) that separates the future epiblast from the blastocoelic cavity (black). At e5.5, at the distal tip of the egg cylinder the distal visceral endoderm (DVE, green) is specified and begins to migrate to the future anterior (green arrow). The white region is the extraembryonic epiblast that is covered with VE. At e6.5, gastrulation has begun and mesoderm cells (red) at the posterior of the embryo migrate between the ectoderm (blue) and endoderm (yellow). The extraembryonic portion (white), including the ectoplacental cone (EPC), is depicted as separate from the embryonic portion for easier visualization. At e7.5, the presence of the notochord (brown) that forms from cells migrating out of the node (white spiral) is evident as well as the allantois in the posterior. A day later at e8.5, the head folds (purple) are apparent in the anterior and the somites (pink) are visible as blocks of tissue. (This figure was adapted from (Wolpert, 2002)).

1.3 ESTABLISHMENT OF THE ANTERIOR-POSTERIOR AXIS

Establishment of the anterior-posterior (A-P) axis is essential for proper development, such that any A-P axis perturbations result in severe developmental defects and often early embryonic lethality (Lu et al., 2001). Knock-out studies in mice have revealed roles for many genes in this process. For example, *Wnt3* (Liu et al., 1999), *Nodal* (Conlon et al., 1994) and *Otx2* (Perea-Gomez et al., 2001a) are all required in the embryo proper to establish the A-P axis. Extraembryonic events also play crucial roles in the initiation of the A-P axis, namely the formation and migration of the visceral endoderm (VE) (Srinivas, 2006). Importantly, the anterior VE (AVE) is essential for generating asymmetric gene expression which underlies positioning of the primitive streak and hence the A-P axis (Bielinska et al., 1999; Coucouvanis and Martin, 1999; Perea-Gomez et al., 2001b; Simeone and Acampora, 2001; Yamamoto et al., 2004). In addition, the AVE is essential for the formation of neural ectoderm such that targeted deletion of AVE specific genes including *Otx2* and *Lim1*, results in the loss of regions of the brain and anterior head structures, respectively (Acampora et al., 1995; Shawlot and Behringer, 1995).

1.3.1 The Role of Visceral Endoderm

Beginning at embryonic day (e) 4.5, approximately the time of implantation, the embryo consists of the ICM surrounded by primitive endoderm cells, which will give rise to the VE and parietal endoderm (Fig. 1). At e5.0, the proamniotic cavity begins to form, and the VE cells surrounding the egg cylinder have a columnar morphology with microvilli that aid the VE in its early role in nutrient exchange. By e5.5, these embryonic VE cells at the distal tip of the embryo proper

become thicker and express a unique set of genes, including *Hex* (Thomas et al., 1998; Rivera-Perez et al., 2003), *mCer1* (Belo et al., 1997) and *Lefty1* (Meno et al., 1999; Perea-Gomez et al., 1999) and are referred to as distal VE (DVE). These DVE cells actively migrate toward the presumptive anterior of the epiblast and this migration is essential for establishing the A-P axis, as failure to migrate generates a host of aberrant axis asymmetries usually resulting in early embryonic lethality (Fig. 1). For example, the DVE of *Otx2* mutants fails to migrate causing misexpression of posterior epiblast markers and leads to the loss of anterior head structures and embryonic lethality by ~e10.5 (Ang et al., 1996; Perea-Gomez et al., 2001a). Once the DVE cells reach the anterior, they are now termed the AVE. The AVE patterns the adjacent embryonic ectoderm via secreted antagonists of BMPs, Wnts, and Nodal (Belo et al., 1997; Shawlot et al., 1998; Perea-Gomez et al., 2001a), which restrict posterior-inducing signals to the future posterior side of the embryo thus establishing the A-P axis.

1.4 GASTRULATION AND MESODERM FORMATION

At e6.5, the appearance of the primitive streak (PS) in the posterior of the embryo indicates the beginning of gastrulation, the process whereby the three germ layers, ectoderm, endoderm and mesoderm are generated (Fig. 1). The ectoderm will later form the neural tissue and epidermis, the endoderm will give rise to the gut and its derivatives, and the mesoderm will give rise to the heart and vessels, gonads, kidneys, dermis of the back, skeletal muscle, ribs and vertebrae (Wolpert, 2002). Mesodermal cells delaminate through the PS and migrate between the inner ectoderm layer and the outer endoderm layer. The PS is the source of all mesoderm including

axial, paraxial (PAM), intermediate, lateral plate and extraembryonic mesoderm. The position of cell emergence from the streak determines the type of mesoderm that it will form. At the anterior-most point of the PS, the node forms. Mesoderm migrates through the node to form the axial mesoderm and the notochord (Fig. 1). From the most anterior to posterior portions of the streak, the PAM cells are next to ingress, followed by intermediate mesoderm, the lateral plate mesoderm in the middle and finally the extraembryonic mesoderm which forms from the posterior end of the streak (Tam and Beddington, 1987). As our laboratory is interested in the formation of ribs and vertebrae, I will focus on the PAM. The PAM gives rise to the somites, epithelial blocks of tissue that will eventually differentiate to form the dermis of the back, vertebrae and ribs, and skeletal muscle of the organism. After moving through the streak, PAM cells move laterally to eventually lie between the axial and intermediate mesoderm forming the unsegmented presomitic mesoderm (PSM). The anterior end of the PSM undergoes segmentation to form the somites, while the PS continues to supply cells to the posterior end of the PSM population resulting in the extension of the body axis. At e10.5 the tailbud becomes the source of PAM until somitogenesis is complete at e13.5 (Tam and Behringer, 1997; Dubrulle and Pourquie, 2004).

1.4.1 Notochord Formation

The notochord is a transient rod-shaped structure forming ventral to the neural tube along the midline of the developing embryo. Signaling molecules emanating from the notochord are critical for neural tube and somite patterning (Placzek et al., 1993; Pourquie et al., 1993)(discussed in Section 1.4.3) and serves as structural support, later being replaced by the vertebral column. Trunk notochord forms from the node through convergent-extension-like

movements (Yamanaka et al., 2007). Caudal (tail) notochord forms from notochord progenitor cells found in the ventral region of the node (Kinder et al., 2001) that actively migrate to the posterior, where they are maintained in the tailbud (Yamanaka et al., 2007). Despite the different mechanisms of notochord formation, thus far there are no known differences in gene expression or morphology along the notochordal A-P axis. However, the distinct regions of notochord formation are under the control of a variety of transcription factors. Notochord formation is completely dependent upon *Foxa2* (*HNF-3β*), a winged-helix transcription factor, such that loss of *Foxa2* results in the loss of all notochord cells (Ang and Rossant, 1994; Weinstein et al., 1994). Trunk notochord formation is dependent upon *Brachyury* (*T*), as loss of *T* results in the loss of trunk notochord (Gluecksohn-Schoenheimer, 1938). Finally, formation of the caudal notochord is dependent upon *Noto*, a homeobox gene, as homozygous loss of *Noto* results in the loss of tail notochord specifically (Abdelkhalek et al., 2004).

1.4.2 Somite Formation

Somite formation is a complex process involving both positive and negative feedback loops between members of the Notch, Wnt, Fgf8 and retinoic acid signaling pathways. The current model of somite formation involves a "clock", which sets up an oscillating pattern of gene expression throughout the PSM that is then translated into the formation of periodic somite boundaries by a "determination front" (Freitas et al., 2005). This front is positioned such that at the anterior end of the PSM, cells become competent to receive the oscillating signals and undergo segmentation. Segmentation involves a mesenchymal-to-epithelial transition of the PAM to form the somite; this process occurs approximately every two hours in the mouse. During somitogenesis, the more anterior somites are more mature than the newly forming

posterior somites. Thus along the anterior-posterior axis, a gradient of somite differentiation can be observed (Dubrulle and Pourquie, 2004; Giudicelli and Lewis, 2004; Freitas et al., 2005).

1.4.3 Somite Differentiation

The epithelial somite receives signals from surrounding tissues to form the sclerotome and dermamyotome compartments (Fig. 3A) (reviewed in (Saga and Takeda, 2001). Ventral-medial somitic cells that receive signals from the notochord and the floor plate of the neural tube undergo an epithelial-to-mesenchymal transition (EMT) to form the sclerotome compartment of the somite (Fig. 3A). Following the EMT transition, the medial sclerotome cells will proliferate and migrate towards the notochord forming the vertebral body anlagen and intervertebral discs (IVD's), while the lateral sclerotome cells will form the pedicles and laminae of the neural arches, and also the ribs (Christ and Wilting, 1992). The more dorsal and lateral regions of the somite will form the dermamyotome that is patterned by signals from the dorsal neural tube, overlying ectoderm and flanking lateral plate mesoderm (Fig. 3A). The dermamyotome will further differentiate into the dermatome, forming the dermis of the back and the myotome, which will form the muscles of the back, body wall, and limb. Cells from all regions of the somites can give rise to vascular and lymphatic endothelium (reviewed in (Christ et al., 2007). Following differentiation, the sclerotome portion of the somite undergoes a resegmentation event, where the caudal half of the more anterior sclerotome will fuse with the rostral half of the next posterior sclerotome, resulting in the formation of a new segment, the vertebrae. However, the myotome compartment does not resegment (Fig. 3B). Altogether, this results in the muscles attaching two successive vertebrae, thus allowing for movement within the axial skeleton (reviewed in (Saga and Takeda, 2001). Proper resegmentation requires molecular distinctions between the rostral

and caudal halves of the somites. The distinct molecular identities begin to be apparent in the anterior portion of the PSM prior to segmentation (Fig. 3B). Alterations in rostral-caudal patterning disrupt resegmentation leading to axial skeleton defects (reviewed in (Sewell and Kusumi, 2007).

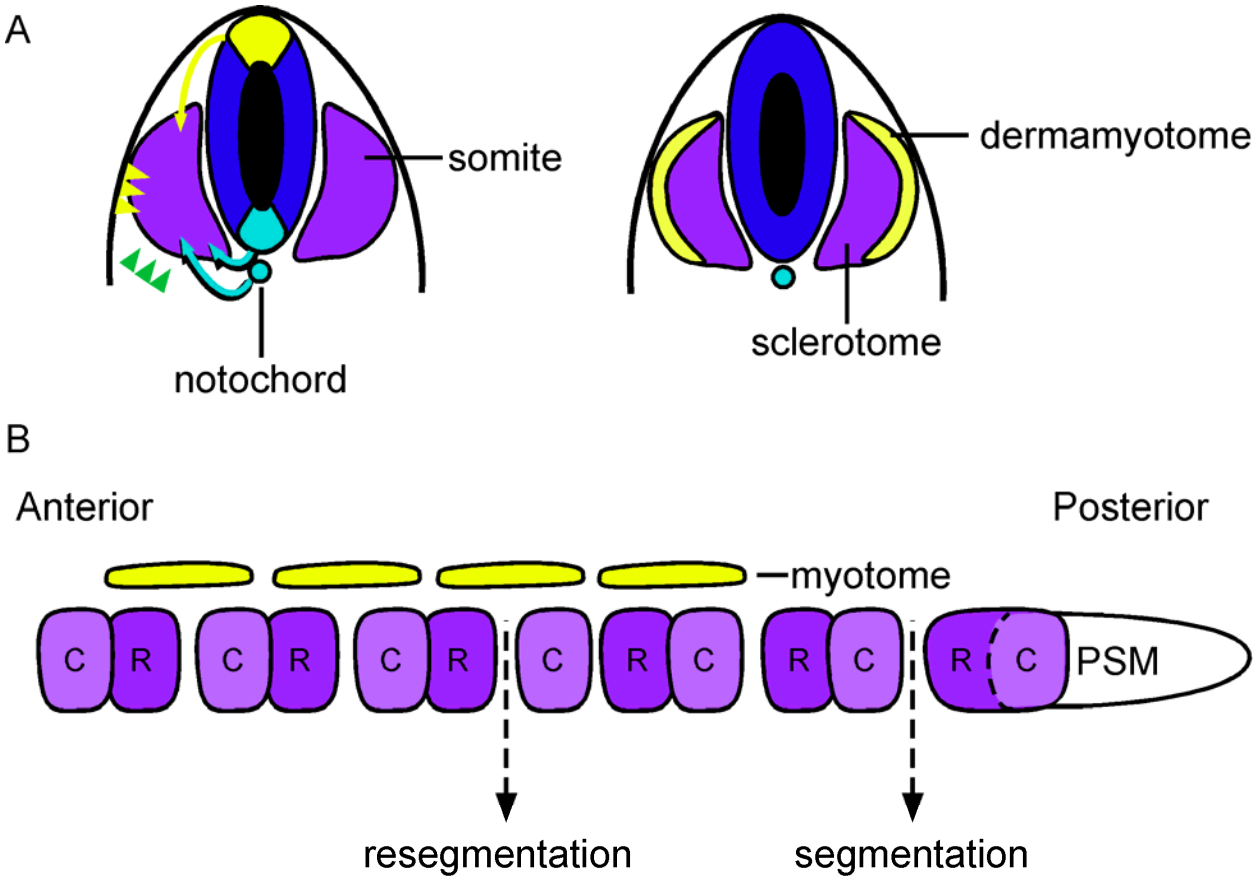

Figure 2: Somite segmentation and differentiation. (A) Upon signals (arrowheads and arrows) from the neural tube (blue), notochord (turquoise), and overlying ectoderm (black), the somite will differentiate to form the dermamyotome (yellow) and sclerotome (purple). (B) Initial segmentation of the somite from the anterior-most region of the PSM, is followed by a later resegmentation event that allows the dermamyotome

(yellow) to connect to two consecutive vertebrae (purple). Note the rostral (R) and caudal (C) polarity of the somites (This figure was adapted from (Saga and Takeda, 2001).

1.5 AIMS OF DISSERTATION RESEARCH

The development of an organism beginning with the fertilized egg requires exquisite cross talk between many different signaling pathways and transcription factors in the proper spatio-temporal patterns. Perturbations of these pathways at different times and places often generate phenotypes that severely affect the functioning and/or vitality of the organism. By understanding the molecular basis of these perturbations, we can learn a great deal about the events that are critical for normal embryogenesis. Developmental biologists use a variety of approaches to understand the processes underlying normal development. In my thesis, I have used two complementary approaches: 1) phenotypic analysis of a spontaneous mutation to identify the responsible gene and 2) genetic manipulation to misexpress a gene of interest to further understand mesoderm formation and patterning during embryogenesis.

My first aim was to characterize a spontaneous mouse mutation that has been named *kinked tail*. Through this characterization, I identified a defect in cell migration and/or adhesion that affected both the establishment of the A-P axis and formation of the axial skeleton. The second aim of my thesis work was to examine the role of Tbx6 in rib and vertebrae formation and patterning through the analysis of embryos in which *Tbx6* is under-, over- and ectopically expressed. These studies revealed the importance of the tight regulation of Tbx6 protein levels for normal vertebral development.

2.0 CHARACTERIZATION OF THE *KINKED TAIL* MUTATION

2.1 INTRODUCTION

The *kinked tail* mutation arose as a spontaneous mutation within a mouse colony in the lab of Dr. Charles McTiernan (University of Pittsburgh Medical Center). He observed that the founder mouse transmitted a kinky tail phenotype to her progeny and, knowing our interest in vertebral defects, generously gave us kinky tail mice to investigate the mutation that generated the phenotype. The goal of my studies was to characterize the mutation since named *kinked tail* (*knk*) using a range of mouse embryological techniques. *Knk* is a spontaneous dominant mutation that results in variable tail lengths in the heterozygotes and early embryonic lethality in the homozygotes.

2.1.1 Musculoskeletal formation in mice

PAM generates the bilaterally positioned somites along the A-P axis. The somites give rise to the dermis, skeletal muscle, ribs and vertebrae. Patterning of the somites along the dorsal-ventral (D-V) axis provides the template from which the vertebrae and overlying musculature will form. Sonic hedgehog (shh) signaling from the notochord and the floor plate of the neural tube induces the ventral portion of the somite to form sclerotome, which will later give rise to the vertebrae of

the axial skeleton and IVDs (Fan and Tessier-Lavigne, 1994). In the chick, removal of the notochord results in failure to specify sclerotome causing the somite to differentiate into only dermamyotome (Monsoro-Burq et al., 1994). Conversely, grafting of an additional notochord lateral to the neural tube in chick embryos induces sclerotome formation at the expense of dermamyotome (Pourquie et al., 1993). Once induced, sclerotome cells express *Pax1,* a transcription factor that is required for proper sclerotome formation. *Pax1* null mutants lack vertebral bodies and have malformed proximal ribs (Wallin et al., 1994). Expressed within the caudal half of the newly formed somite and sclerotome is the homeobox gene, *Uncx4.1*, which is required for pedicles, transverse processes and proximal rib formation (Leitges et al., 2000; Mansouri et al., 2000). *Tbx18* is expressed within the rostral half of the somite and the sclerotome and is required to maintain the distinction between the rostral and caudal compartments, such that in its absence the pedicles fuse (Kraus et al., 2001; Bussen et al., 2004). Additional patterning of the somite comes from the dorsal neural tube via *Wnt1*/*Wnt3a* to specify the myotome to form the epaxial muscles of the back (Ikeya and Takada, 1998).

In addition to its role in patterning, the notochord is also essential for IVD formation. Notochordal cells eventually become enclosed within the sclerotome and form the perinotochordal sheath. As the sclerotome cells undergo chondrogenesis, they exert a mechanical force on these notochord cells, resulting in their eventual removal from the intravertebral regions and their accumulation in the intervertebral regions. Here the notochord cells will undergo hypertrophy to form the nucleus pulposa, which becomes the center of the IVD (Paavola et al., 1980; Aszodi et al., 1998).

Generating a functional musculoskeletal system requires the precise coordination of somite formation, patterning, and differentiation with interactions between nearby structures

including the notochord, neural tube, lateral plate mesoderm and overlying ectoderm. Defects along each step of this pathway could lead to phenotypes not unlike those observed in the *knk* mice.

2.2 *KNK* GENETIC ANALYSIS

Kinked tail heterozygotes were first detected by the presence of a curled tail tip at e13.5. Adult heterozygotes were viable and fertile, displaying variable degrees of tail kinks resulting in axial shortening. Analysis of the number of live births from *knk/+* intercrosses and *knk/+* x wildtype crosses, resulted in 66% (n=58) and 53% (n=86) mice with affected tails, respectively (Farkas and Chapman, 2009). These numbers represent the expected Mendelian frequencies for a mutation that is inherited dominantly. *knk/+* embryos were indistinguishable from wildtype embryos from e5.5 to approximately e13.5. Thereafter, the heterozygotes can be distinguished by tail defects (discussed in Section 2.3). Analyses of litters dissected from *knk/+* intercrosses revealed a population of embryos with distinct phenotypes between e6.5-e8.5, and decidual resorptions starting at e8.5. These mutant phenotypes were found in ~25% of embryos, the expected Mendelian transmission for the *knk/knk* embryos.

2.3 *KNK* HETEROZYGOUS ANALYSIS

2.3.1 *kinked tail* heterozygous mice exhibited variable tail kinks and shortened axes

The *kinked tail* mutation arose as a spontaneous dominant mutation that results in variable tail kink phenotypes in heterozygotes mice. *knk/+* mice were viable and fertile, displaying vertebral defects that were confined to the tail region (Fig. 3A). To investigate the vertebral defects that generated the kinky tail phenotype, skeleton preparations of adult tails stained with Alizarian red were made. Adult tails showed that the evenly segmented tail vertebrae of wildtype mice are replaced by wedge, block and hemi-vertebrae in the *knk/+* tails (Fig. 3B, compare B to B'-B"; Fig. 15). These vertebral abnormalities resulted in a range of phenotypes from an almost full-length tail with one or two kinks to a curly-Q tail, representing the most severe axis shortening observed (Fig. 3A) (Farkas and Chapman, 2009).

Observation of the vertebral defects found in the adult tails suggested that development of the axial skeleton was defective. However, it was unclear from the adult phenotypes whether vertebral malformations were restricted to the tail region. To address this question, timed dissections were performed at e12.5 and e13.5 to visualize the anterior axial skeleton as well as determine at what stage these defects can first be observed. At e13.5, *knk* heterozygotes were characterized by a curled tail tip (Fig. 3C-C', outlined regions). At this stage, alcian blue staining revealed that vertebrae and ribs in the thoracic and trunk regions in the *knk*/+ and normal (N) were indistinguishable, thus vertebral defects were restricted to the tail region (Fig. 3C-C'). Alcian blue also stains the glycosaminoglycans in the notochord sheath (Paavola et al., 1980) and examination of *knk/+* tails revealed branching and thickening of the notochord (Fig. 3C"') (Farkas and Chapman, 2009). To confirm that this observed staining represented branched

notochordal tissue, histological analyses were performed on normal and heterozygous tails. Transverse sections though e13.5 *knk*/+ tails confirmed the alcian blue staining results, namely the presence of a dorsally branched notochord (Fig. 3D', D") (Farkas and Chapman, 2009). Similar to the vertebral defects, notochord defects were also restricted to the tail region. The role of the notochord in the formation of IVD's prompted me to carefully examine the IVD's of the *kinked tail* mice. In tails of normal embryos, the IVD's were uniform in size between the vertebrae, whereas the *knk*/+ tail displayed variably sized IVDs or none at all (Fig. 3B-B", arrowheads).

Given the role of the notochord and shh in patterning the somites, a branched notochord could result in aberrant somite patterning and hence vertebral formation would be affected. To analyze the potential for aberrant shh signaling from the notochord, *shh* expression was assayed by whole mount *in situ* hybridization (WISH). *shh* transcripts were found in both the axial notochord and its branches in the *knk*/+ embryos at e12.5 (Fig. 3E-E') (Farkas and Chapman, 2009). A thickened and branched notochord expressing the patterning molecule shh would be predicted to exert sclerotome induction on the neighboring somite at the expense of myotome. To determine whether the myotome is compromised in tails, I examined *myogenin* expression by WISH. Given the branching and thickening of the notochord, the effect on the myotome was much less dramatic than expected. I did not observe any missing myotome, but instead observed the occasional fusion of the myotomes (Fig. 3F-F") (Farkas and Chapman, 2009). Mispatterning of the somite's anterior-posterior halves, could later lead to resegmentation defects, which could result in some of the vertebral fusions observed. Examination of the posterior halves of the somites, via *Uncx4.1* WISH staining, revealed subtle differences between normal and *knk*/+ tails, namely variable size and spacing between the *Uncx4.1* expressing segments (Fig. 3G-G").

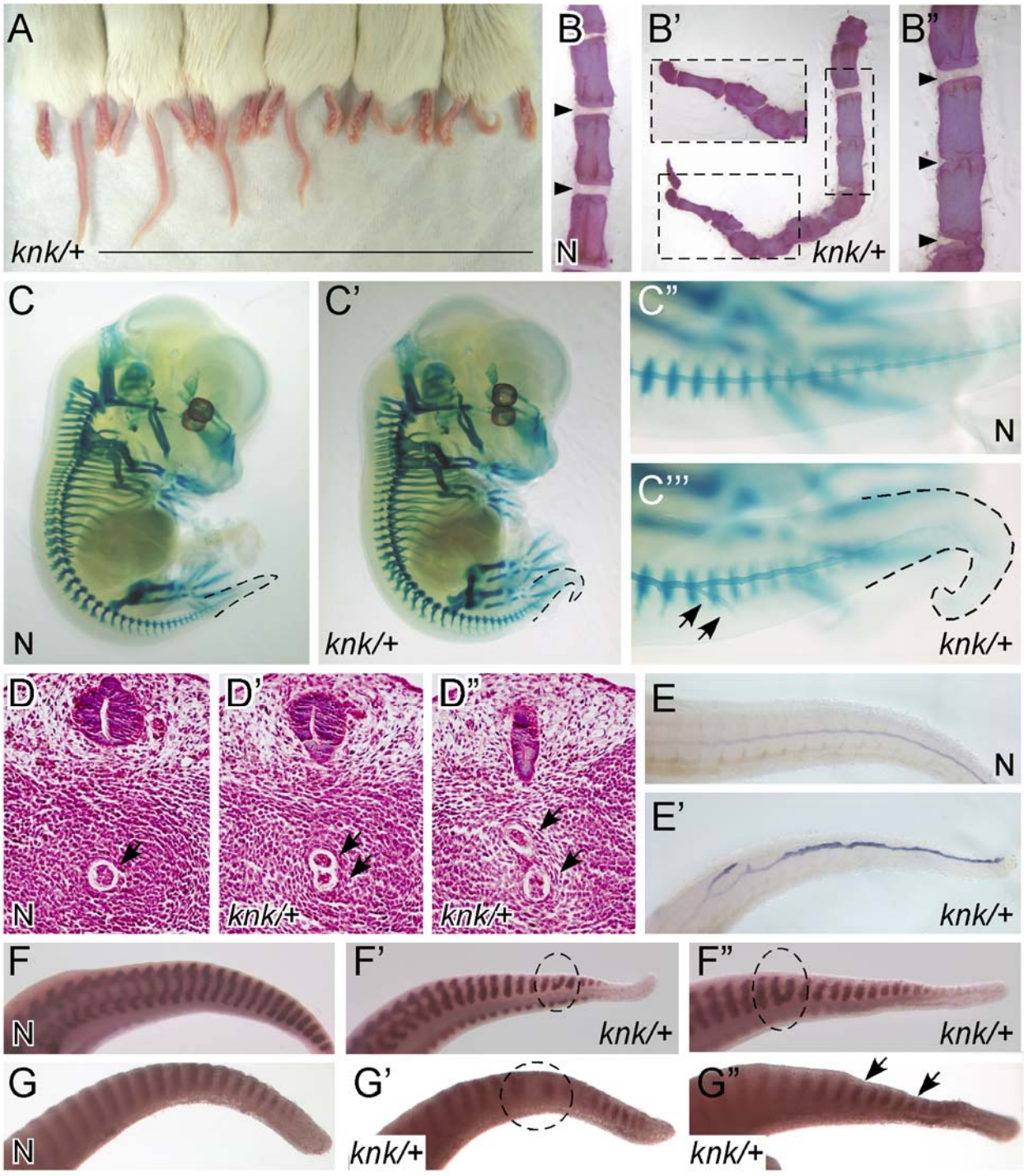
A
knk/+
B
N
B'
knk/+
B"
C
N
C'
knk/+
C"
N
C'''
knk/+
D
N
D'
knk/+
D"
knk/+
E
N
E'
knk/+
F
N
F'
knk/+
F"
knk/+
G
N
G'
knk/+
G"
knk/+

Figure 3: *knk* heterozygous mice exhibited vertebral malformations. (A) *kinked tail* heterozygous mice exhibit variable tail kinks and a shortened axis. Alizarian red staining of adult normal (N; panel B) and *knk*/+ (B'-B") tails revealed severe vertebral defects including fusions and hemi-vertebrae (B-B") as well as defects in IVD formation (arrowheads, B") in *knk* heterozygotes compared to the evenly segmented vertebrae and evenly spaced IVD's in normal tails (arrowheads, B). Alcian blue staining of e13.5 normal (C, C") and *knk*/+ (C´, C'") embryos revealed the curled tail tip and a thick and branched notochord (arrows, C'") in the *knk*/+ embryo. Transverse sections through the posterior of e13.5 N (D) and *knk*/+ (D', D") tails stained with H & E. Arrowheads indicate notochord; note the presence of 2 notochords in the *knk*/+ sections (D'-D"). (E-E') WISH of *shh* expression in e12.5 tails revealed the aberrant morphology of the notochord that is thickened and has multiple branches in the *knk*/+ tail compared to the normal tail. (F) *Myogenin* expression showed subtle fusions of the myotome in the *knk*/+ tails (dashed circles, F'-F"). (G) *Uncx4.1* expression revealed altered spacing between posterior somite halves (dashed circle, G') and variable sized compartments (arrows, G") (Farkas and Chapman, 2009).

2.3.2 Discussion

The *kinked tail* mutation is a spontaneous dominant mutation in an unknown gene(s). The observed kinky tail phenotype in the heterozygotes is a product of vertebral malformations likely resulting from a primary notochord defect. Mutations in a variety of genes adversely affect notochord formation. *T/T* homozygous embryos lack a trunk notochord (Wilkinson et al., 1990) and *Foxa2* homozygous mutants lack all notochord cells (Ang and Rossant, 1994). Homozygous loss of *Noto*, a homeobox gene, specifically affects the tail notochord after e9.5 in homozygous mutants (Abdelkhalek et al., 2004). Similar to *kinked tail* heterozygotes, *Noto* phenotypes are limited to the tail, supporting the hypothesis that there is a separate mechanism for notochord morphogenesis in the anterior and posterior portions of the embryo.

Disruption of D-V patterning of the somite by aberrant shh signaling could generate the vertebral fusions observed in the *knk* heterozygotes. Conversion of dermamyotome to sclerotome may lead to malformation of vertebrae, possibly the converted myotome would not undergo resegmentation causing vertebral fusions. However, the *myogenin* (myotome) WISH results suggest that if D-V patterning is affected by the *kinked tail* mutation, it is a subtle effect and may not completely explain the vertebral defects and axis shortening observed. Two alternative explanations for the *knk* heterozygous phenotypes are based on characterization of the *Pax1* and *Noto* mutant embryos. Notochord signals induce *Pax1* expression in the ventromedial part of the somite that will form the sclerotome. *Pax1* mutant embryos exhibit abnormal sclerotome compartments and excessive notochordal cell proliferation, suggesting that in a normal situation, signals from the sclerotome to the notochord help regulate notochord cell proliferation and morphology (Wallin et al., 1994). Similarly, the kinky tail phenotype observed in *knk*/+ mice could result from excess notochord cell proliferation that is secondary to defective sclerotome signals. In the *Noto* homozygous mutant, the primary defect is in the notochord where notochord precursor cells contributing to the posterior notochord are transfated from axial to paraxial mesoderm, resulting in caudal notochord and axial truncations (Abdelkhalek et al., 2004; Yamanaka et al., 2007). Therefore, the defects in the *knk*/+ mice could be primarily caused by notochord defects. However, these defects alone might not completely explain the axial truncations observed in the *knk*/+ mice. Axis extension results from mesoderm production within the PS and later in the tailbud. It is therefore possible that mesoderm production may also be affected in the *kinked tail* heterozygotes. Finally, while A-P somite patterning defects were not analyzed extensively, it is possible that the very slight mispatterning revealed by *Uncx4.1*

WISH may later lead to resegmentation defects. Subtle A-P and D-V axis defects may compound to generate the vertebral malformations observed in the affected mice.

knk heterozygotes were characterized by both a malformed notochord and IVDs. Interestingly, defects in notochord formation and subsequent IVD formation can result in vertebral defects such as wedge, fused and hemi-vertebrae similar to those seen in human scoliosis patients (Semba et al., 2006). There are currently no known differences in trunk versus tail somite formation and differentiation, and ultimately vertebral formation. Therefore, it is possible to examine vertebral malformations in the tail of the *knk* heterozygotes and apply that to trunk vertebral malformations found in human patients. While the etiology of congenital scoliosis is still unknown, the *kinked tail* mutation might lend insight into the genetic basis of this disorder.

2.4 *KNK* HOMOZYGOUS MUTANT ANALYSIS

2.4.1 Introduction

Analyses of litters dissected from *knk*/+ intercrosses revealed a population of embryos with distinct phenotypes between e6.5-e8.5, and decidual resorptions starting at e8.5. These mutant phenotypes were found in ~25% of embryos, the expected Mendelian transmission for the *knk/knk* embryos. Presumptive *knk*/*knk* mutant embryos were not found after e8.5.

2.4.1.1 Basement membrane deposition during early development

Basement membranes play fundamental roles during embryogenesis such as promotion of cellular differentiation, growth and cell attachment. They are composed of extracellular matrix (ECM) glycoproteins including laminins, collagen IV, perlecan, and nidogen (Timpl, 1996). Laminins, heterotrimeric proteins consisting of three chains, α, β, and γ, are essential for basement membrane formation, which begins with laminin deposition, polymerization and subsequent integration of other ECM glycoproteins (Li et al., 2003). During early development, from e5.5 to e7.5, laminin chains α1, α5, β1 and γ1, representing laminins 1 and 10, are the only laminins detected and have unique and overlapping expression domains (Miner et al., 2004). One of these domains is the embryonic basement membrane that lies between the embryonic ectoderm and the visceral endoderm (Fig. 4). The visceral endoderm cells are thought to contribute to this membrane through laminin secretion (Coucouvanis and Martin, 1999; Smyth et al., 1999; Miner et al., 2004).

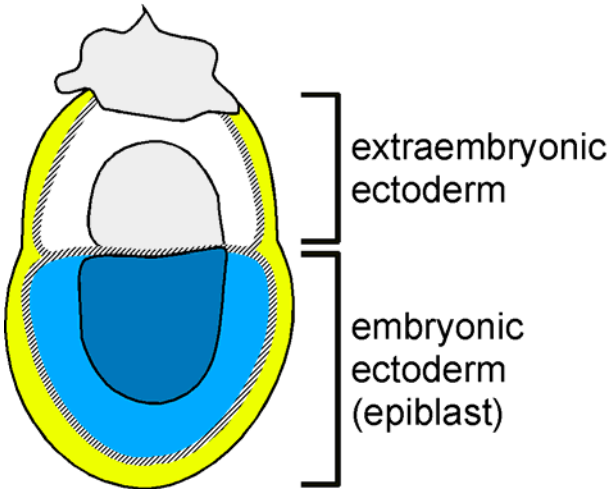

Figure 4: Laminin embryonic distribution. Laminin is deposited in the embryonic basement membrane beginning at e5.5; hatched lines (laminin deposition) between visceral endoderm (yellow) and embryonic ectoderm or epiblast (blue) and extraembryonic ectoderm (white).

2.4.1.2 DVE migration and AVE formation

The migration of DVE cells anteriorly establishes the AVE, a signaling center that is required for asymmetric gene expression within the epiblast and hence the A-P axis (Bielinska et al., 1999; Coucouvanis and Martin, 1999; Perea-Gomez et al., 2001b; Simeone and Acampora, 2001; Yamamoto et al., 2004). If the DVE fails to be specified and/or to migrate, these asymmetric gene expression patterns will not be established and the embryos will fail to gastrulate. These types of defects are observed in *Cripto* (Ding et al., 1998), *Otx2* (Kimura et al., 2000), β-*catenin* (Huelsken et al., 2000) and *Nodal* mutants (Brennan et al., 2001).

Nodal, a TGFβ family member is essential for DVE induction as *Nodal* mutants lack typical DVE specific markers, including *Hex*, *Lefty1*, and *Otx2* (Brennan et al., 2001). Nodal is required for proliferation of the epiblast which is critical for growth of the embryo along its proximo-distal axis and is necessary to separate the DVE from unknown inhibitory signals in the extraembryonic ectoderm (Brennan et al., 2001; Rodriguez et al., 2005; Mesnard et al., 2006). Once the epiblast reaches ~180 μm, the distal tip is far enough removed from these inhibitory signals to become receptive to Nodal signaling and the DVE cells thicken (Mesnard et al., 2006). Upon induction, these DVE cells actively migrate toward the presumptive anterior of the epiblast concomitant with a cell shape change from their previous columnar morphology to a squamous one (Srinivas et al., 2004). This active migration is accompanied by a passive migration event which results from an asymmetric increase in cell proliferation on the future posterior side of the embryo (Yamamoto et al., 2004). However, even before induction can take place, Nodal appears to be required for specifying general embryonic VE identity because loss of *Nodal* expression results in the loss of general VE markers including *Fgf8* (Mesnard et al., 2006).

Nodal signaling both directly and indirectly specifies DVE cells which then express a unique subset of genes including *Hex, Lefty1, mCer1* and *Otx2*. *Hex*, a homeobox gene, is one of the first genes expressed upon DVE induction and is later found in the extraembryonic mesoderm and endothelial cell precursors (Thomas et al., 1998). Loss of *Hex1* in the mouse results in defective definitive endoderm and forebrain development followed by embryonic lethality by e15.5 (Martinez Barbera et al., 2000). *Lefty1*, a TGFβ family member, is secreted from the DVE cells as they migrate towards the future anterior of the embryo and antagonizes Nodal signaling (Meno et al., 1996; Perea-Gomez et al., 2002). *mCer1*, a secreted BMP and Nodal antagonist, shares an overlapping expression domain with *Lefty1* in the DVE and AVE (Belo et al., 1997; Shawlot et al., 1998). However, neither *Lefty1* (Meno et al., 1998) nor *mCer1* (Belo et al., 2000) homozygous mutant embryos do not display any gastrulation abnormalities, despite the role of DVE cell migration and gene expression in A-P axis establishment. However, compound mutants of *Lefty1* and *mCer1* result in ectopic primitive streak formation followed by embryonic lethality at e9.5, revealing their role in proper A-P patterning (Perea-Gomez et al., 2002).

Once the DVE cells reach the anterior, they are now termed the AVE. The AVE cells continue to express DVE specific genes, *Hex, Lefty1, mCer1* and *Otx2*. In addition its role in establishing the A-P axis through secreted inhibitors of BMPs, Wnts and Nodal, the AVE also has a role in patterning the anterior of the embryo. *Otx2*, a homeodomain containing transcription factor, is expressed in the VE beginning at approximately e5.5, becomes localized to the anterior of the embryo by e7.5, and continues to be expressed in the head region later in development (Simeone et al., 1993; Ang et al., 1994). The knockout of murine *Otx2* results in severe gastrulation and axial mesoderm defects, loss of anterior neural tissue and embryonic

lethality around e10.5 (Ang et al., 1996). Importantly, *Otx2* is also required for the movement of VE cells: *Otx2* -/- mutant VE cells do not migrate, expression of DVE/AVE specific genes, *Lefty1* and *Dkk1* is lost, and *mCer1* expression is mislocalized (Perea-Gomez et al., 2001a).

2.4.2 Results of *knk*/*knk* mutant analysis

Characterization of early embryonic lethal phenotypes involved analysis of marker genes for appropriate patterning, presence of germ layers, and cell and tissue morphology. Attention was also paid to the DVE/AVE transition, including cell morphology and ECM component localization. Below I describe the analyses of the *knk* homozygous mutant (Farkas and Chapman, 2009).

2.4.2.1 *knk*/*knk* mutants had small, disorganized embryonic portions

Analyses of litters dissected from *knk*/+ intercrosses revealed a population of embryos with mutant phenotypes between e6.5-e8.5, and decidual resorptions starting at e8.5. These mutant phenotypes were found in ~25% (n=35) of embryos, the expected Mendelian transmission for the *knk/knk* embryos. Although genotyping of the *kinked tail* mice and embryos is not possible at this time because the gene(s) affected by the *knk* mutation is not known, I have interpreted the affected population of embryos as *knk* homozygotes based on its Mendelian transmission.

Examination of litters from e5.5 to e6.5 (n=47 embryos) revealed that at e5.5 there were no discernable differences between the majority of presumptive mutant and normal embryos. However, some very severe *knk* mutant embryos were distinguishable at this stage. At e6.5 the *knk/knk* mutant phenotype could be recognized by a smaller embryonic portion that generally lacked organization when compared to normal embryos (Fig. 5A). At e7.5 the yolk sac and

Reicherts' membrane often appeared to be loosely adhered to the egg cylinder (Fig. 5B, arrow). Despite the smaller embryonic portions, there were no observable differences in the size of the extraembryonic ectoderm and ectoplacental cone in *knk*/*knk* embryos compared with normal embryos, and the separation between the embryonic and extraembryonic regions were similarly distinct (Fig. 7 *BMP4* panel). The severity of the homozygous mutant phenotype was variable, which might be expected based on the variability of the *knk*/+ phenotypes. By e7.5, normal embryos had already begun gastrulation with prominent anterior head folds (Fig. 5B). At e7.5, the *knk/knk* mutant embryos were consistently smaller than their normal littermates and were approximately the size of normal e6.5 embryos (n=35) (Fig. 5B and Fig. 6B, Fig. 10), suggesting that they may be developmentally delayed. However, the dysmorphic *knk*/*knk* epiblast suggests that the phenotype is not merely a developmental delay. Very few mutant embryos survived to e8.5. Those that did survive appeared to generate a more organized epiblast that was somewhat similar to normal e6.5 embryos (compare Fig. 5C' to 5A). *knk/knk* embryos were not found in decidua past e8.5 (Farkas and Chapman, 2009).

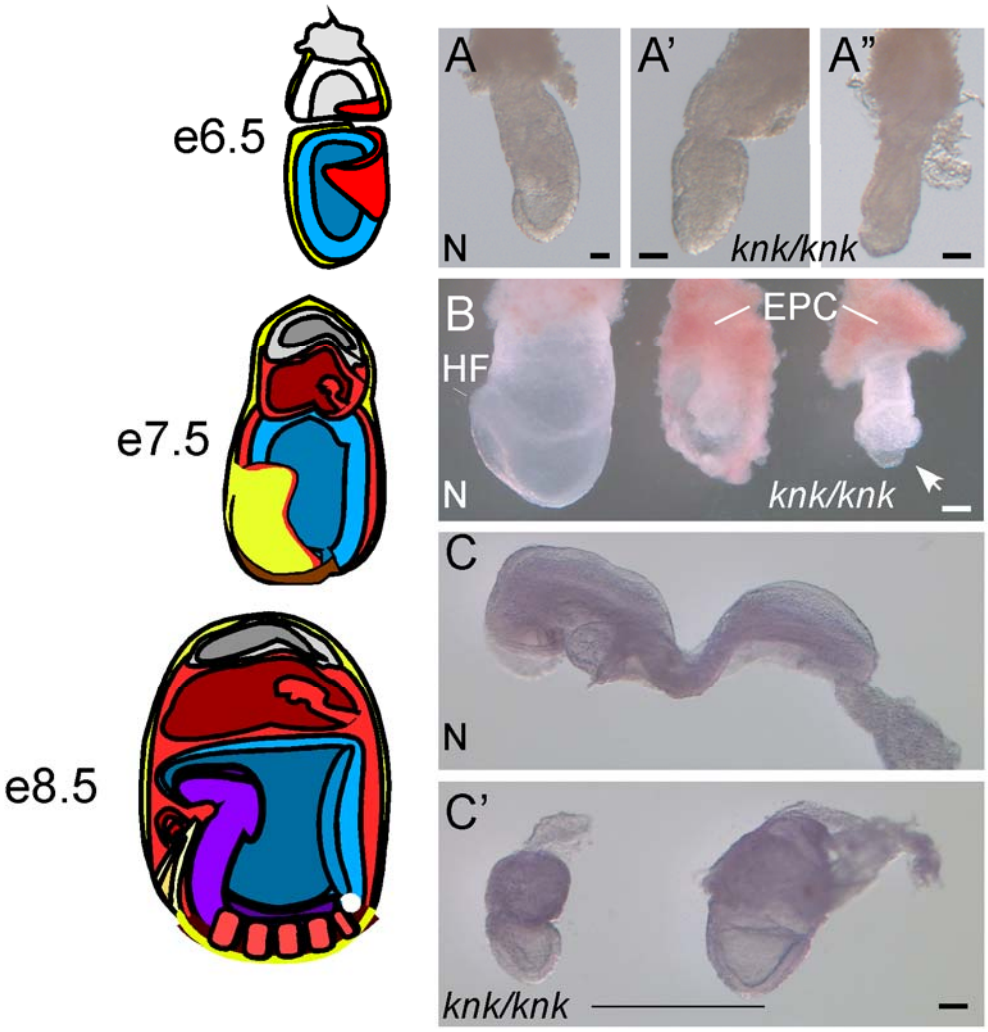

Figure 5: *knk*/*knk* mutants had small, disorganized embryonic portions. Gross morphology at e6.5 (A), e7.5 (B) and e8.5 (C) revealed that *kinked tail* homozygous mutants were severely dysmorphic compared to normal (N) littermates. Scale bars in panel A represent 50 μm. The few embryos that survived to e8.5 slightly resembled e6.5 normal embryos (compare C' to A). Scale bars in panels B and C represent 100 μm. Abbreviations: headfolds (HF); ectoplacental cone (EPC) (Farkas and Chapman, 2009).

2.4.2.2 Cell proliferation was unaffected in *kinked tail* homozygous mutants

To investigate whether the smaller embryonic portion observed in the *knk*/*knk* mutants was due to a defect in cellular proliferation, I examined mutant embryos by whole mount

immunohistochemistry. Phospho-Histone H3 is a marker of actively proliferating cells (Hendzel et al., 1997). Analysis of stained normal and mutant embryos by confocal microscopy revealed the presence of proliferating cells in both phenotypes (Fig. 6A). Quantitation of actively proliferating cells calculated as a percentage of relative total cell number indicated that there was no significant difference in the percentage of proliferating cells between normal (13 ± 8%) and *knk*/*knk* mutant embryos (16 ± 4%) (Fig. 6B, n=4 *knk*/*knk*). However, relative total cell numbers indicated that the *knk*/*knk* mutant embryos (919 ± 52) were significantly smaller than normal embryos (3138 ± 1165) (Fig. 6B). The possibility of cell death affecting the *knk*/*knk* mutant embryos will be discussed in section 2.6.3.

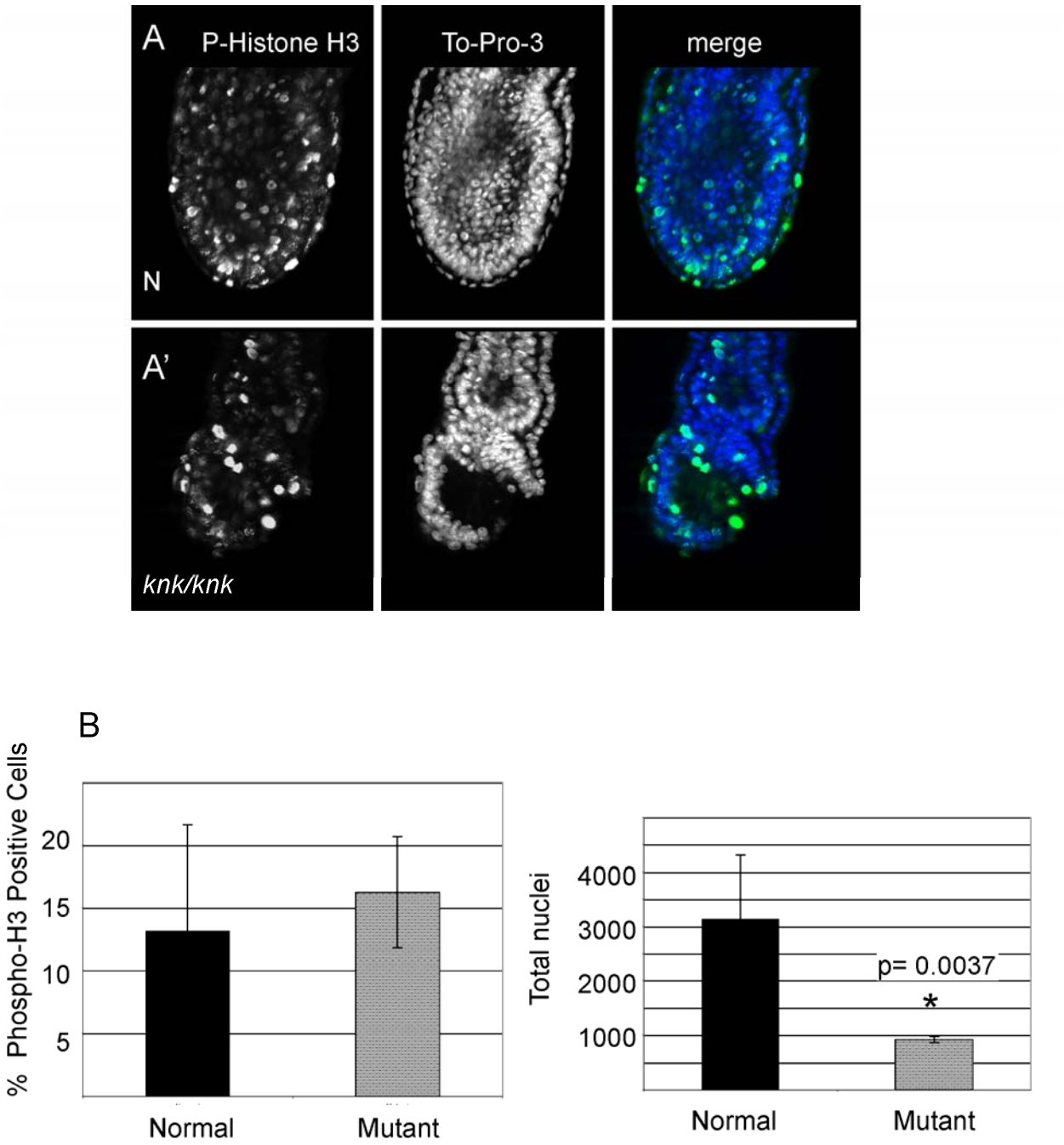

Figure 6: Cellular proliferation is unaffected in *knk*/*knk* mutants. (A) e7.5 normal (N) and *knk*/*knk* mutant embryos were stained for actively proliferating cells with phospho-Histone H3 (green) and nuclei with TO-PRO-3 (blue). Single optical sections are shown. (B) The percent proliferating cells was calculated by counting the number of phospho-Histone-H3 positive cells and dividing by the number of TO-PRO-3 positive

cells within the embryonic portion, in representative optical sections from the top, middle and bottom of the embryo. This calculation revealed that there was no significant difference in the percent proliferating cells in normal or mutant embryos. However, the relative total cell number (represented by positive TO-PRO-3 cells from the previous calculation) indicated that the *knk*/*knk* mutant embryos have significantly smaller embryonic portions than the normal embryos based on Student's T-test, p=0.0037.

2.4.2.3 *knk*/*knk* mutants fail to gastrulate

I performed marker gene analysis using WISH at e6.5-e7.5 to further characterize the homozygous *kinked tail* phenotype. Morphological analyses showed that the *knk*/*knk* mutant embryos were smaller than normal embryos. These phenotypes could be due to a general failure to specify the embryonic portion. To test this possibility, I examined *Oct3/4* (a.k.a. *Pou5f1*), a pluripotency marker, that is normally expressed in the entire embryonic ectoderm and is later restricted to the posterior of the embryo (Nichols et al., 1998; Rosner et al., 1990). Comparisons of *Oct3/4* expression in early- and late-staged e7.5 normal and *knk/knk* mutant embryos revealed that the small, disorganized embryonic portion of the mutants at the distal tip was indeed a pluripotent embryonic region, but that *Oct3/4* did not become restricted to the posterior region as was observed in normal littermates (Fig. 7 *Oct3/4* panel, n=7 *knk*/*knk*) (Farkas and Chapman, 2009). To confirm that the *knk*/*knk* mutant *Oct3/4* expression domain represented the embryonic portion, I analyzed *BMP4* expression, a marker of the extraembryonic ectoderm at e6.5 (Coucouvanis and Martin, 1999). *BMP4* expression demarcated the extraembryonic/embryonic boundary and revealed the smaller than normal embryonic portion in obvious mutants (Fig. 7 *BMP4* panel, n=4 *knk*/*knk*). At e6.5, the number of obvious *knk*/*knk* embryos was less than expected based on Mendelian transmission, therefore some *knk*/*knk* embryos at e6.5 could not be distinguished morphologically or by *BMP4* expression from normal littermates. This again

reflects the variability of the *kinked tail* phenotype. *BMP4* expression was also examined at e7.5, when the *kinked tail* phenotype is more obvious. This analysis clearly showed the smaller embryonic portion of the *knk*/*knk* embryos demarcated by the extraembryonic *BMP4* expression. In addition, *BMP4* expression does not become restricted to the posterior in *knk*/*knk* mutant embryos as compared to normal e7.5 embryos (Fig. 7 *BMP4* panel, n=5 *knk*/*knk*) (Farkas and Chapman, 2009). Comparisons of the embryonic portions of e6.5 and e7.5 *knk*/*knk* mutants revealed that relatively little growth occurred during this time period.

To determine whether the *knk/knk* embryos undergo gastrulation, I examined markers of mesoderm production, *T* and *Foxa2*, at e7.5. *T* is normally expressed in the PS and is essential for mesoderm specification (Wilkinson et al., 1990; Herrmann, 1991). Expression of *T* in the *knk*/*knk* mutants was either absent or non-distinct (Fig. 7 *T* panel, n=5 *knk*/*knk* no stain, n=1 *knk/knk* non-distinct stain) (Farkas and Chapman, 2009). *Foxa2* (a.k.a. *Hnf-3β*) is normally expressed in the node, notochord, and prechordal mesoderm and is essential for their formation (Ang and Rossant, 1994; Monaghan et al., 1993). *knk* homozygous mutants did not express *Foxa2* (Fig. 7 *Foxa2* panel, n=3 *knk*/*knk*) (Farkas and Chapman, 2009). Altogether *knk*/*knk* mutants do not specify significant amounts of mesoderm, thereby suggesting a failure to undergo gastrulation.

There are several reasons for gastrulation failure, one of which is the defective establishment of the AVE. To determine whether the AVE is compromised in the *knk* embryos, I examined the expression of *Otx2* and *mCer1*, markers of mature AVE (Fig. 7). At e7.5, *Otx2* is expressed in the AVE and is essential to pattern the anterior head structures of the embryo (Ang et al., 1996). *Otx2* expression was variable in *knk/knk* mutants, with mutants expressing either low levels of *Otx2* throughout the presumptive embryonic ectoderm/VE (Fig. 7 *Otx2* panel, n=2 *knk*/*knk*), or

not expressing *Otx2* at all (n=1) (Farkas and Chapman, 2009). *mCer1*, a secreted Nodal antagonist, is expressed in the AVE and plays a role in patterning the A-P axis (Belo et al., 1997; Yamamoto et al., 2004). *knk/knk* embryos displayed weak or no expression of *mCer1* (Fig. 7 *mCer1* panel, n=4 *knk*/*knk*), suggesting a failure to establish the mature AVE (Farkas and Chapman, 2009).

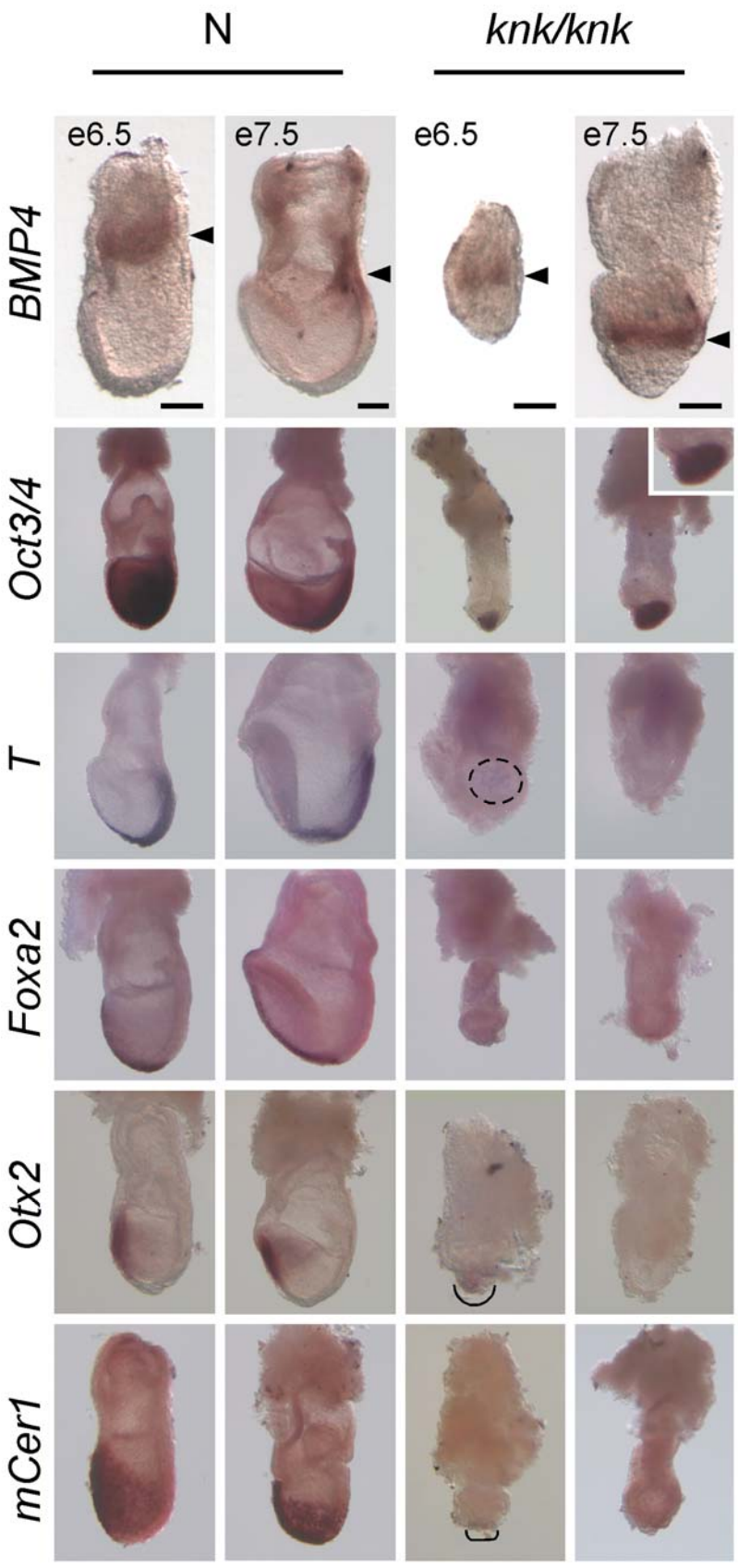
N
knk/knk
e6.5
e7.5
e6.5
e7.5
BMP4
Oct3/4
T
Foxa2
Otx2
mCer1

Figure 7: Marker gene analysis of *knk*/*knk* embryos. As shown by *BMP4* WISH at e6.5 and e7.5, *knk*/*knk* mutants establish a clear embryonic/extraembryonic boundary (black arrowheads) but the embryonic portion is smaller than normal littermates. Scale bars in *BMP4* panel represent 20 μm at e6.5 and 100 μm at e7.5. For all remaining panels, marker genes were analyzed at e7.5 with two examples of each to demonstrate the variability of the *knk/knk* phenotype. For these panels, all embryos were photographed at the same magnification and the normal embryos were oriented with anterior to the left and posterior to the right. The *knk*/*knk* embryos specified an epiblast (*Oct3/4* panel, high magnification inset; black arc *Otx2* panel) but this area was significantly smaller than normal littermates. *knk*/*knk* embryos specified little (dashed circle, *T* panel) to no mesoderm (*T* and *Foxa2* panels). *knk*/*knk* mutants did not form mature AVE as shown by the lack or mislocalization of *Otx2* and little (black arc) to no *mCer1* expression (*Otx2* and *mCer1* panels) (Farkas and Chapman, 2009).

2.4.2.4 Abnormal VE morphology of *kinked tail* mutants

The above studies suggest that a mature AVE does not form in the *knk/knk* mutants. Prior to AVE formation, the DVE must be specified, followed by migration to the future anterior, finally forming the mature AVE. I hypothesized that *knk/knk* mutant embryos do not gastrulate due to a defect in the embryonic VE. To further examine the morphology of the *knk*/*knk* VE, I performed histology on normal and mutant embryos beginning at e5.5. At the gross morphological level, the majority of *knk*/*knk* mutant embryos cannot be distinguished from normal littermates at this stage. Even at the histological level, *knk*/*knk* embryos were difficult to distinguish (data not shown). By e6.5, DVE cells in normal embryos have already migrated anteriorly and the embryonic VE cells have adopted a squamous cell morphology, while the extraembryonic VE cells maintain a cuboidal morphology (Fig. 8A). At this stage, the amniotic cavity was also well formed in normal embryos (Fig. 8A). In comparison, the VE cells of the

knk/*knk* embryos maintained a cuboidal morphology around the entire egg cylinder and the amniotic cavity was only beginning to form (Fig. 8A'-A"). At e7.5, normal embryos have established all three germ layers indicative of successful gastrulation (Fig. 8B). In contrast, *knk/knk* embryos had small, grossly malformed embryonic portions with no apparent mesoderm. This supports the conclusion that *knk/knk* mutant embryos fail to undergo gastrulation. In addition, the VE cells maintained their cuboidal morphology and were not organized (Fig. 8B'-B") (Farkas and Chapman, 2009). The failure of embryonic VE adopting a squamous morphology was apparent in the *knk*/*knk* mutant embryos with some *knk*/*knk* embryos displaying an accumulation of VE cells at the distal tip by e7.5 (Fig. 8B").

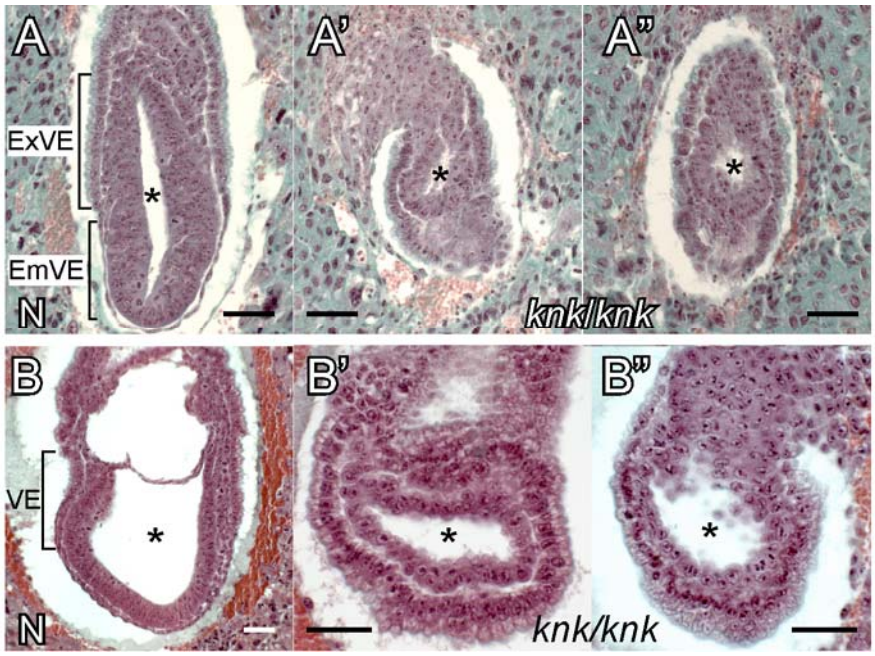

Figure 8: Abnormal VE morphology in *knk/knk* mutants. Mason's trichrome staining of e6.5 (A) and e7.5 (B) sections. Scale bars represent 50 μm. (A) The embryonic VE surrounding the embryonic portion of the *knk/knk* embryo does not adopt a squamous cell morphology as seen in normal (N) embryos. (B) At e7.5, normal embryos have established all 3 germ layers, while the *knk*/*knk* embryos have a disorganized

embryonic portion and have not undergone gastrulation (B', B"). Abbreviations: embryonic visceral endoderm (EmVE); extraembryonic visceral endoderm (ExVE); visceral endoderm (VE) * (amniotic cavity) (Farkas and Chapman, 2009).

2.4.2.5 *knk*/*knk* mutant embryos are competent to receive inductive *Nodal* signals

While the *knk*/*knk* mutant VE cells have a distinct morphological phenotype, I wanted to further characterize the mutants by analyzing VE cell gene expression and overall embryo size. Due to its critical role in general VE and DVE specification, I examined *Nodal* expression in the *knk*/*knk* mutants. At e5.5, *Nodal* is normally expressed throughout the entire embryonic portion (Varlet et al., 1997), however the *knk/knk* mutant did not express *Nodal* (Fig. 9A-A', n=1 *knk*/*knk*). By e7.5, *Nodal* transcripts are normally confined to the node, but in the *knk/knk* mutants *Nodal* was now expressed throughout the presumptive embryonic portion, thus resembling normal *Nodal* expression at e5.5 (Fig. 9B-B', n=5 *knk*/*knk*) (Farkas and Chapman, 2009). Aberrant *Nodal* expression in the *kinked tail* homozygous mutants could indicate a general failure of embryonic VE specification. To further analyze general VE specification, I examined *Fgf8* expression. Prior to gastrulation (~e5.75), *Fgf8* is expressed in the VE, but by e7.5 becomes localized to the PS (Crossley and Martin, 1995). As previously described, *knk/knk* embryos fail to undergo gastrulation and therefore do not form a PS, and at e7.5 are similar to normal e5.5-e6.5 embryos. I therefore examined e7.5 *knk/knk* embryos for *Fgf8* expression. Interestingly, *Fgf8* was expressed throughout the embryonic portion, thus resembling the normal pattern of *Fgf8* expression prior to gastrulation (Fig. 9C-C', n=6 *knk/knk*) (Farkas and Chapman, 2009). In addition, *Otx2* which is also expressed in the VE prior to gastrulation (Simeone et al., 1993), was present in some of the *knk*/*knk* embryos at e7.5 (Fig. 7, *Otx2* panel, black arc) (Farkas

and Chapman, 2009). Altogether, these results support that VE is specified in the *knk*/*knk* embryos.

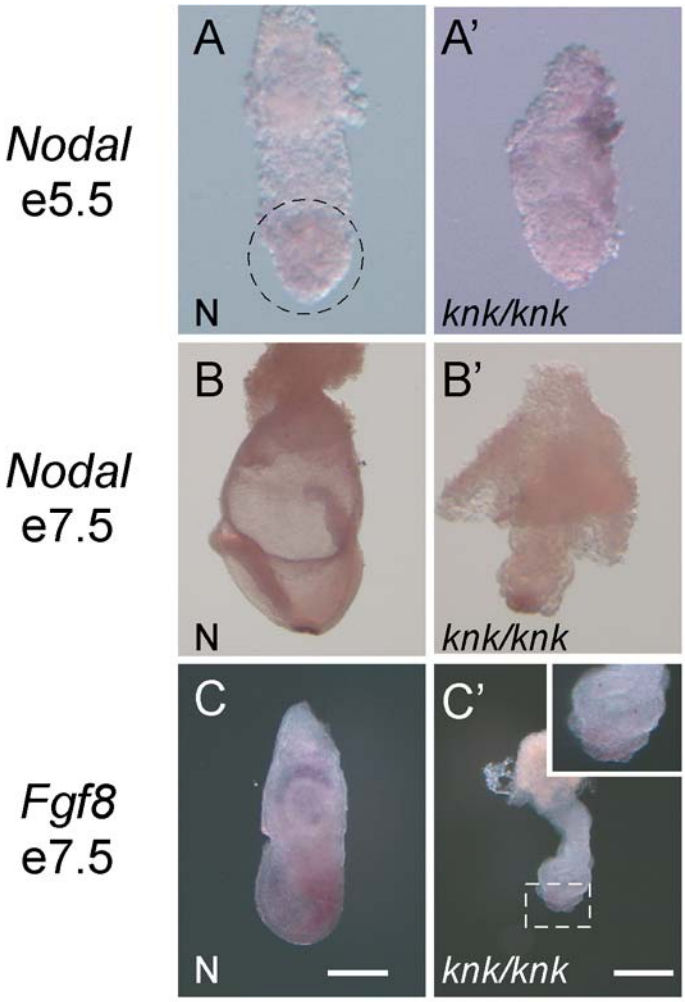

Figure 9: General VE marker genes were expressed in *knk*/*knk* embryos. (A) At e5.5, normal embryos expressed *Nodal* throughout the epiblast (A, dashed circle), while a *knk*/*knk* mutant embryo did not express *Nodal* (A'). (B) However, by e7.5, *Nodal* transcripts were found throughout the small *knk*/*knk* embryonic portion (B') in contrast to its normal expression in the node (B). (C) While *Fgf8* at e7.5 becomes localized to the posterior of the normal embryo (C), expression in the *knk*/*knk* embryo appears in the presumptive embryonic portion (C', dashed square, inset). For these panels, embryos were photographed with anterior to the left and posterior to the right. Scale bars represent 100 μm. (Farkas and Chapman, 2009).

Based on the morphology and marker gene expression, general VE cells in *kinked tail* homozygotes are specified. To determine if the *knk*/*knk* mutant embryos reached the critical size of ~180 μm required for DVE induction, I measured the proximo-distal size of the embryos. By e7.5, ~50% of the *knk*/*knk* mutant embryos were indeed large enough to be receptive to inductive *Nodal* signaling, while others were considerably smaller (Fig. 10).

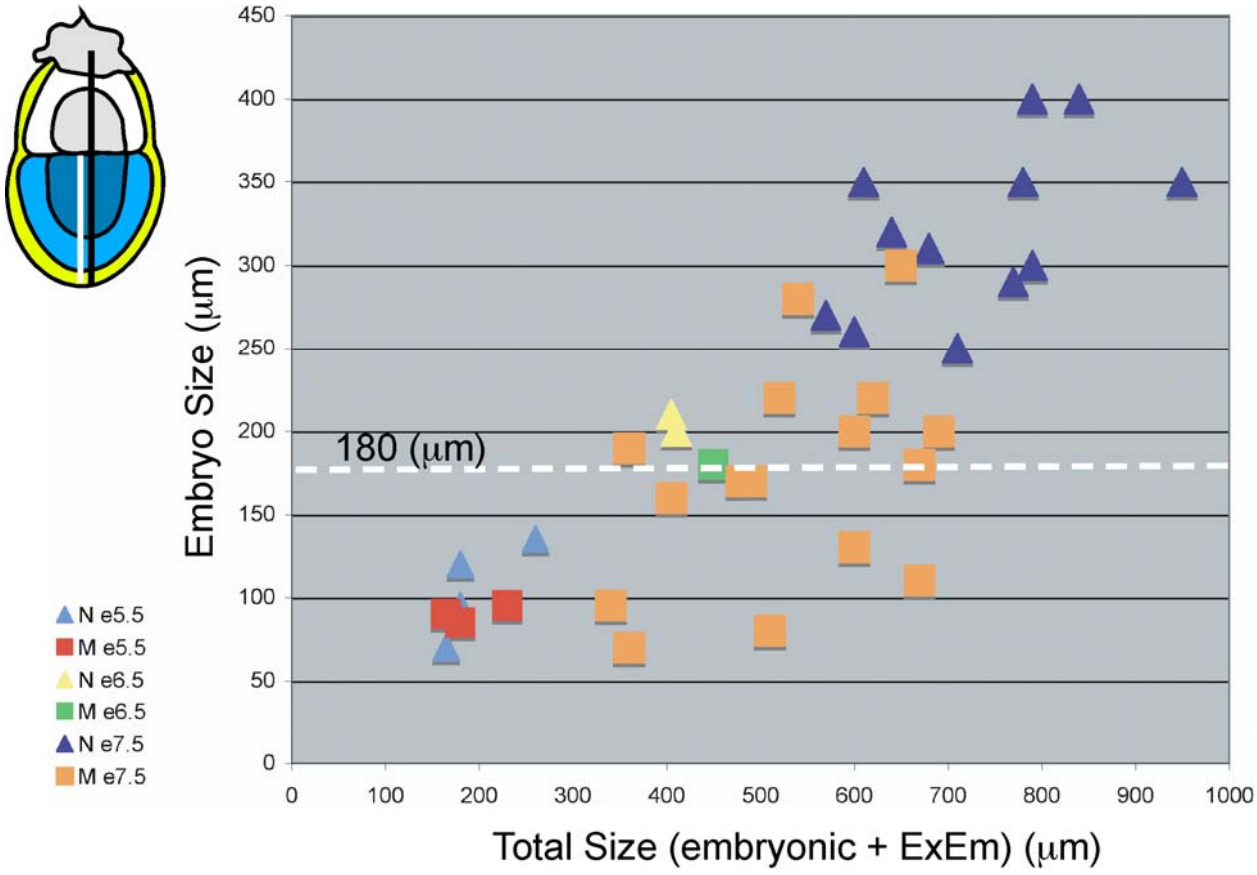

Figure 10: Reduced embryonic portions of *knk/knk* mutants compared to normal littermates. Schematic describing the measurements made for the embryonic portion (white line) versus the total embryonic plus extraembryonic portion (ExEm) (black line). *knk/knk* mutant (M) embryos display variable growth characteristics, ranging from smaller than normal (N) e6.5 embryos to larger than normal e7.5 (~180

μm, dashed white line). Embryo diagram: yellow (visceral endoderm); turquoise (epiblast); white (extraembryonic). (Farkas and Chapman, 2009)

2.4.2.6 *kinked tail* mutants specify the DVE

The failure of mutant VE cells to adopt a squamous cell morphology suggested that the distal VE cells do not migrate to the future anterior. As migration is dependent on DVE specification, I hypothesized that the cell shape change did not occur because the DVE was not specified. To test this, I analyzed the expression of DVE specific genes in normal and *knk*/*knk* mutant embryos by WISH. *mCer1* is secreted from the DVE cells as they migrate towards the future anterior of the embryo and is required for proper A-P patterning (Belo et al., 1997; Yamamoto et al., 2004; Torres-Padilla et al., 2007). Examination of e6.5 normal and *knk*/*knk* mutant embryos revealed that *mCer1* expression was absent in the mutants (Fig. 11A-A', n=3 *knk*/*knk*) (Farkas and Chapman, 2009). However at e7.5, some *knk*/*knk* embryos had weak *mCer1* expression (Fig. 7, *mCer1* panel, bracket). Another DVE-specific Nodal antagonist, *Lefty1*, has an overlapping expression domain with *mCer1* (Meno et al., 1996; Perea-Gomez et al., 2002). At e6.5, both normal and less severe *knk*/*knk* embryos expressed *Lefty1* in the migrating DVE cells (Fig. 11B'), however more severe *knk*/*knk* mutants (Fig. 11B", dashed circle) exhibited diffuse *Lefty1* expression in the middle portion of the embryo (Fig. 11B-B", n=3 *knk*/*knk*). At e7.5, *Lefty1* continues to be expressed as the DVE cells migrate and reach the anterior of the embryo. This expression pattern was seen in normal embryos, as well as *knk*/*knk* mutant embryos. However the mutant embryos appeared to have a distinct expression domain located at the boundary between the embryonic and extraembryonic portions (Fig. 11C-C"', arrowheads, insets, n=2 *knk*/*knk*) (Farkas and Chapman, 2009). Finally, *Hex*, which encodes a homeodomain protein, is expressed in the newly specified DVE and in the DVE cells as they

migrate toward the future anterior of the embryo (Thomas et al., 1998). This expression pattern was seen in normal early and late stage e7.5 embryos (Fig. 11D-D', arrows). Homozygous mutant embryos expressed *Hex* in the small embryonic portion (Fig. 11D"-D"', arrows, inset, n=3 *knk*/*knk*) (Farkas and Chapman, 2009). Eventual expression of all three DVE-specific markers suggests that the DVE is specified in *knk*/*knk* embryos.

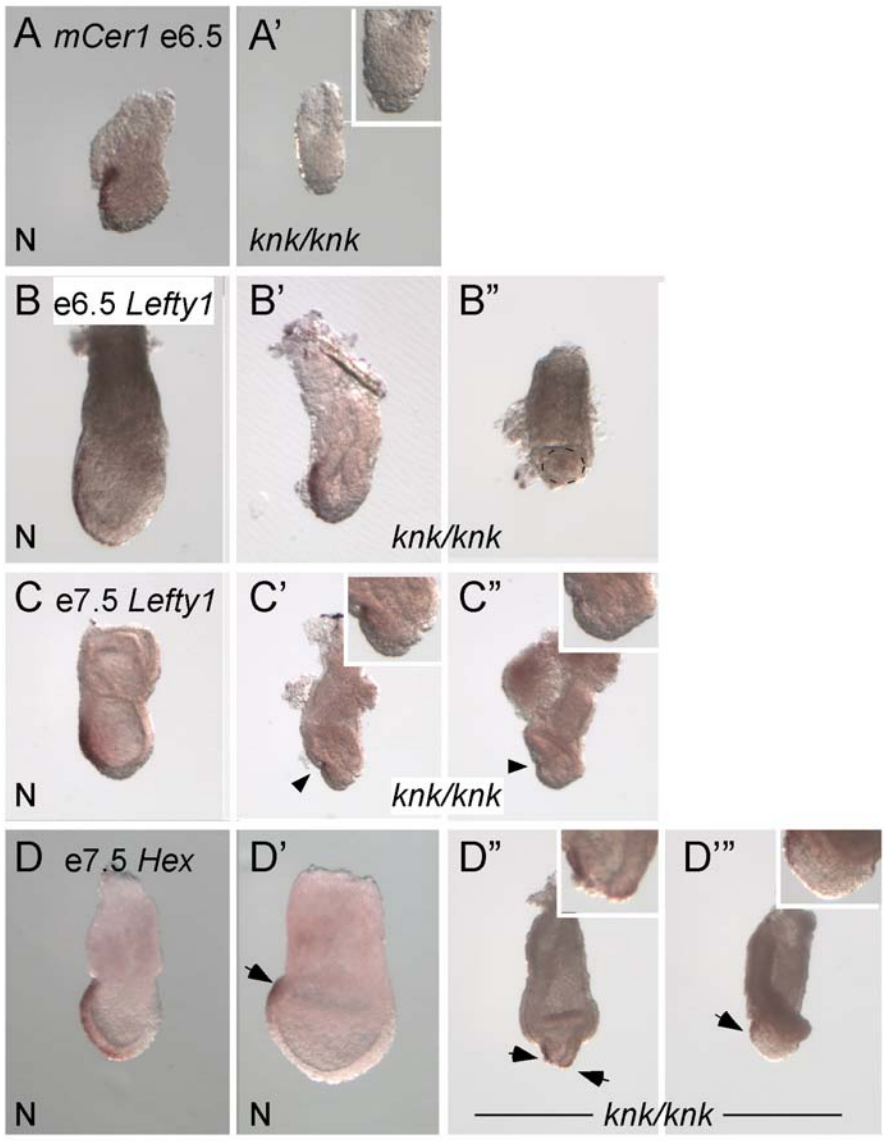

Figure 11: *knk*/*knk* mutant embryos specify the DVE. (A) At 6.5, *mCer1* is normally expressed in the VE in the future anterior of the embryo (A), however *mCer1* expression was absent in *knk*/*knk* mutant embryos (A', inset). (B) WISH at e6.5 showed *Lefty1* expression in the migrating DVE cells in both the normal (B) and a mild *knk*/*knk* mutant (B'). A severe *knk*/*knk* mutant had a diffuse *Lefty1* expression domain (B", dashed circle). (C) At e7.5, migrating cells in normal embryos continued to express *Lefty1* (C), while the *knk*/*knk* mutant embryos appeared to have a distinct domain of *Lefty1* expression at the boundary between

the extraembryonic and embryonic portions (C'-C", arrowheads, and insets). (D) WISH at e7.5 showed *Hex* expression in VE cells of both normal (D, D') and *knk*/*knk* embryos (arrows D"-D'", and insets). (Farkas and Chapman, 2009).

2.4.2.7 E-cadherin and laminin expression in *kinked tail* homozygous mutants

Another possible cause for the failure to establish mature AVE could be problems in DVE migration resulting from aberrant cell adhesion. Since the DVE appears to be specified, it is possible that the DVE cells are unable to migrate either because they adhere to each other and/or the underlying embryonic basement membrane too tightly or because they cannot adhere properly. The failure to migrate would result in the maintenance of the VE squamous cell morphology and subsequent failure to set up the A-P axis and gastrulation. To test for the localization of molecules involved in cell adhesion and migration, I examined E-cadherin expression in normal and *knk/knk* embryos. E-cadherin localizes to the adherens junctions of epithelial cells where it is essential for cell-cell adhesion (Damsky et al., 1993). Whole-mount immunofluoresence of E-cadherin expression at e6.5-e7.5 revealed that there was no detectable difference in E-cadherin expression or localization in the VE of normal and *knk/knk* embryos (Fig. 12A-A'", n=3 *knk*/*knk*). E-cadherin staining verified the squamous cell morphology of the normal VE cells (Fig. 12A') as compared to the cuboidal morphology of the *knk/knk* VE cells (Fig. 12A'") (Farkas and Chapman, 2009).

While cell-cell junctions appeared to be intact in the *knk*/*knk* embryos (based on E-cadherin expression), VE cells may have an altered ability to adhere to the embryonic basement membrane. To investigate this possibility, I examined the expression of laminin by whole-mount immunofluoresence. Laminins 1 and 10 are normally localized to the basement membrane

between the VE and embryonic and extraembryonic ectoderm and are essential for basement membrane formation (Miner et al., 2004; Smyth et al., 1999) (Fig. 12B). Examination of e6.5 *knk/knk* embryos revealed discontinuous laminin localization (Fig. 12B-B", n=5 *knk*/*knk*) (Farkas and Chapman, 2009). A disruption in the basement membrane due to a lack of laminin deposition may result in VE cells that subsequently aggregate. Aggregation of VE cells could be observed in some mutant embryos (Fig. 12B', Fig. 8B").

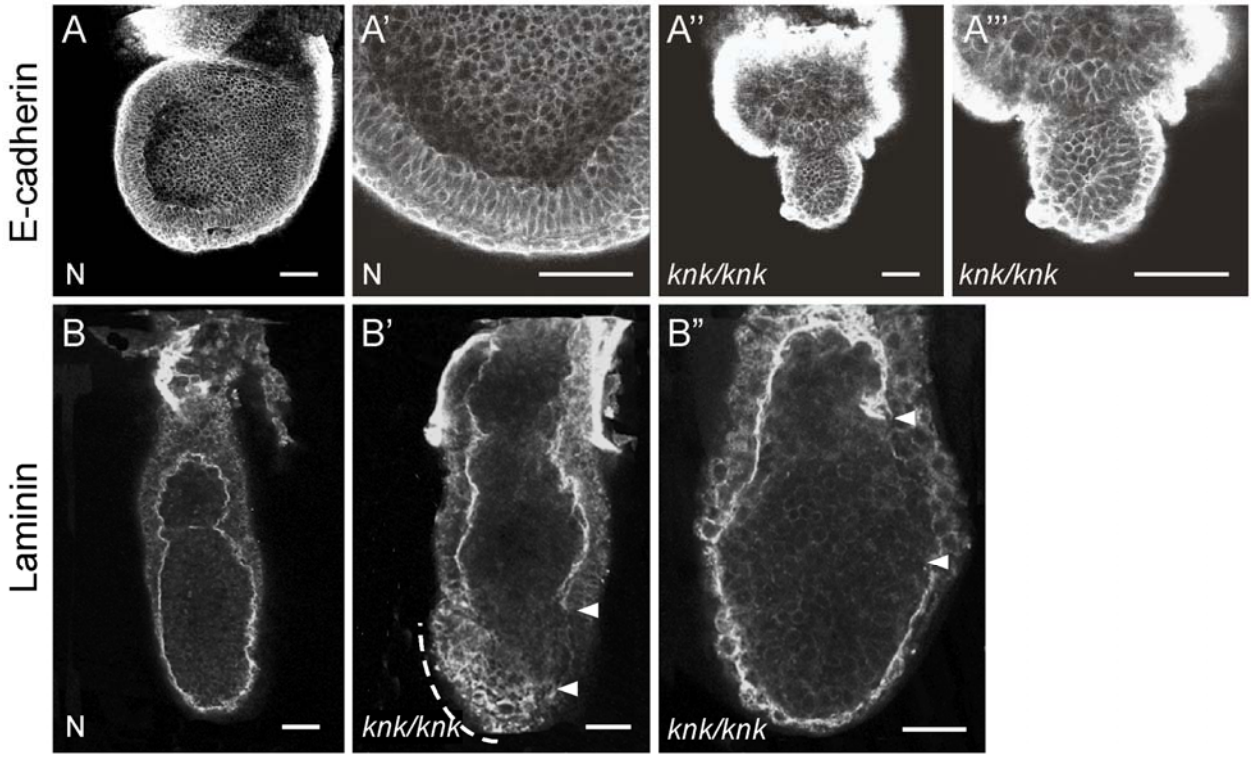

Figure 12: E-cadherin and laminin expression in *knk/knk* mutants. Whole mount immunofluoresence was used to visualize E-cadherin (e7.5) and laminin (e6.5) localization in normal and *knk/knk* embryos. (A) E-cadherin localized to the adherens junctions in both normal (N) and *knk*/*knk* embryos (single optical sections). A' and A'" are high magnifications of normal and *knk*/*knk* mutants, respectively. (B) Laminin is expressed continuously between the VE and the embryonic and extraembryonic ectoderm in normal embryos. Laminin localization was discontinuous in the mutants at e6.5 (compare B to

B' and B", arrowheads mark boundary of laminin breaks, dashed arc marks accumulation of cells). Scale bars represent 21.5 μm. (Farkas and Chapman, 2009).

2.4.2.8 Discussion of *knk*/*knk* mutant phenotype

Based on morphology, histology and marker gene analysis, *knk* homozygous mutant embryos are unable to gastrulate. This observed gastrulation failure is likely due to the improper temporal expression of DVE specific genes, as well as laminin deposition defects that together result in the absence of the AVE. These defects were compounded by the severe embryonic dysmorphology and developmental delay that ultimately result in the early embryonic lethality of the *knk* homozygotes.

To further investigate the small embryonic portions of the *knk*/*knk* embryos, I examined the embryos for the presence of proliferating cells. Although, there was no significant difference in proliferation rates between normal and mutant embryos at e7.5, this analysis provided a way to quantitate the relative number of cells in mutants versus normal littermates for statistical comparison. To minimize counting error, total cell numbers were calculated from optical sections representing the top, middle and bottom of the embryo. Therefore, the significant decrease in cell number between normal and *knk*/*knk* embryos calculated was a relative rather than absolute number (Fig. 6). However, this quantitation confirmed the data obtained from overall size measurements that showed that mutant embryos were approximately 33% smaller than the normal embryos (Fig. 10). An additional reason for the observed decrease in cell number would be an increase in cell death in the *knk*/*knk* mutant embryos. Attempts to assay this via acridine orange staining were made, but they have proved unsuccessful due to high background staining.

Oct3/4 expression showed that *knk*/*knk* embryos formed a small epiblast region. The presence of this small epiblast was further supported by examining *BMP4* expression, which demarcated the embryonic/extraembryonic boundary. The failure of the *Oct3/4* expression domain to become restricted to the posterior, however suggested that development was not progressing properly. *knk*/*knk* embryos failed to undergo gastrulation as demonstrated by little to no expression of mesodermal markers, *T* and *Foxa2*, and mature AVE markers, *Otx2* and *mCer1* (Fig. 7).

Interestingly, *Otx2* expression in the e7.5 *knk*/*knk* embryos appeared similar to that expected for e5.75 wildtype embryos at which time it is normally expressed throughout the epiblast (Acampora et al., 1995). This "delay" in marker gene expression was also observed for *mCer1* and *Nodal* and highlighted the severely compromised development of the *knk*/*knk* embryos (Figs. 7 and 9). The presence of *Nodal* signaling and the average size of the *knk* mutant embryonic portion at e7.5 should have been enough for proper DVE induction. In fact, I did observe the presence of DVE specific genes, *Hex* and *Lefty1* in mutant embryos. However, I was unable to orient these embryos making it difficult to determine whether their expression was properly localized to the presumptive anterior (Fig. 11). While *Nodal* mutants display a similar VE phenotype to *kinked tail* homozygotes, laminin deposition is not affected in the *Nodal* mutants (Mesnard et al., 2006). Therefore the *knk*/*knk* phenotype is distinct from a simple loss of *Nodal* expression.

Finally, histology and gross morphology revealed defective amniotic cavity formation for the majority of *kinked tail* mutant embryos analyzed (Fig. 8). The compromised amniotic cavity suggested that proper VE morphology/function might be playing a role in amniotic cavity formation (Coucouvanis and Martin, 1999).

2.5 MAPPING OF THE *KINKED TAIL* LOCUS

The *kinked tail* mutation arose spontaneously in mice on a C57Bl/6:FVB/N background. Single nucleotide polymorphism (SNP) mapping of affected and unaffected embryos isolated from the backcross of *knk*/+ mice (C57Bl/6J:FVB/N) one generation onto a DBA background was performed by Harvard Partners Center for Genomics and Genetics. SNP mapping revealed that the gene(s) affected by the *kinked tail* mutation occurred on the C57Bl/6 background. Affected (heterozygous) progeny were determined by the presence of a malformed tail. Based on the location of recombination events, the affected interval was narrowed down to a 6.3 Mb region on proximal Chromosome 1 between 37.4 and 43.7 Mb (NCBI build 33) (Fig. 13). Analysis of the most recent NCBI build 37 revealed that within this region there are 48 genes including 5 novel predicted proteins (Table 1). Candidates were further characterized by RT-PCR analysis, with the assumption that the gene(s) affected by the *kinked tail* mutation would be expressed within the embryo at e7.5 due to the observed *knk*/*knk* phenotype (Table 1).

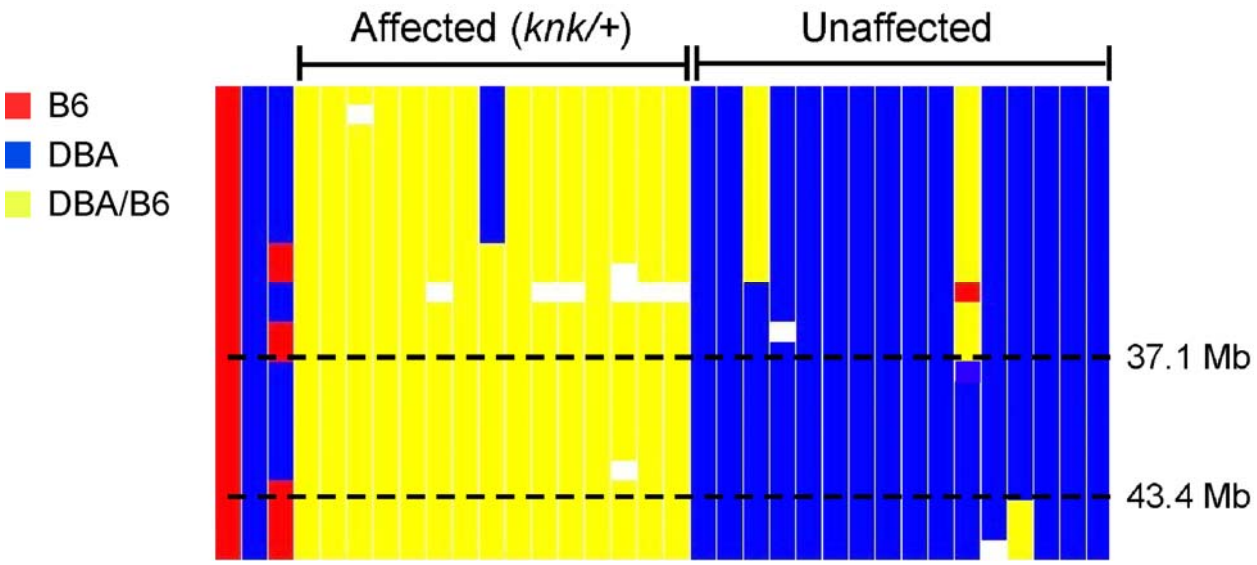

Figure 13: Single nucleotide polymorphism (SNP) mapping of the *knk* affected locus. SNP mapping was performed on affected and unaffected embryos by Harvard Partners Center for Genomics and Genetics. The red represents SNPs unique to the C57Bl/6 background, the blue represents SNPs unique to the DBA background, the yellow represents SNPs shared between both the DBA and C57Bl/6 backgrounds and the white represents misreads. The *knk* mutation was found to be on proximal Chromosome 1 between 37.1 and 43.4 Mb, based on a region of unique SNPs to the affected versus unaffected embryos.

Kinked tail candidates: proximal chromosome 1 from 37.1-43.4 Mbp (Build 37)

Gene name	RT-PCR SW e7.5	Gene Description
Aff3	+	AF4/FMR2 family, member 3; transcription factor activity; lymphoid development
D1Bwg0212e	ND	DNA segment; uncharacterized protein
Inpp4a	NT	inositol polyphosphate-4-phosphatase, type I; "weeble" mice; regulates cell growth; neuronal
Il1r1	ND[1]	interleukin 1 receptor, type I; mouse mutant defective immune response
Il1r2	ND	interleukin 1 receptor, type II
Idd26	NT	insulin dependent diabetes susceptibility 26
Il1rl1	ND[2]	interleukin 1 receptor-like 1; mouse mutant defective immune response
Npas2	+	neuronal PAS domain protein 2; circadian sleep/wake cycle; mutants have sleeping problems
Slc9a2	*	solute carrier family 9, member 2; mutants have gastric secretion problems
Slc9a4	+	solute carrier family 9, member 4; mutants have gastric problems
Dbsty1	NT	diabesity 1
Pou3f3	+	POU domain transcription factor; initiate migration in neural cells; mutants lethal 36hrs PN brain defects
1500015O10Rik	ND	RIKEN cDNA 1500015O10 gene; esophagael cancer-related gene
8430432A02Rik	ND	RIKEN cDNA 8430432A02 gene
Cnga3	NT	cyclic nucleotide gated channel alpha 3; mutants have a loss of cone photoreceptor cells
Gpr45	ND	G protein-coupled receptor 45
Il18r1	ND	interleukin 18 receptor 1; mutants have defective immune response
Lyg1	NT	lysozyme G-like 1
Map4k4	+	mitogen-activated protein kinase kinase kinase kinase 4; NIK; mutants embryonic lethal
Mitd1	NT	MIT, microtubule interacting and transport, domain containing 1
Mrpl30	NT	mitochondrial ribosomal protein L30
Nck2	+	non-catalytic region of tyrosine kinase adaptor protein 2; no mutant phenotype; role in cell migration
Rev1	+	REV1 homolog (*S. cerevisiae*); DNA repair
Tbc1d8	+	TBC1 domain family, member 8; integral to membrane
Tsga10	NT	testis specific 10; required for sperm tail sheath formation
Unc50	NT	unc-50 homolog (*C. elegans*)
2610017I09Rik	ND	RIKEN cDNA 2610017I09 gene
AI597479	ND	expressed sequence AI597479

Chst10	+	carbohydrate sulfotransferase 10; mutants have altered learning
Creg2	**	cellular repressor of E1A-stimulated genes 2; novel neuronal ECM secreted glycoprotein
Eif5b	+	eukaryotic translation initiation factor 5B; implicated in joining ribosomal subunits
Fhl2	ND	four and a half LIM domains 2; mutants have no phenotype
Il18rap	ND	interleukin 18 receptor accessory protein; -/- defective immune response
Il1rl2	+	interleukin 1 receptor-like 2
Lipt1	NT	lipoyltransferase 1
Lonrf2	ND	LON peptidase N-terminal domain and ring finger 2; thioredoxin related
Lyg2	ND	lysozyme G-like 2
Mfsd9	NT	major facilitator superfamily domain containing 9
Mgat4a	NT	mannoside acetylglucosaminyltransferase 4, isoenzyme A; affects growth/size, liver
Mrps9	ND	mitochondrial ribosomal protein S9
Nms	**	neuromedin S; GPCR
Pdcl3	+	phosducin-like 3; apoptosis; phototransduction
Rfx8	NT	regulatory factor X 8
Rnf149	+	ring finger protein 149; zinc finger; ring domain (ubiquitin ligase?); proteolysis
Rpl31	+	ribosomal protein L31; protein biosynthesis
Snord89	NT	small nucleolar RNA, C/D box 89
Tgfbrap1	+	transforming growth factor, beta receptor associated protein 1
Tmem182	+	transmembrane protein 182

+ RT-PCR positive

[1] published e3.5 ICM and e4.0 by RT-PCR

[2] published e9.5 RNase protection

ND not determined

NT not tried

Table 1: *Kinked tail* candidates on proximal Chromosome 1: Within this region there are 48 genes, potential candidate genes are highlighted in yellow, dark yellow represents higher interest candidates and light yellow represents lower interest candidates. Candidate analysis can be found in section 2.5.1. RT-PCR was performed in wildtype e7.5 Swiss Webster (SW) embryos to determine whether the genes were expressed. "+" indicates the

presence of the gene in SW embryos by RT-PCR. ND indicates that RT-PCR was not successful due to technical difficulties or the gene was not present in SW e7.5 embryos. NT indicates that RT-PCR was not attempted due to new build data. "*" indicates that RT-PCR detected the presence of the gene in adult intestines, but not e7.5 SW embryos. "" indicates that RT-PCR detected the presence of the gene in adult brain, but not in SW e7.5 embryos.**

2.5.1 Mapping candidate analysis

Preliminary examination of two potential candidates (chosen based on their phenotypes and expression domains) *NIK* and *Chst10* by WISH was performed to identify if there were any differences between normal and *knk*/*knk* embryos (Table1, yellow highlight) (see Section 2.5.2 for in depth candidate discussion). WISH of e7.5 embryos revealed ubiquitous *NIK* expression throughout the embryo proper in both normal and *knk/knk* mutants (Fig. 14, n=1 *knk*/*knk*). *Chst10* WISH in e7.5 normal and *knk/knk* embryos revealed expression between the embryonic ectoderm and embryonic VE in normal embryos and no expression in the *knk/knk* mutants (Fig. 14, n=2 *knk*/*knk*).

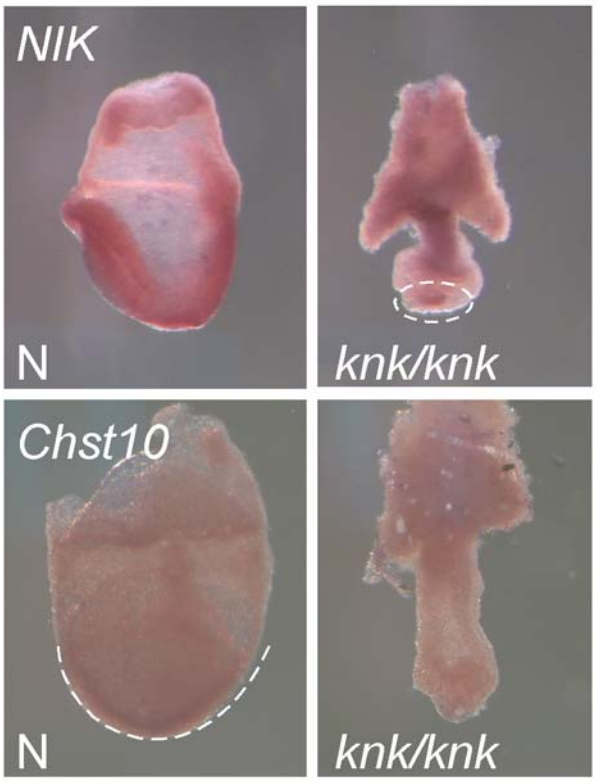

Figure 14: *Kinked tail* candidate gene expression. At e7.5, *NIK* appears to be expressed ubiquitously throughout the embryonic portion of the normal (N) embryos. The *knk*/*knk* embryo analyzed also expresses

***NIK* in the presumptive embryonic region (dashed circle, *NIK* panel). *Chst10* is expressed in the region between the embryonic visceral endoderm and ectoderm (above white dashed arc) in the normal e7.5 embryos, however it is completely absent in the *knk*/*knk* mutants (*Chst10* panel).**

2.5.2 Discussion of candidate genes

Further mapping will be needed to refine the region affected by the *kinked tail* mutation. In the simplest scenario, the affected gene(s) would be expressed during embryonic development perhaps in the VE and later in the notochord. However, as the nature of the mutation is not known other scenarios are possible. It is possible that a multigenic region, rather than a single gene, is lost due to the spontaneous *kinked tail* mutation that could generate many unrelated phenotypes in heterozygous and mutant embryos. Alternatively, the mutation could have generated a loss-of-function, a gain-of-function or a neomorphic allele making candidate and phenotypic analysis difficult to interpret. Finally, chromosomal alterations might have also occurred such as chromosomal duplications or inversions as a result of the *kinked tail* mutation. It is also important to note that the mapping interval is also based on data obtained from unaffected progeny that could cause a problem if there is incomplete penetrance of the mutation.

Within this region there are three interesting candidates. The first candidate is *NIK*, the mammalian homolog of *Drosophila Misshapen*, a Map kinase kinase kinase kinase (Map4k4) that is ubiquitously expressed at e7.5 and e8.5. However earlier expression has not been investigated (Xue et al., 2001). The knock out embryos die ~e9.5-e10.5 due to a failure of mesoderm and endoderm cells to migrate to their correct location (Xue et al., 2001). Based on my studies of the *knk/knk* embryos and migration, this migration defect makes *NIK* an interesting candidate. However, I did not observe a loss of *NIK* transcript expression in *kinked tail* mutants,

but this does not rule out other types of mutations since the nature of the *knk* mutation is still unknown. *NIK's* candidacy was further supported by the discovery of p38-Interacting Protein (p38-IP) in a forward ENU mutagenesis screen. p38-IP interacts with p38, a MAP kinase, downstream of NIK. A mutation in p38-IP results in gastrulation defects. Specifically, the mutants fail to down-regulate E-cadherin, which is an essential event for the migration of mesoderm through the primitive streak (Zohn et al., 2006). This failure prevents mesoderm from migrating, resulting in an accumulation of mesodermal cells in the embryo later leading to lethality (Zohn et al., 2006). Interestingly, these p38-IP mutants look very similar to the few *knk/knk* mutants that survive to e8.5.

The second candidate is *Chst10* (*Hnk-1ST*), carbohydrate sulfotransferase 10. Sulfotransferases add sulfate groups to carbohydrate moieties and this modification is necessary for cell adhesion. *Chst10* plays a role in cell-cell and cell-substratum interactions and is the sulfotransferase responsible for the formation of the cell surface carbohydrate, HNK-1, which is found on many migrating neural cells (Ong et al., 1998). Interestingly, HNK-1 on small cerebellar neurons binds the laminin α1 chain. When binding is prevented using HNK-1 monoclonal antibodies, cell adhesion to laminin is partially ablated (Hall et al., 1995; Hall et al., 1997). Expression analyses of murine *Chst10* have not been published. However my WISH data of e7.5 normal embryos revealed *Chst10* expression between the embryonic ectoderm and embryonic VE, which is lost in *knk*/*knk* mutants. This expression domain is interesting because it colocalizes with laminin expression, including laminin α1, both spatially and temporally. Since *Chst10* appears to be absent in the *knk/knk* mutants then the possibility arises that VE cells may not be properly modified with HNK-1 and cell migration would be defective. However, it is unknown whether VE cells are modified with HNK-1. If HNK-1 is expressed on migrating VE

cells, then it is possible that defective modification or formation of HNK-1 caused by mutations in *Chst10* could therefore adversely affect the ability of those cells to migrate, compounded by the laminin deposition defects I observed in the *knk*/*knk* mutant embryos.

The third candidate is *Nck2*, an adaptor protein containing three SH3 domains and one SH2 domain. Nck proteins play a role in coordinating many signaling pathways, including those involved with cell adhesion (Lehmann et al., 1990). Nck2 was first identified through its association with the LIM4 domain of PINCH, a protein involved in integrin signaling (Tu et al., 1998). It is expressed in two domains: the anterior of the embryo and between the embryonic ectoderm and VE at e7.5. *Nck2* later becomes highly expressed in the mesoderm-derived structures, particularly the notochord. By e10.5, expression is ubiquitous but is strong in the sclerotome compartment of the somites (Bladt et al., 2003). Targeted knockout of *Nck2* causes no observable defects, suggesting that Nck1 (the other murine Nck protein) is able to compensate for the loss of Nck2. Double mutants of *Nck1* and *Nck2* are developmentally delayed by e8.5, have malformed and discontinuous notochords as revealed by *shh* WISH and embryonic lethality at e9.5. Furthermore, mouse embryonic fibroblasts derived from *Nck1*/*Nck2* double homozygous mutants have significant defects in their cell motility (Bladt et al., 2003). Responses to Nck are mediated by its binding to Nap1 (Nck-associated protein) within a complex of proteins, which in turn regulates WAVE. WAVE mediates the dynamic changes in the actin cytoskeleton that take place during cell migration. Loss of *Nap1* in mouse embryos results in the loss of both polarized cell morphology and movement of the DVE (Rakeman and Anderson, 2006). Interestingly, the *Drosophila* ortholog of Nck interacts with Misshapen (NIK) (Ruan et al., 1999).

Nck2 is a very strong candidate to be the gene affected by the *kinked tail* mutation. Since Nck2 interacts with the laminin receptor integrin, then mutations in *Nck2* may cause the laminin

deposition defects that I observed in the *knk/knk* mutants due to the loss of integrin signaling (Hamill et al., 2009). The developmental delay and smaller size of *Nck1/Nck2* double mutant embryos at e8.5 is also reminiscent of the *knk* homozygous mutants. However, if *Nck2* is affected by the *knk* mutation, then it is possible that mutated *Nck2* may be functioning as a dominant-negative as phenotypes are only observed in *Nck1*/*Nck2* double mutants. Further support for its candidacy is the absence of DVE movement in the *Nap1* mutant, which also occurs in the *knk/knk* mutant VE. In addition, *Nck2* is expressed in the notochord and sclerotome compartment of the somites, which is the right place to generate some of the observed phenotypes in the *knk*/+ mice. Importantly, the observed notochord defects in the *knk/+* embryos are very similar to those seen in the *Nck1/Nck2* double knockout. Alterations of *Nck2* expression in the notochord or sclerotome could lead to notochord branching or generate aberrant sclerotome formation and subsequent vertebral abnormalities. Interestingly, NCK interacts with NIK (Su et al., 1997), which may explain the seemingly pleiotropic defects caused by the *kinked tail* mutation.

2.6 CONCLUSIONS AND FUTURE PROSPECTUS

2.6.1 Cell-cell adhesion or migration defects in the *knk* heterozygotes

In summary, I hypothesize that the *kinked tail* mutation affects cell migration and/or adhesion. The initial defect in the *knk* heterozygotes appears to be abnormal thickening and branching of the tail notochord, which in turn leads to the vertebral fusions and dysmorphology that generate the *kinked tail* heterozygous phenotype. The failure of notochord cells to migrate or adhere to

one another properly could generate the observed phenotypes including notochord abnormalities and axes truncation. Interestingly, time-lapse microscopy showed that subpopulations of notochord cells actively migrate to the posterior of the embryo to specifically form the tail notochord (Yamanaka et al., 2007). At this point, analysis of notochord cell migration in the *kinked tail* heterozygotes would likely require the ability to genotype the embryos. To assay for improper cell adhesion, histological analyses followed by antibody staining for cell-cell adhesion molecules, such as E-cadherin could also be performed (Sakamoto et al., 2008).

2.6.2 Cell-ECM defects in *knk* heterozygotes

Given the defective laminin deposition observed in the *knk*/*knk* mutants, there could be a similar defect of laminin in the *knk*/+ notochord and surrounding notochordal sheath. While the role of laminin in notochord formation has been difficult to study in the mouse, several zebrafish mutants reveal that laminin is necessary for notochord cell differentiation. Specifically, defective laminin deposition in the notochordal sheath results in a failure of the notochord cells to differentiate and ultimately leads to apoptosis (Parsons et al., 2002). Examination of ECM components such as laminin and collagen IV in the *knk*/+ notochords, might clarify why the notochord is branching and thickening (O'Shea, 1987). s*hh* signaling is also essential for laminin synthesis in the myotomal basement membrane of mice and loss of *shh* results in defective basement membrane assembly (Anderson et al., 2009). It is yet to be determined if *shh* plays a role in laminin synthesis in the notochord, but the *knk*/+ embryos might provide a useful tool for investigating this process. Ectopic *shh* signaling from the branched notochord could also affect sclerotome formation itself, which would later generate vertebral defects. To assay for this, *knk*/+ e12.5 and e13.5 tails could be analyzed for *Pax1* expression via WISH.

2.6.3 Defective morphogenesis in *kinked tail* embryos

The truncated axes in *knk*/+ mice may result from improper mesodermal cell migration. However, examination of mesodermal markers as well as histological analyses in the *kinked tail* heterozygotes is limited by the inability to genotype at this time. An alternative explanation for the truncated axes is excessive cell death in the caudal region or tailbud of heterozygous mice (Shum et al., 1999). Attempts to assay cell death in e7.5 embryos with acridine orange were unsuccessful, therefore future studies could stain for activated Caspase-3, a marker of apoptosis. If cell death is caspase-independent, alternative assays including, TUNEL or LysoTracker Red can be used. Excessive cell death could also contribute to the small size of the *knk*/*knk* mutant embryos. Therefore, cell death is a potential avenue to investigate in both *knk* hetero- and homozygotes, which might be contributing to the *kinked tail* phenotypes.

2.6.4 *knk*/*knk* basement membrane defects

In the *knk/knk* mutants the epiblast is small and grossly disorganized and the DVE cells are specified but do not migrate properly. This defective DVE migration in addition to the severe embryonic dysmorphogenesis results in a failure to establish asymmetric gene expression necessary to pattern the A-P axis, and ultimately gastrulation failure and early embryonic lethality. Improper VE cell migration and/or adhesion are likely to be responsible for the observed phenotypes. While cell-cell adhesion (based on E-Cadherin expression) does not appear to be affected in the *knk*/*knk* embryos, cell-ECM adhesion defects are likely to contribute to the mutant phenotype.

It is possible that the laminin defect observed in the *knk*/*knk* mutant embryos might be a secondary result of basement membrane failure. To address this, other ECM components, such as integrins, nidogen, perlecan, collagen type IV, and hensin could be analyzed in the *knk*/*knk* mutants. *Integrinβ1* null mice display ICM growth retardation resulting in a failure of endodermal and epiblast differentiation, followed by embryonic lethality at approximately e5.0 (Fassler and Meyer, 1995). Based on the similarity between *integrin β1* and *knk*/*knk* phenotypes as well as the close association of integrin with laminin (Tarone et al., 2000), it is possible that integrin expression could be affected in the *knk* homozygous mutants due to the loss of laminin deposition. It is also interesting to note that *integrin β1* null embryoid bodies are marked by a failure of visceral endoderm differentiation (Liu et al., 2009).

Alternatively, laminin defects in the *kinked tail* homozygous mutant might result in aberrant signaling between the VE and embryonic ectoderm accounting for the observed failure in A-P axis establishment. Signaling pathways including TGF-β/Nodal, BMPs and FGFs all play a role in signaling between the VE and embryonic ectoderm. Candidate targets can be analyzed within the *knk*/*knk* embryos to address this possibility (Coucouvanis and Martin, 1999; Li et al., 2004; Costello et al., 2009). Finally, laminin has been shown to cause VE cells to differentiate to a squamous cell morphology in an embryoid body system. This event is critical to DVE migration (Takito and Al-Awqati, 2004). Therefore, defects in laminin deposition might prevent the observed columnar *knk*/*knk* mutant VE cells from adopting the normal squamous cell morphology that is necessary for migration to the presumptive anterior. Interestingly, another ECM protein, hensin, is expressed throughout the VE at e5.0, becoming mostly restricted to the DVE at e5.5, with expression in a variety of tissues at later stages, including the notochord (Takito and Al-Awqati, 2004). Loss of *hensin* in the mouse results in lethality between e4.5 and

e5.5, most likely due to the failure of proper VE cell morphology, similar to that observed from the *laminin γ1* knockout (Smyth et al., 1999). This observation demonstrated that basement membranes are essential during primitive endoderm differentiation. Embryoid body analysis further revealed that hensin induces VE cells to adopt a columnar morphology (Takito and Al-Awqati, 2004). The role of hensin in the *knk*/*knk* mutant embryo has yet to be determined.

2.6.5 Mapping analysis

The fine mapping analysis narrowed the *kinked tail* interval to a relatively reasonable number of genes amenable to cDNA sequencing. These sequences can be examined for polymorphisms in an attempt to identify the gene(s) affected by the mutation. Alternatively, current tools for mapping, including whole genome sequencing, has the capability of determining down to a point mutation the gene(s) affected by the *kinked tail* mutation.

Ideally, the gene(s) affected by the *kinked tail* mutation will be identified through refined mapping. Until then and pending genotyping possibly through the use of SNP's flanking the affected *knk* region, it is possible to use genetics to identify the gene(s) affected by the *knk* mutation. Heterozygous crosses between *knk*/+ and *candidate*/+ mice should yield progeny (*knk*/*candidate*) that are similar in phenotype to *knk*/*knk* mutant embryos. Depending on the level of genetic interaction, I should observe an enhancement of both the *knk*/+ and/or *knk*/*knk* phenotypes, assuming that a parallel pathway has not been affected. For example, if the *knk* mutation is a loss-of-function (LOF) mutation, it would be possible to examine knk^{LOF}/$candidate^{LOF}$ embryos, which should phenocopy the *knk*/*knk* mutant embryos allowing us to determine the gene affected by the mutation. Interestingly, none of the discussed candidate gene mutations, *NIK*, *Nck2* or *Chst10*, exhibit a phenotype when heterozygous (Xue et al., 2001;

Senn et al., 2002; Bladt et al., 2003), allowing for easier analysis to determine the gene(s) affected by the *knk* mutation.

2.6.5.1 Candidate gene analysis

Expression analysis of high potential candidates, *NIK* and *Chst10*, was initially performed via WISH at e7.5. Expression of *Nck2* was not analyzed due to difficulties in producing a useful riboprobe. However, *Nck2* is still an important candidate to analyze further due to its interacting partners and mutant phenotypes (see also Section 2.5.2 for discussion). It is known that *Nck2* is expressed in the notochord (Bladt et al., 2003), however it is unknown if *NIK* or *Chst10* are expressed there. WISH of *NIK*, *Chst10* and *Nck2* in normal and *knk*/+ tails from e12.5 to e13.5 can be performed to answer this question and identify any alterations in notochordal expression in *knk*/+ embryos.

2.6.6 Implications

The *kinked tail* mutation presents an opportunity to answer many basic research and potentially clinical questions. Basic research questions that may be answered using the *knk*/*knk* mutant embryos include addressing A-P axis establishment. There is a large debate as to when initial asymmetries are established within the embryo. It is possible, that the gene(s) affected by the *kinked tail* mutation may play a role in establishing these asymmetries. Additionally, there are many unanswered questions regarding basement membrane formation and the migration of the DVE cells. The *knk*/*knk* mutant could be a tool to study those processes as well.

From a basic research standpoint, little is known about caudal notochord formation. Therefore, identification of the gene(s) affected in the *knk* mutation and the function of the protein encoded by *knk*, may uncover the mechanisms required for proper caudal notochord formation. Interestingly, aside from *Nck2*, none of the other discussed candidates (see Section 2.5.2) within the *kinked tail* region generate a notochord phenotype when they are mutated. Additionally, the *knk*/+ mice could be important in determining the causes of congenital scoliosis (CS). The current mouse model of CS involves the use of carbon monoxide (a teratogen) exposure to the pregnant mice followed by analysis of vertebral abnormalities including hemi-, bar and curved vertebrae in the resulting litters (Farley et al., 2006). The observed vertebral defects in CS are very similar to what is observed in the *knk*/+ tails (Fig. 15). It is estimated that 0.5-1/1,000 births are clinically classified as CS that is based on the presence of vertebral segmentation failure (fused vertebrae), vertebral formation failure (hemivertebrae) and/or a combination of both (Giampietro et al., 2003). It will be very interesting to investigate the role of the gene(s) affected by the *kinked tail* mutation in CS, potentially contributing a novel gene to this growing field of research.

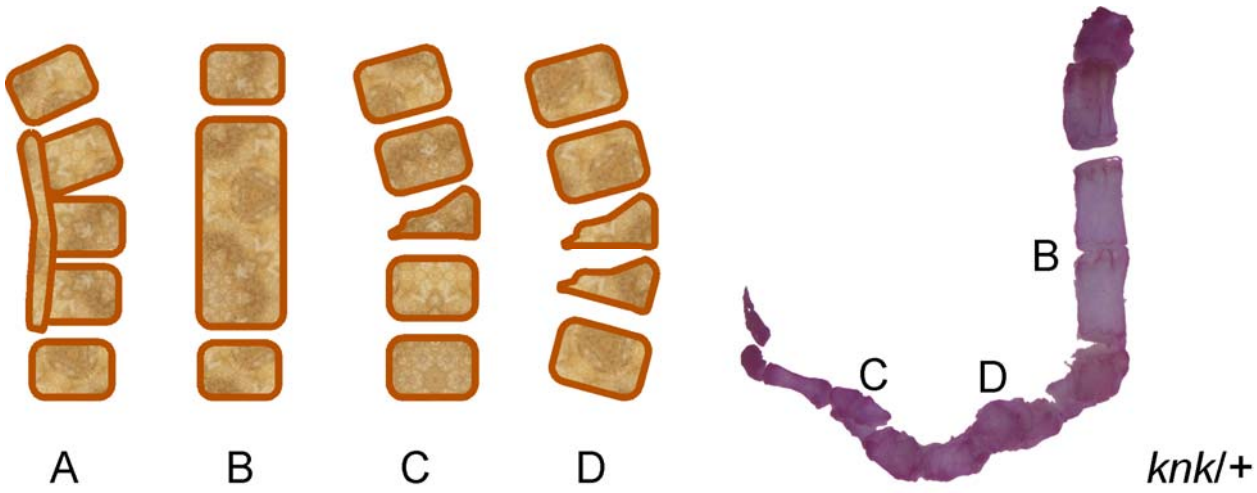

Figure 15: Vertebral defects found in congenital scoliosis. Diagram of the common vertebral malformations found in CS. (A) unsegmented bar vertebrae (B) block vertebrae (C) hemivertebrae (D) wedge vertebrae. Examples of three of the four vertebral abnormalities are observed in this *knk*/+ tail.

3.0 EXAMINATION OF TBX6 PROTEIN STABILITY AND EXPRESSION LEVELS

3.1 INTRODUCTION

3.1.1 T-box family of transcription factors

T-box genes encode a family of transcription factors that are expressed in unique and overlapping embryonic tissues and domains throughout vertebrate development. As transcriptional regulators, these proteins control many developmental processes including cell fate decisions. The T-box family is characterized by the presence of a conserved T-box DNA binding domain, termed the T-domain, and as such all T-box proteins recognize a core 5'-AGGTGT-3' sequence (Naiche et al., 2005). Conservation, however, is limited to the T-domain and therefore regulatory regions are divergent for the different family members. These divergent regions can contribute to their interactions with other proteins, their function as transcriptional activators or repressors, and their stability. Haploinsufficiency for T-box genes results in human diseases including Holt-Oram, Ulnar-mammary and DiGeorge syndromes highlighting the importance of maintaining proper levels of these factors for normal development (Packham and Brook, 2003).

3.1.2 *Brachyury* (*T*) - the founding T-box family member

In 1927, the *Brachyury* or *T* heterozygous phenotype was first described as having an effect on tail length and axial elongation in mice (Dubrovolskaia-Zavadskaia, 1927). *T* is first expressed in the PS at approximately e6.5, the start of gastrulation. *T* expression persists in the PS and later in the tailbud until the tailbud is no longer able to generate mesoderm at e13.5. *T* is also expressed in axial mesoderm, the notochord (Wilkinson et al., 1990). Homozygous loss of *T* results in early embryonic lethality by e10.0 with mesodermal defects including the loss of posterior mesoderm, disorganization of the notochord, and failure to form the allantois resulting in lethality (Gluecksohn-Schoenheimer, 1938; Gluecksohn-Schoenheimer, 1944). Chimeric analyses revealed that *T*/*T* mutant cells cannot exit the PS due to increased cellular adhesion (Wilson et al., 1995). This inability to move away from the streak results in cell accumulation and eventually cell death due to loss of cell attachment, anoikis (Conlon and Smith, 1999). Loss of PS cells leads to the failure of axis extension.

3.1.3 Tbx6 is essential for posterior paraxial mesoderm (PAM) formation and patterning

Tbx6, a T-box transcription factor, is first expressed at e7.0 in the PS and PAM, and later in the tailbud. Expression within the unsegmented presomitic PAM is sharply downregulated as the new somite forms and is no longer found in the tailbud after e12.5 (Chapman et al., 1996). Homozygous loss of *Tbx6* results in the mispatterning of anterior somites, the formation of ectopic neural tubes at the expense of posterior somites, an enlarged tailbud and embryonic lethality by e12.5 (Chapman and Papaioannou, 1998). While the enlarged tailbud does not

result from changes in cell proliferation or death, it is thought that *Tbx6* mutant cells are unable to leave the tailbud due to defective migratory or adhesive properties (Chapman et al., 2003).

3.1.4 Over-expression of *Tbx6* in its endogenous domain generates a short tail phenotype

In an attempt to determine the regulatory regions of *Tbx6*, a transgene was generated that contained the entire coding region of *Tbx6*, including upstream and downstream flanking regions, driving *lacZ* expression. This transgene, *Tg46*, recapitulated the endogenous expression domain of *Tbx6* within the PS and PSM (White et al., 2003; White et al., 2005). Since the transgene contained the entire *Tbx6* coding and regulatory regions necessary for proper expression, it was used for rescue studies. These experiments demonstrated that a single copy of *Tg46* could partially rescue the *Tbx6* mutant phenotype, namely that posterior somites were formed and the tailbud was reduced in size compared to *Tbx6* nulls. However, the somites that formed were improperly patterned. Single-copy *Tg46* rescued embryos were short in stature, due to severe vertebral and rib fusions, and had truncated axes. These experiments in conjunction with WISH revealed that hemizygosity for *Tg46* generated less than heterozygous levels of *Tbx6* (White et al., 2003). Interestingly, wildtype embryos with two copies of the *Tg46* transgene are also short in stature however vertebrae and ribs are properly formed. These *Tg46*/*Tg46* embryos have truncated axes and often end with a filamentous tail, and often die by e18.5 due to unknown causes (Figs. 16 and 23, DLC unpublished). Based on genetic and biochemical data, our laboratory hypothesizes that axial truncation is due to the competition of Tbx6 with T for T downstream targets. The competition would cause a downregulation of T target genes, resulting in phenotypes including small tailbuds and axial truncations, similar to those seen in *T* hetero- and homozygotes (Dubrovolskaia-Zavadskaia, 1927).

3.1.5 Tbx6 hypomorphic allele: rib-vertebrae (rv)

rib-vertebrae (*rv*) is a spontaneous, recessive mutation that results in fusions of posterior ribs and vertebral malformations (Theiler and Varnum, 1985). *rv*/*rv* embryos are recognized by an enlarged and branched tailbud, as well as the formation of ectopic neural tissue in the tail. Vertebral defects are caused by defective somite formation and patterning (Beckers et al., 2000; Nacke et al., 2000). *rv* is a mutation within the regulatory region of *Tbx6*, specifically a duplication from the *Tbx6* coding region that results in overall decreased in *Tbx6* mRNA which generates a hypomorphic allele of *Tbx6* (Watabe-Rudolph et al., 2002; White et al., 2003).

3.1.6 Regulation of Tbx6 at the protein level

In wildtype embryos, Tbx6 protein is expressed in the tailbud and PSM and is sharply downregulated as the new somites form, overlapping with the *Tbx6* mRNA expression domain (White and Chapman, 2005). How this protein expression domain is regulated *in vivo* is not clear. However two studies suggest that it may be through ubiquitin-mediated degradation. Oginuma *et al*. showed that Tbx6 protein but not *Tbx6* mRNA is expanded into the segmented PAM, approximately into the region of the fourth most recently formed somite, in a *Mesp2* knockout embryo. They further showed that the Mesp2-dependent regulation of Tbx6 protein is likely to occur through a proteasome-dependent mechanism, as the expression domain of Tbx6 was expanded anteriorly into the region of the newly forming somites in embryonic tails treated with MG132, a proteasome inhibitor, but not with the vehicle control (Oginuma et al., 2008). These experiments suggested that Tbx6 protein is degraded by the proteasome as the new somite forms. However, the target(s) of Mesp2 signaling that resulted in Tbx6 degradation are

unknown. Examination of the Tbx6 sequence reveals a PEST domain (phosphodegron) within the C-terminal amino acids 320-332 of Tbx6 (PESTfind Analysis). PEST domains are hypothesized to be a signal sequence for degradation by the proteasome (Rogers et al., 1986). Using HEK293 cells and coimmunoprecipitation experiments, Chen *et al*. identified Smurf1 as the E3 ubiquitin ligase that targets mouse Tbx6 for ubiquitin-mediated degradation (Chen et al., 2009). Furthermore, they showed that Smurf1 was recruited to Tbx6 in a Smad6-dependent manner. Smad6 is an inhibitory Smad that functions downstream of BMP signaling. While these experiments showed Tbx6 ubiquitination *in vitro*, there is little to no evidence for Smad6 or BMP expression in an overlapping domain with Tbx6 *in vivo*. Taken together these studies suggest that one level of Tbx6 protein regulation is through ubiquitin-mediated degradation.

It is clear that both under- and over-expression of *Tbx6* has severe consequences on the development and patterning of the embryo (Fig. 16). Homozygous loss of *Tbx6* results in loss of posterior paraxial mesoderm and embryonic lethality. Lower than heterozygous levels of *Tbx6* such as that found in $Tbx6^{rv/rv}$ and *Tg46* rescue embryos result in rib and vertebrae defects caused by somite mispatterning. Finally, over-expression of *Tbx6* found in *Tg46*/*Tg46* embryos results in a shortened axis and a small tailbud. Clearly, the expression levels of Tbx6 mRNA and protein need to be tightly regulated for the embryo to develop properly. Using both *in vitro* and *in vivo* techniques, I examined the relationship between Tbx6 protein regulation and embryonic phenotypes.

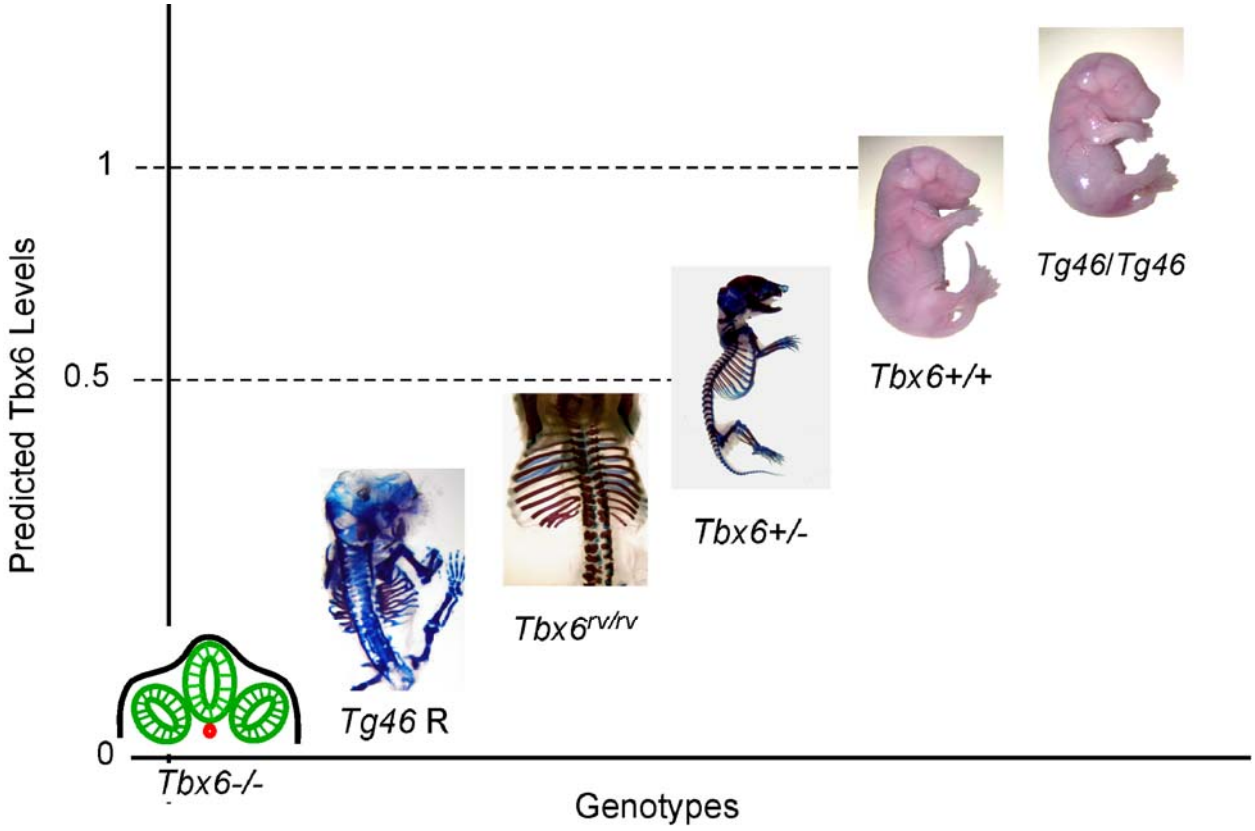

Figure 16: The predicted relationship between Tbx6 protein levels and embryonic phenotypes. Examination of phenotypes from complete loss of *Tbx6* to over-expression of *Tbx6* revealed the relationship between *Tbx6* levels and embryonic phenotypes. The complete loss of *Tbx6* (*Tbx6*-/-) resulted in the loss of posterior PAM, ectopic neural tube formation and embryonic lethality. Hemizygosity for *Tg46* resulted in incomplete rescue in a *Tbx6* -/- background (*Tg46* R) generating severe vertebral and rib malformations. The hypomorphic allele of *Tbx6* (*Tbx6*$^{rv/rv}$) displayed rib and vertebral defects but to a lesser degree than observed in *Tg46*R embryos. *Tbx6*+/- embryos are phenotypically normal as compared to wildtype embryos (*Tbx6*+/+). Over-expression of *Tbx6* in *Tg46*/*Tg46* embryos resulted in loss of tailbud tissue that leads to axial shortening.

3.2 TBX6 PROTEIN STABILITY *IN VITRO*

Using tissue culture cells that were transiently transfected with pCS3-myc-Tbx6, a Tbx6 expression construct that produces a myc-tagged full length Tbx6 protein, I performed a steady state analysis to examine Tbx6 protein stability. COS-7 cells (lacking endogenous Tbx6) were transiently transfected with pCS3-myc-Tbx6 and the cells were cultured either in the presence of DMSO (vehicle control) or MG132. Cells were collected at 0.5, 2, 4, 6, and 24 hours post-treatment and lysates were prepared for Western blot analysis. Western blot analysis revealed that Tbx6 protein levels remained relatively constant when cells were treated with DMSO. However, in the presence of the proteasomal inhibitor MG132, Tbx6 protein appeared to accumulate over time (Fig. 17A). One caveat to the steady state experiment is that MG132 can induce a stress response which needs to be taken into account when interpreting the data (discussed in Section 3.4) (Bush et al., 1997). Quantification of Tbx6 protein levels normalized to tubulin revealed a significant increase by 6 hours post-treatment (Fig. 17B). To verify the experimental design of the *in vitro* steady state assays, I examined the stability of the Notch intracellular domain (NICD), a known target of ubiquitin-mediated degradation (Oberg et al., 2001; Wu et al., 2001). As expected, the NICD protein, which runs as two bands, greatly accumulated in response to MG132 treatment (Fig. 17A). This suggested that like NICD, Tbx6 is a target of proteasome-mediated degradation.

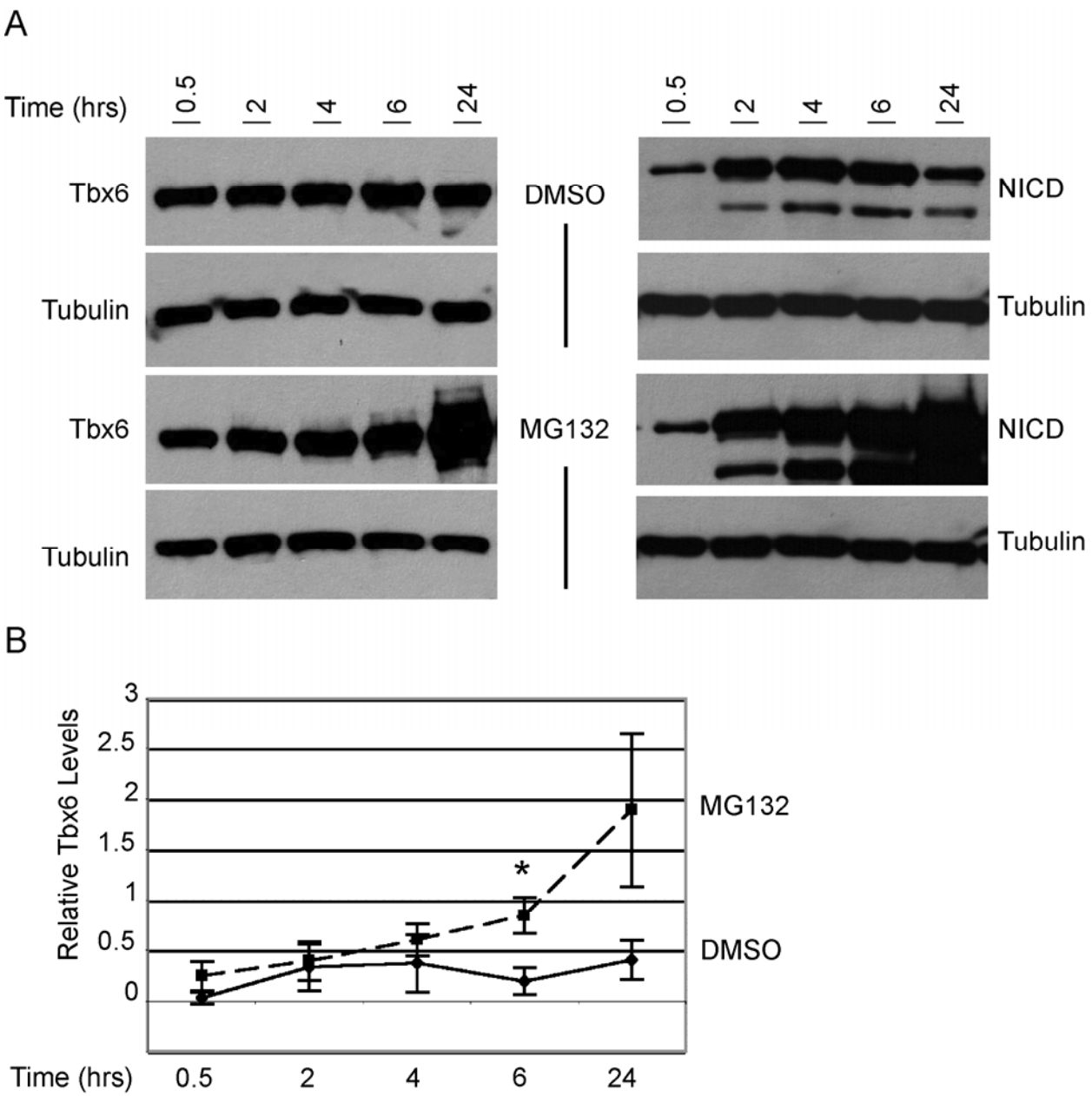

Figure 17: Proteasome inhibition resulted in the accumulation of Tbx6 protein in transfected COS-7 cells. (A) Protein lysates were prepared from COS-7 cells transiently transfected with pCS3-myc-Tbx6 treated with DMSO or MG132 (50 μm), resolved by SDS-PAGE, and subjected to Western blot analysis using anti-myc and anti-tubulin antibodies. During the time period analyzed the level of Tbx6 protein remained relatively stable in the DMSO treated samples as compared to the accumulation of Tbx6 protein in the MG132-treated samples. NICD, a positive control, also accumulated in the presence of MG132 but not in the

presence of DMSO. (B) Western blot data for Tbx6 was quantified using Kodak Image Station software by normalizing the amount of protein per sample to tubulin. Experiments were performed in triplicate. A significant increase of Tbx6 protein levels occurred at 6 hours in MG132 treated samples, DMSO 0.19 ± 0.13; MG132 0.84 ± 0.18 * p=0.04 by Student's t-test. Error bars represents standard error around the mean (SEM).

To investigate the functional consequence of Tbx6 accumulation, I performed standard luciferase assays of similarly transfected cells cultured in the presence of DMSO or MG132. If the population of Tbx6 protein that accumulated in the presence of MG132 was functional, then I would expect an increase of Tbx6 transcriptional activity. To test this hypothesis, increasing amounts of pCS3-myc-Tbx6 were transiently transfected into COS-7 cells along with a *Dll1-msd* reporter luciferase construct, which our laboratory has shown is responsive to Tbx6 (When *et al*, unpublished). Twenty-four hours post-transfection cells were treated with DMSO or MG132, and at 6 hours post-treatment luciferase readings were measured. Tbx6 transcriptional activity at the *Dll1-msd* enhancer was measured as luciferase units and normalized to CMV-Renilla luciferase (a control for transfection efficiency and cell number). These normalized data were again normalized to the empty vector control and presented as relative fold induction. Increasing the concentration of Tbx6 in the presence of DMSO resulted in an expected increase of luciferase activity. In the presence of MG132, there was an even greater increase of Tbx6 transcriptional activity as compared to the DMSO control (Fig. 18). This suggested that upon proteasomal inhibition with MG132 Tbx6 protein accumulated (Fig. 17) and that this population was transcriptionally active (Fig. 18).

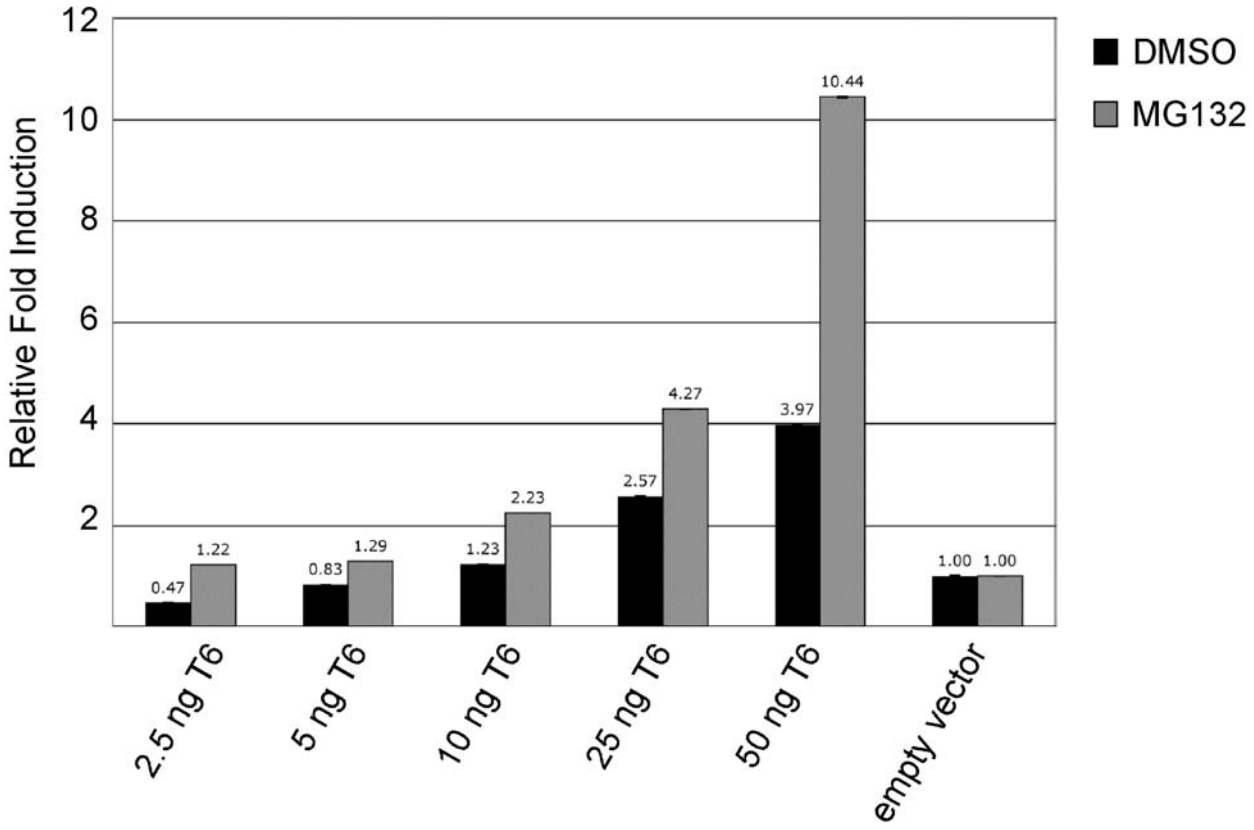

Figure 18: Tbx6 transcriptional activity increased in the presence of MG132. (A) Luciferase assays were performed in triplicate on COS-7 cells transiently transfected with pCS3-myc-Tbx6 and *Dll1-msd* enhancer. Twenty-four hours post-transfection cells were treated with DMSO or MG132 (50 μm). Luciferase activity was determined six hours later. Luciferase readings were normalized to CMV-Renilla and empty vector control. As the concentration of Tbx6 increased, its transcriptional activity at the *Dll1-msd* enhancer also increased. This activity was greatly enhanced in the presence of MG132. Error bars represent SEM.

Taken together, *in vitro* steady state and luciferase assays suggested that Tbx6 protein is targeted for proteasome-mediated degradation and that misregulation of Tbx6 protein turnover could generate excessive Tbx6 activity. To determine the dynamics of Tbx6 turnover, I

performed *in vitro* cycloheximide chase assays. These assays were performed by transiently transfecting COS-7 cells with pCS3-myc-Tbx6 in the presence of vehicle (water) or cycloheximide (CHX). In the presence of vehicle, Tbx6 protein remained relatively stable over the 24-hour time-course, supporting the steady state assays performed over the same time-course (Fig. 19A). In the presence of CHX, a slight decrease in the amount of Tbx6 protein was observed around four hours with a statistically significant decrease to below 50% at 24 hours post-treatment (Fig. 19A,B). These data suggested that *in vitro* Tbx6 protein was degraded with a half-life between 6 and 24 hours.

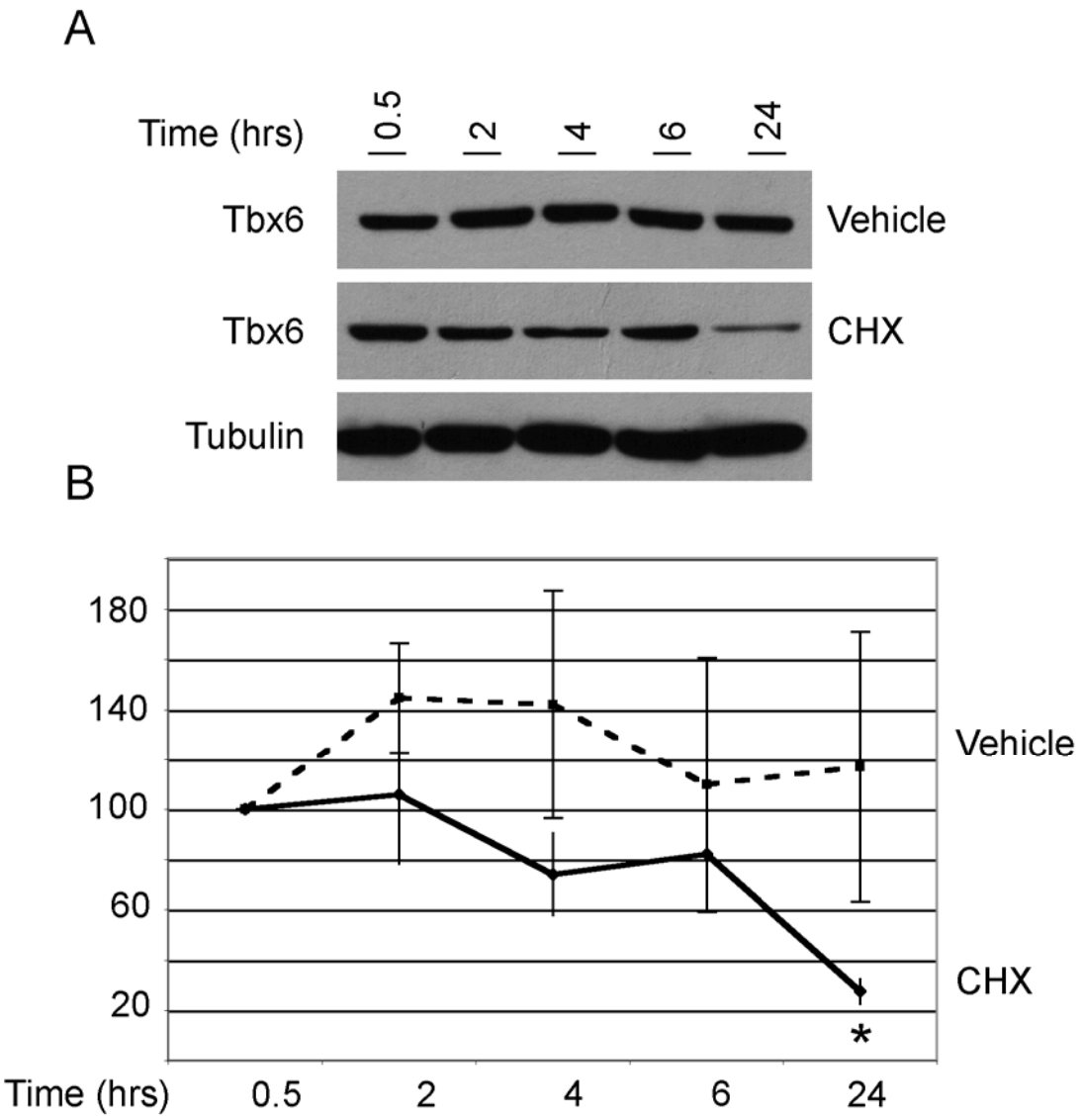

Figure 19: Tbx6 is a relatively stable protein. (A) Protein lysates were prepared from COS-7 cells transiently transfected with pCS3-myc-Tbx6, treated with vehicle (water) or cycloheximide (CHX, 250 μg/ml), resolved by SDS-PAGE, and subjected to Western blot analysis using anti-myc and anti-tubulin antibodies. Tbx6 remained stable in vehicle-treated cells as compared to the CHX-treated cells, where Tbx6 protein levels began to decrease after 4 hours. (B) Western blot data was quantified by normalizing the amount of protein per sample to tubulin and then calculating the relative fold change compared to the 0.5-hour time point. Experiments were performed in triplicate. The level of Tbx6 protein was significantly

reduced by 24 hours, vehicle 1.17 ± 0.54; CHX 0.25 ± 0.05 *p=0.02 by Student's T-test. Error bars represent SEM.

While the CHX experiments revealed that Tbx6 protein was being turned over, perhaps through a proteasome-dependent mechanism, two questions remained. Firstly, the CHX experiments followed two populations of Tbx6 protein, both existing and newly synthesized pools that were unaffected by the low concentration of cycloheximide used. Therefore, it was difficult to determine the actual rate of Tbx6 protein turnover. Secondly, the time-course over which Tbx6 protein was analyzed was missing key time points between 6 and 24 hours. To analyze Tbx6 protein turnover more effectively, pulse-chase analyses were performed using COS-7 cells transiently transfected with pCS3-myc-Tbx6 in the presence of DMSO or MG132. Based on the steady state and CHX assays I predicted that Tbx6 protein would be degraded around 6 hours. Examination of one pool of ^{35}S-labeled Tbx6 protein in DMSO-treated cells revealed that Tbx6 had a half-life of approximately four to six hours *in vitro*. In the presence of MG132, Tbx6 half-life was extended by two hours as compared to the DMSO control (Fig. 20). These data suggested that some component of Tbx6 degradation is a proteasome-dependent process.

Altogether, the *in vitro* steady state, CHX and pulse chase assays revealed that Tbx6 is a relatively stable protein and that Tbx6 protein turnover is in part governed by proteasome-dependent degradation. These experiments gave me a better understanding of how Tbx6 protein might be regulated *in vivo*, thus lending insight to interpretation of phenotypic studies.

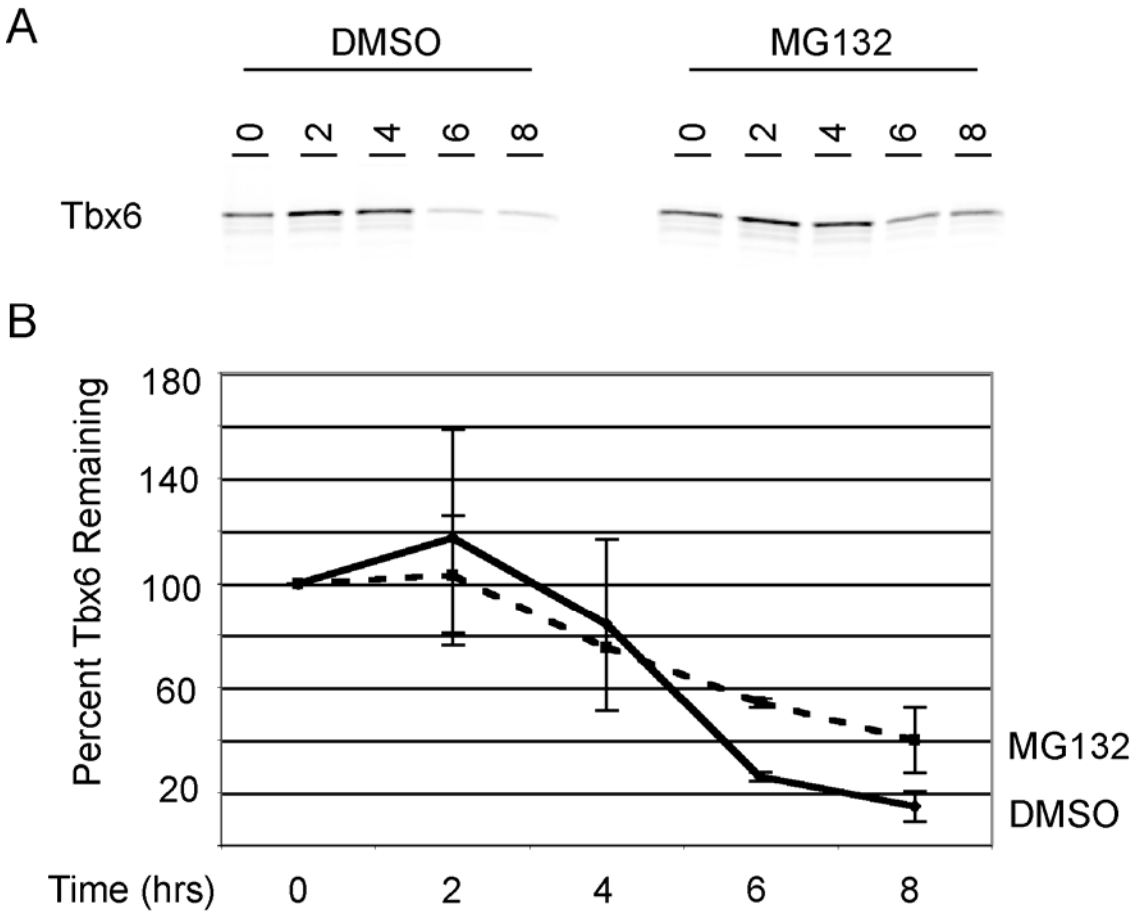

Figure 20: Tbx6 protein half-life was modestly extended in the presence of a proteasomal inhibitor. (A) Protein lysates were prepared from COS-7 cells transiently transfected with pCS3-myc-Tbx6, Tbx6 was immunoprecipitated with an anti-Tbx6 anitbody, labeled with ^{35}S-methionine and ^{35}S-cysteine, treated with DMSO or MG132 (50 μm), resolved by SDS-PAGE, and subjected to Fuji Fluroimager analysis. A labeled population of Tbx6 protein began to decrease after four hours in the DMSO control as compared to eight hours in the MG132-treated samples. (B) Quantification of Fuji imager data, normalized to the 0 hour time point. The half-life of Tbx6 was approximately four to six hours, which was extended by two hours in the MG132-treated samples. These experiments were performed in duplicate. Error bars represent the range of data.

3.3 PHENOTYPIC CONSEQUENCES OF MODULATING TBX6 PROTEIN LEVELS *IN VIVO*

3.3.1 Tbx6 protein levels varied among *Tbx6* under- and over-expressing mouse lines

Examination of the *rib-vertebrae* mouse line revealed decreased *Tbx6* mRNA expression in *Tbx6*$^{rv/rv}$ tails as compared to *Tbx6*$^{rv/+}$ tails (White et al., 2003). This decreased level of *Tbx6* in *Tbx6*$^{rv/rv}$ embryos results in an enlarged, branched tailbud and rib and vertebral fusions (Watabe-Rudolph et al., 2002; White et al., 2003). Conversely, homozygosity for *Tg46*, a transgene that contains the entire coding region of *Tbx6*, results in smaller tailbuds than their hemizygous or wild type littermates (Figs. 22-23). The phenotypic consequences of under- and over-expressing *Tbx6* are obvious. However, Tbx6 protein expression had not been analyzed in either the *Tbx6*$^{rv/rv}$ or *Tg46* embryos. I wanted to determine the amount of Tbx6 protein that was required to generate these phenotypes.

To address this question, I analyzed Tbx6 protein levels in *Tbx6*$^{rv/rv}$, *Tbx6*+/-, and *Tg46*/*Tg46* tailbuds and their respective wildtype background strains. I isolated and pooled e10.5 tailbuds from the various lines and analyzed Tbx6 and actin protein levels by Western blot quantification. This experiment revealed varying Tbx6 protein levels among the different genetic background strains analyzed (Fig. 21A). To quantify relative Tbx6 protein levels among the lines examined, Tbx6 protein amounts were normalized to total actin levels. As predicted, *Tbx6*$^{rv/rv}$ tailbuds contained the lowest amount of Tbx6 protein, followed by a slight increase of relative Tbx6 protein in *Tbx6*+/- tailbuds, and the greatest amount of Tbx6 protein was found in the *Tg46*/*Tg46* tailbuds (Fig. 21B). One caveat to the above experiment is the extremely low actin levels that *Tg46*/*Tg46* Tbx6 protein levels were normalized to. This could result in Tbx6

protein levels that appear significantly higher than they actually are (see Section 3.4 for discussion). Interestingly, there were also varying Tbx6 levels among the different background strains, C57Bl6/J (*Tbx6*$^{rv/rv}$ background strain) had the lowest levels of Tbx6 protein, followed by mixed C57Bl6/J/129SvEv (*Tbx6+/-* background strain) and finally FVB/N (*Tg46*/*Tg46* background strain) had the most Tbx6 protein (Fig. 21B).

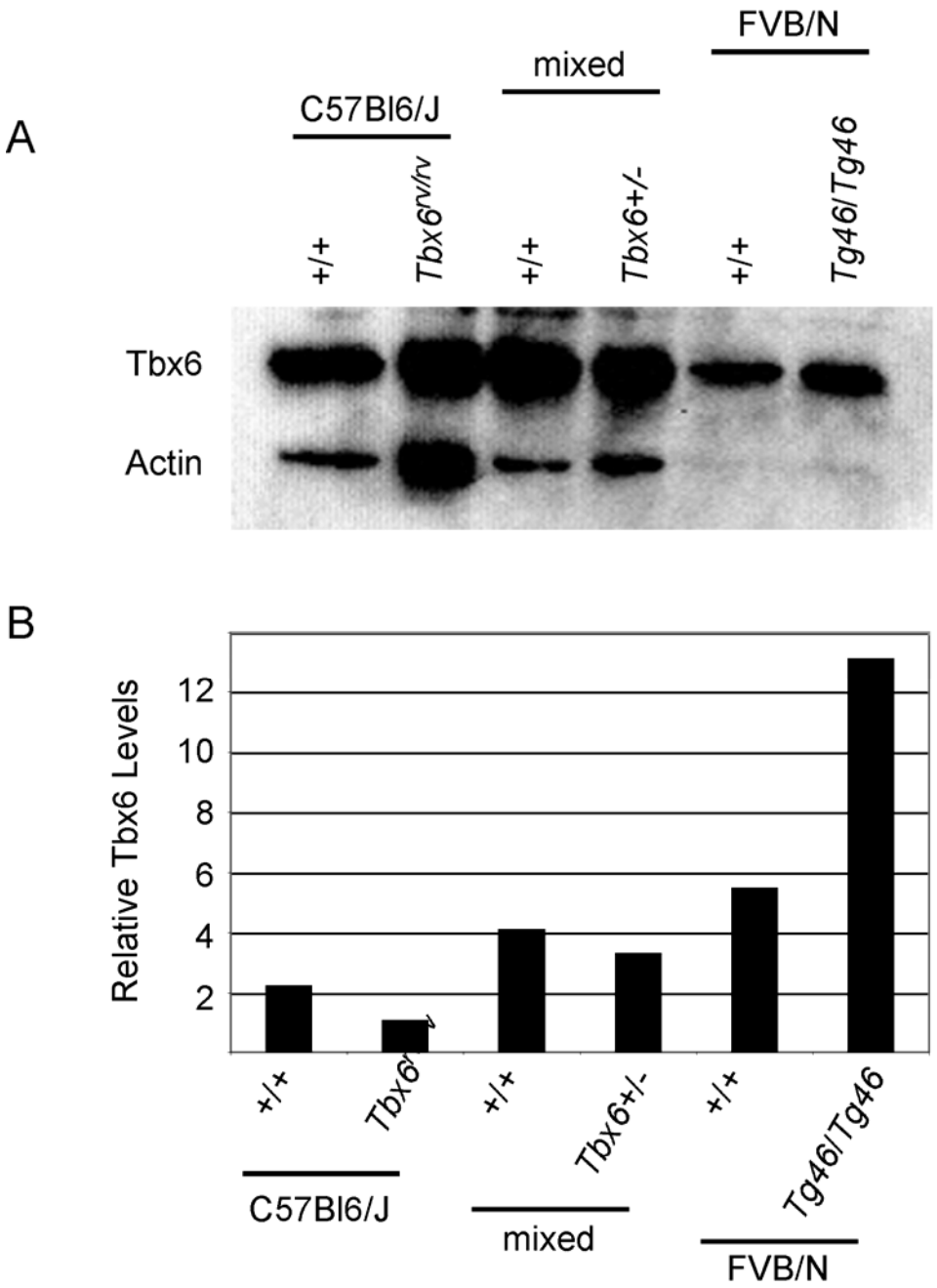
A
FVB/N
mixed
C57Bl6/J
+/+
Tbx6rv/rv
+/+
Tbx6+/-
+/+
Tg46/Tg46
Tbx6
Actin
B
Relative Tbx6 Levels
12
10
8
6
4
2
+/+
Tbx6rv
+/+
Tbx6+/-
+/+
Tg46/Tg46
C57Bl6/J
mixed
FVB/N

Figure 21: Endogenous Tbx6 protein levels varied across genotypes. (A) Protein was isolated from pooled e10.5 tailbuds and subjected to Western blot analysis using anti-Tbx6 and anti-actin antibodies. Varying amounts of Tbx6 protein were found in *Tbx6*$^{rv/rv}$, *Tbx6*+/-, and *Tg46*/*Tg46* lines and in their respective background strains as indicated. (B) Tbx6 protein levels were quantified using Kodak Image Station software and normalized to total actin levels. Increasing amounts of Tbx6 protein were found in the *Tbx6*$^{rv/rv}$, *Tbx6*+/-, *Tg46*/*Tg46* lines as well as their respective background strains.

Western blot data generated from pooled tailbud tissue, suggested that there were increasing amounts of Tbx6 protein from the *Tbx6*^{rv} to *Tg46* lines. I predicted that the relative amount of Tbx6 protein in *Tbx6*$^{rv/rv}$ tailbud tissue would be less that *Tbx6* heterozygotes (Fig. 16) and found there was approximately half as much Tbx6 protein compared to wildtype embryos. Similarly, I predicted that the level of Tbx6 protein found in *Tg46*/*Tg46* tailbud tissue would be above wildtype levels and I found that there was more Tbx6 protein in *Tg46*/*Tg46* tailbuds as compared to wildtype. To confirm total Tbx6 protein levels and localization, I performed whole embryo immunohistochemistry to qualitatively examine Tbx6 protein levels among the genotypes. Although Tbx6 protein appeared to be properly localized in the various genetic strains, different staining intensities were observed. As predicted, staining intensity in *Tbx6*$^{rv/rv}$ tailbuds was less than that observed in *Tbx6*+/- tailbuds, whereas greater staining intensities were observed in *Tg46*/*Tg46* tailbuds as compared to wildtype (Fig. 22). The noticeable absence of Tbx6 staining in the *Tbx6*$^{rv/rv}$ tailbud is neural tissue which does not express Tbx6 (Theiler and Varnum, 1985). In addition, at e9.5 *Tg46*/*Tg46* embryos appeared to express more Tbx6 protein as compared to *Tbx6*$^{rv/rv}$ and *Tbx6*+/- embryos at e10.5 (Fig. 22). In order to make accurate comparisons between *Tbx6*^{rv} and *Tg46*, one would have to perform the immunohistochemistry experiment with e10.5 *Tbx6*$^{rv/rv}$, *Tbx6*+/-, *Tg46*/*Tg46* and their respective wildtype littermates in

the same tube. In the presented data e9.5 *Tg46*/*Tg46* and e10.5 *Tbx6*$^{rv/rv}$, *Tbx6*+/-, and their respective wildtype littermates were tested in the same tube. However, the e10.5 *Tg46*/*Tg46* with its wildtype littermate experiment was performed on a separate date. Comparisons between the wildtype background strains of the examined genotypes showed the same trend that the Western blot data revealed, where the least amount of Tbx6 protein was found in the *Tbx6*$^{rv/rv}$ C57Bl6/J background strain and the greatest amount was expressed in the *Tg46*/*Tg46* FVB/N background strain.

Taken together, both the quantitative Western blot and qualitative immunohistochemistry data suggested that Tbx6 protein expression increased in the different genotypes with the lowest amounts expressed in *Tbx6*$^{rv/rv}$ embryos, followed by *Tbx6*+/-, *Tbx6*+/+, and *Tg46*/*Tg46* embryos, which had the highest level of Tbx6. From these data I were able to determine that approximately half as much protein compared to the heterozygous levels of Tbx6 protein resulted in an enlarged tailbud as seen in *Tbx6*$^{rv/rv}$ tailbuds. The reduced levels of Tbx6 protein appeared throughout the enlarged tailbud of *Tbx6*$^{rv/rv}$ tailbuds, except for in the ectopic neural tissue. Conversely, an increased amount of staining compared to wildtype was observed in *Tg46*/*Tg46* tailbuds. The observed increase of Tbx6 protein appeared throughout the reduced tailbud of the *Tg46*/*Tg46* embryos, suggesting that even though there are fewer cells within the *Tg46*/*Tg46* tailbud they express greater levels of Tbx6 as compared to wildtype tailbuds.

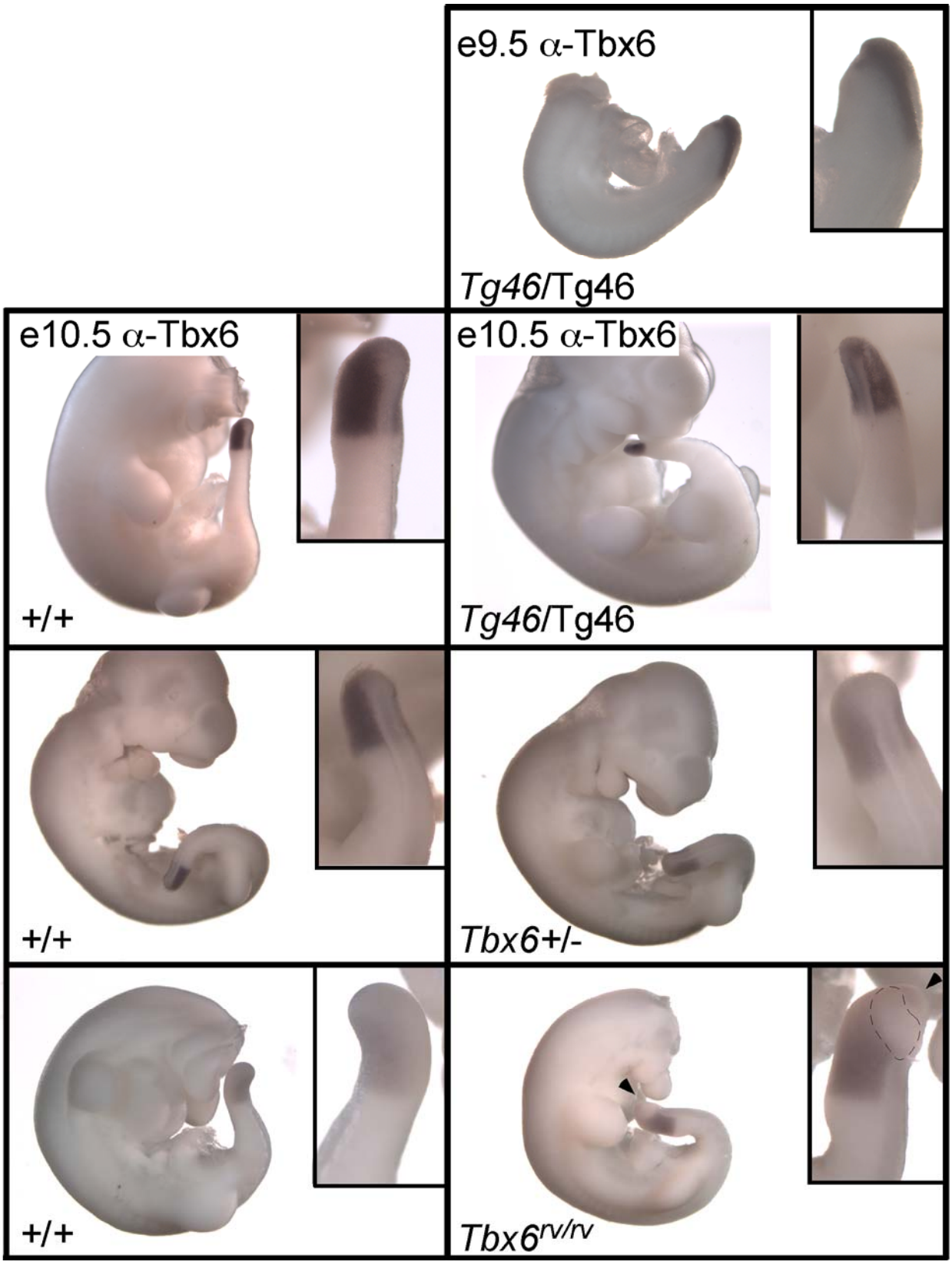
e9.5 α-Tbx6
Tg46/Tg46
e10.5 α-Tbx6
+/+
e10.5 α-Tbx6
Tg46/Tg46
+/+
Tbx6+/-
+/+
Tbx6rv/rv

Figure 22: Endogenous Tbx6 protein expression varied across genotypes. e9.5 and e10.5 embryos were analyzed by immunohistochemistry for Tbx6 protein expression. Overall the expression domain of Tbx6, within the tailbud and PSM, remained the same across genotypes. However tailbud morphology was affected. *Tg46*/*Tg46* e9.5 and e10.5 embryos had small tailbuds and expressed increased levels Tbx6 protein as compared to *Tbx6*+/- e10.5 embryos. e10.5 *Tbx6*$^{rv/rv}$ embryos have enlarged tailbuds and expressed the least amount of Tbx6 protein as compared to *Tbx6*+/- and *Tbx6*+/+ tailbuds. Absence of Tbx6 staining in the *Tbx6*$^{rv/rv}$ tailbud (black arrowhead and dashed outline) was neural tissue.

I have previously shown that increasing the amount of Tbx6 protein using MG132 in tissue culture cells increases the amount of Tbx6 protein that is functional based on luciferase assays (Fig. 18). I have also observed variable levels of Tbx6 protein in *Tbx6*$^{rv/rv}$, *Tbx6*+/-, *Tg46*/*Tg46*, and wildtype embryos. Since varying Tbx6 protein levels in embryos is sufficient to generate phenotypes, I hypothesized that Tbx6 downstream targets may be affected. Tbx6 is a transcriptional activator therefore target genes may be under- (*Tbx6*$^{rv/rv}$) or over-expressed (*Tg46*/*Tg46*) in our various *Tbx6* mutants and transgenic lines. In an attempt to correlate the increased amount of Tbx6 protein expressed within the *Tg46* line with the observed phenotype, I analyzed Tbx6 downstream targets *Dll1* and *Ripply2* in *Tg46*/*Tg46* e10.5 embryos. *Dll1* is expressed in and overlapping expression domain with *Tbx6* and the caudal halves of the somites (Bettenhausen et al., 1995). WISH of *Dll1* revealed no obvious differences between wildtype and *Tg46*/*Tg46* embryos in the expected expression domain within the PSM and tailbud (Fig. 23, *Dll1* panel). *Ripply2* has a dynamic expression profile and is found expressed either as a single strong stripe or as two weaker stripes within the anterior PSM in wildtype embryos (Biris et al., 2007). In *Tg46*/*Tg46* embryos *Ripply2* was expressed in a slightly more diffuse stripe as compared to the more defined stripe seen in the wildtype embryo (Fig. 23, *Ripply2* panel). Despite the clear over-expression of Tbx6 protein in *Tg46*/*Tg46* embryos (Figs. 21-22), there

was no significant up- or misregulation of these two Tbx6 downstream targets based on WISH data. These data suggest that additional factors are required for expression of *Dll1* and *Ripply2,* and that perhaps expression of these other factors may need to be upregulated to generate obvious differences in target gene expression. For example, both Tbx6 and β-catenin are required for *Dll1* (Hofmann et al., 2004) and Wnt and Mesp2 are required for *Ripply2* regulation (Biris et al., 2007; Morimoto et al., 2007; Dunty et al., 2008).

Figure 23: No discernable differences in Tbx6 downstream target gene expression. Expression of Tbx6 downstream targets, *Dll1* and *Ripply2,* was unaffected in e10.5 *Tg46*/*Tg46* embryos. *Dll1* was expressed in the PSM and tailbud at approximately equivalent levels in both wildtype (+/+) and *Tg46*/*Tg46* embryos. *Dll1* is also seen in the caudal half of the somite in *Tg46*/*Tg46* embryos. Note smaller tailbud in *Tg46*/*Tg46* (*Dll1* panel). *Ripply2* had a slightly broader expression domain in the *Tg46*/*Tg46* embryo as compared to wildtype. The white dotted line outlines the *Tg46*/*Tg46* tailbud (*Ripply2* panel).

3.3.2 3-component embryos misexpress Tbx6

The lower than wildtype levels of Tbx6 protein in its endogenous domain in *Tbx6*$^{rv/rv}$ embryos resulted in rib and vertebral fusions and an enlarged tailbud. Increased levels of Tbx6 protein relative to wildtype in *Tg46*/*Tg46* embryos resulted in smaller tailbuds. To clarify the role of Tbx6 protein levels *in vivo* as well as to determine the consequences of Tbx6 misexpression, I utilized a 3-component transgenic system. Briefly, the 3-component system allows spatial control through the use of a tissue specific *Cre recombinase* transgenic line. It also allows temporal control through another transgenic line consisting of a reverse tetracycline-transactivator (rtTA) inserted at the ubiquitous *ROSA26* locus downstream of a floxed stop of transcription cassette (Belteki et al., 2005). Upon addition of doxycycline (DOX) to the water of pregnant females, *rtTA* will activate transcription at the tetracycline responsive element (TRE) upstream of *myc-Tbx6*, the third component of the system (Fig. 24). Using this technique, I misexpressed myc-tagged Tbx6 protein in the *T* expression domain (*T-Cre)*, as well as in its downstream mesodermal derivatives including paraxial, intermediate and lateral mesoderm (Perantoni et al., 2005). I hypothesized that misexpressing *Tbx6* within the *T* expression domain, would result in the competition of Tbx6 with T, resulting in a smaller tailbud/axial shortening similar to *T*/+ phenotypes.

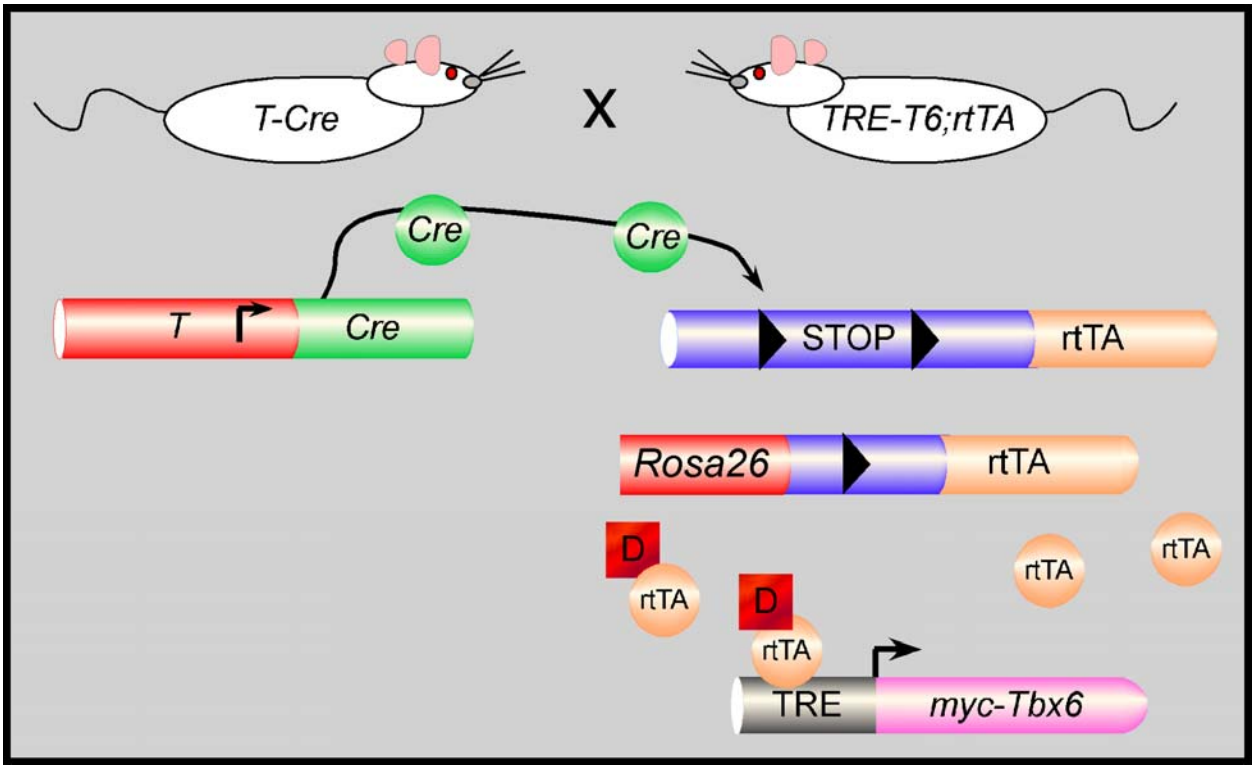

Figure 24: Diagram of the 3-component transgenic system. *T-Cre* transgenic mice were mated to *TRE-myc-Tbx6+/-;rtTA/rtTA* transgenic mice to generate 3-component embryos that misexpress full-length myc-tagged Tbx6 in the *T-Cre* expression domain and in cells derived from this population upon the addition of doxycycline (D) to the pregnant females' drinking water.

To verify the published *T-Cre* expression domain, I crossed *T-Cre*/*T-Cre* mice with *ROSA26-lacZ*/*ROSA26-lacZ* Cre mice in which *lacZ* is silenced until removal of the floxed stop of transcription by Cre recombinase, generating 2-component embryos (Soriano, 1999). 2-component embryos isolated and stained for β-galactosidase activity revealed mosaic staining within the expected mesodermal derivatives and a high degree of variability between littermates (Fig. 25). At e10.5, β-galactosidase activity appeared to be the highest in the heart and forelimb, with one littermate showing β-galactosidase staining throughout the embryo (Fig. 25, e10.5

panel). At e12.5, the variability was more evident among littermates, with some embryos showing restricted β-galactosidase activity within the limbs and PSM, and others exhibiting a more ubiquitous staining pattern (Fig. 25, e12.5 panel). The observed staining patterns differed from previously published data possibly due to the differences in staining times.

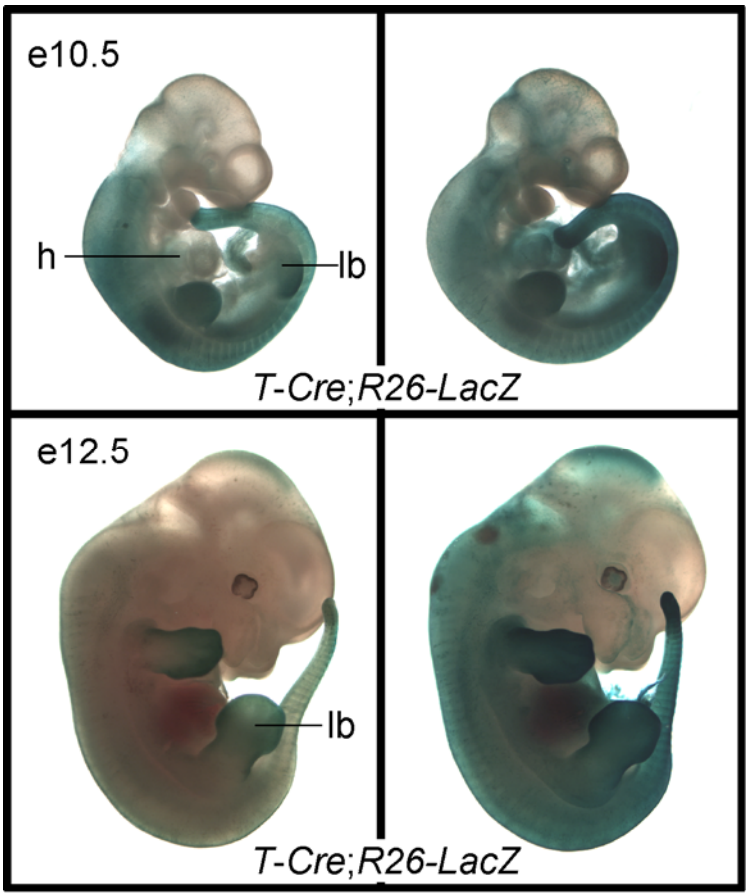

Figure 25: β-galactosidase expression in *T-Cre;R26-LacZ* 2-component embryos was mosaic and variable. Embryos that expressed *LacZ* in the *T-Cre* expression domain were stained for β-galactosidase activity. At e10.5, variable β-galactosidase staining was found within mesodermal derivatives, including a high degree of staining in the limb buds (lb), heart (h) and PSM (e10.5 panel). At e12.5, littermates continued to exhibit highly variable β-galactosidase staining, with increased staining within the limb buds and PSM (e12.5 panel). Abbreviations: limb buds (lb); heart (h).

Despite the variability of the *T-Cre* line, I generated 3-component embryos that misexpress myc-Tbx6 in the domain defined by this β-galactosidase staining pattern and examined the resulting phenotypes. DOX was administered to the pregnant females in their drinking water at e7.5 and timed dissections were performed. To verify that *Tbx6* was misexpressed in the 3-component system, I visualized *Tbx6* mRNA and protein expression at e10.5. *Tbx6* mRNA was mosaically expressed with the highest levels of *Tbx6* found within the limb buds and the heart (Fig. 26A). As expected from the β-galactosidase results, there was a high degree of variability between embryos even within a litter. Tbx6 protein was expressed within the PSM and the tailbud in control embryos, as well as the heart and distinct regions of the forelimb bud in 3-component embryos (Fig. 26B). Interestingly, Tbx6 protein expression did not appear as widespread as mRNA, perhaps due to the detection limits of this technique. Since the PSM and tailbud is expected to express both endogenous and ectopic *Tbx6* it is not possible to determine the amount of ectopic *Tbx6* in those regions by whole mount antibody staining.

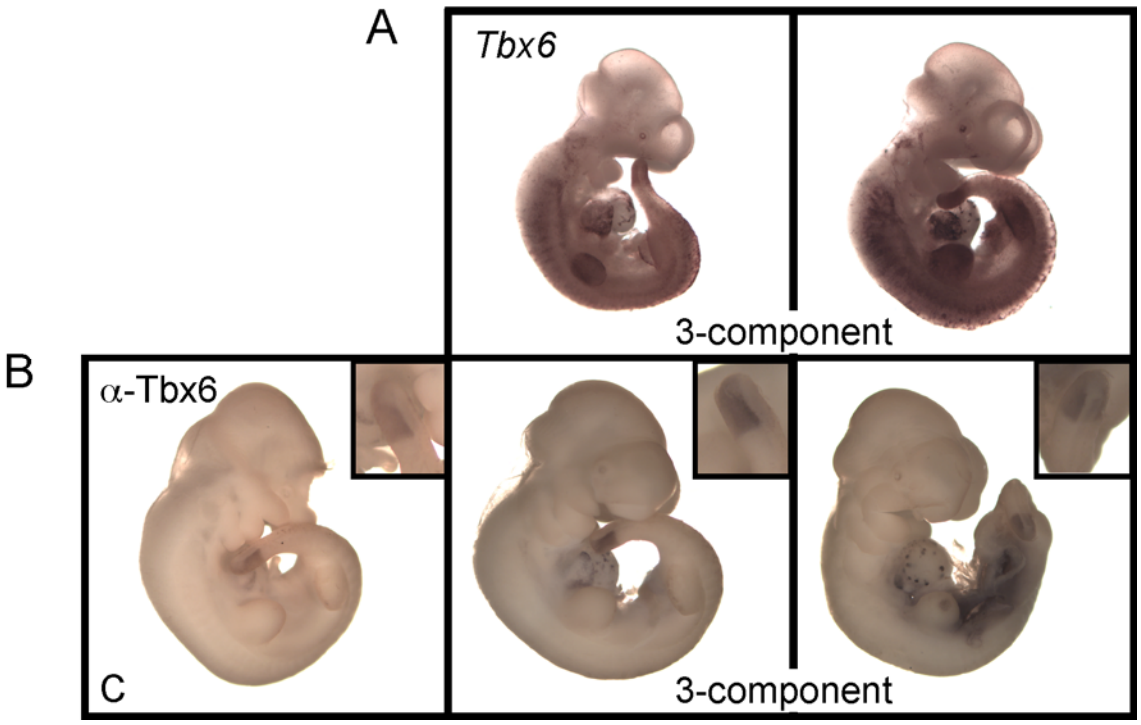

Figure 26: Tbx6 localization in *T-Cre* 3-component embryos. (A) WISH of *Tbx6* mRNA in e10.5 3-component embryos revealed mosaic and variable *Tbx6* expression throughout mesodermal derivatives, with higher expression in the forelimb and heart (*Tbx6* panel). (B) Tbx6 protein was expressed in its endogenous domain, as well as in the heart and regions of the forelimb in 3-component embryos as compared to control (C) embryos (α-Tbx6 panel).

Analysis of Tbx6 mRNA and protein revealed that the 3-component system results in variable expression of ectopic Tbx6. The variability made it difficult to analyze potential phenotypes. I predicted that if ectopic Tbx6 competes with T, I should have seen a smaller tailbud similar to *Tg46* homozygotes and *T* heterozygotes (Fig. 22). However, I did not observe any tailbud phenotypes in the 3-component embryos. To further confirm that the tailbud was unaffected in the 3-component embryos, I analyzed the expression of tailbud specific markers, *T* and *Fgf8* by WISH (Kispert and Herrmann, 1994; Crossley and Martin, 1995). There were no

detectable differences in *T* or *Fgf8* expression between control and 3-component embryos (data not shown), supporting that *T-Cre* 3-component embryos did not have tailbud phenotypes.

While no tailbud phenotypes resulted from ectopic myc-Tbx6 expression, heart and hindlimb abnormalities were observed (data not shown). To determine if there were any skeletal phenotypes associated with 3-component embryos, I analyzed a skeletal preparation of an e13.5 embryo. Only one 3-component embryo survived to e13.5; by e13.5, 3-component littermate embryos were often edemic and lacked beating hearts. Both the edema and death are likely attributed to the severe heart defects observed. The surviving 3-component embryo lost the distal ribs, had severe malformation of the proximal ribs, fusions of the axis and atlas, a hole in the scapula, and malformed fore- and hindlimbs. However, the body axis was fully extended (Fig. 27). Since a functional PS and tailbud are required for axis elongation, the fully extended axis of 3-component embryos supports the absence of overt tailbud phenotypes. These data revealed that Tbx6 misexpression in the PAM and lateral mesoderm caused vertebral and limb malformations, similar to those seen using a *Dll1-msd-Cre* transgenic line which drives expression in the PAM and lateral plate mesoderm (When and Chapman, submitted unpublished).

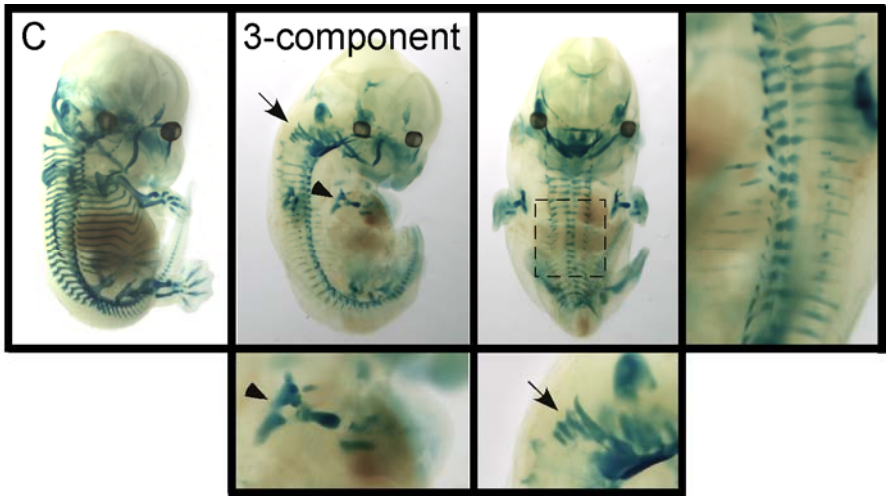

Figure 27: Skeletal defects of a *T-Cre* 3-component embryo. An e13.5 control (C) and 3-component embryo were stained with alcian blue to visualize the cartilaginous skeleton. The surviving 3-component embryo exhibited vertebral malformations including loss of distal ribs, severe malformation of proximal ribs (boxed region), a hole in the scapula (arrowhead), fusions of the atlas and axis (arrow), and fore- and hindlimb abnormalities. Lower panels are higher magnifications of the scapula and atlas and axis defects.

To determine why overt tailbud phenotypes were not observed in the 3-component embryos, I isolated and pooled e10.5 tailbud, somites S1-4 where S1 is the most newly formed somite, and limb bud tissue from 3-component embryos. To compare protein levels between tissues, protein extracts were analyzed for endogenous and ectopic Tbx6 expression. Western blot analysis revealed that ectopic myc-Tbx6 was expressed at relatively low levels within the tailbud, at higher levels in the somitic tissue and at the highest level in the limbbud (Fig. 28A). Quantification of Tbx6 levels normalized to actin indicated that the tailbud contained about half as much ectopic protein as compared to endogenous protein (Fig. 28B). These data suggested that the levels of ectopic Tbx6 expressed in the tailbuds of 3-component embryos were not high enough or myc-Tbx6 was not expressed in enough cells to result in tailbud phenotypes.

Alternatively, the tailbud may be refractory to increased levels of Tbx6 and as such may not be competing with T as hypothesized.

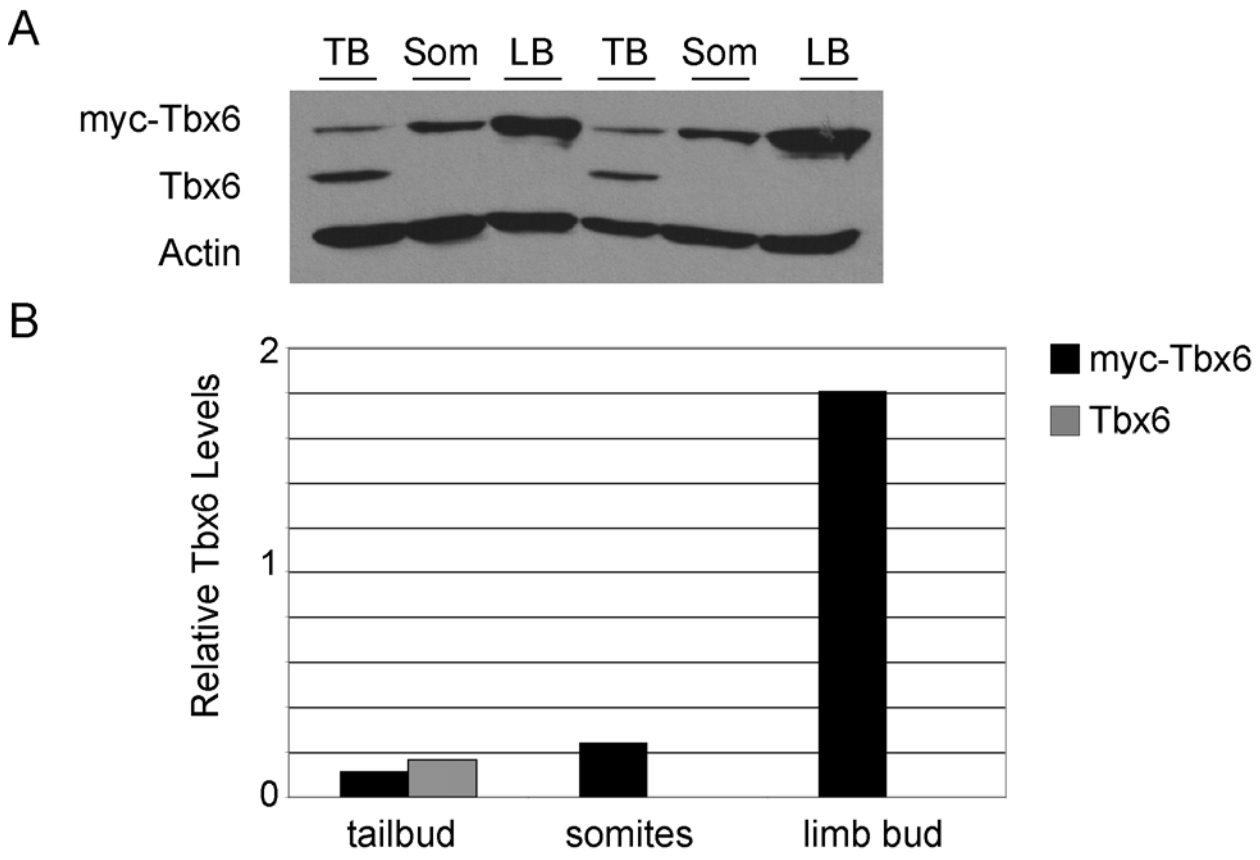

Figure 28: Tbx6 protein levels in *T-Cre* 3-component tissue. (A) Approximately, ten e10.5 3-component embryos were isolated and tailbud, somites S1-4 and limb bud tissue were pooled for Western blot analysis using anti-Tbx6 antibody. Both ectopic (myc-Tbx6) and endogenous Tbx6 protein was expressed in the tailbud (TB). Ectopic Tbx6 was expressed in the somitic tissue (Som) and highly expressed within the limb bud (LB). The second data set were samples from a separate experiment, which revealed the same trend. (B) Quantification of Western blot data, normalized to actin levels, revealed the relative Tbx6 expression levels within the tissues, with the lowest amount of ectopic Tbx6 found in the tailbud.

Interestingly, misexpression of Tbx6 within the somitic region and the limb bud was able to generate phenotypes, including vertebral malformations and scapulae defects. These phenotypes support our previous observations, namely that Tbx6 may be competing with other resident T-box factors in this region (When and Chapman, submitted unpublished). The *T-Cre* line should have resulted in recombination in all PS cells. Once the transcriptional stop is removed, rtTA should be expressed in these cells and all of their derivatives, thus myc-Tbx6 should also be expressed in these cells. However in my experiments recombination appeared mosaic.

To understand the consequences of Tbx6 misexpression in the PS, I next utilized a ubiquitous Cre line, *Sox2-Cre*. Others have shown previously that the *Sox2-Cre* line mediates recombination in all epiblast cells but not extraembryonic tissue by e6.5 and by e9.5 β-galactosidase activity was also found within the yolk sac and amnion (Hayashi et al., 2002). Using the *Sox2-Cre* driver I generated 3-component embryos that misexpressed myc-Tbx6 in all epiblast cells. DOX was administered at e8.5 to the pregnant females drinking water. Dissection of e10.5 3-component embryos revealed head and jaw malformations, mildly eodemic hearts and limb defects. Importantly, these embryos had a short, flattened, stubby tailbud and shortened axes as compared to control littermates (Fig. 29). The alteration of tailbud size and shape was predicted from my analyses of the *Tg46* homozygous phenotype, which also expresses high levels of Tbx6 (Figs. 21-22). Thus, the more efficient recombination by the *Sox2-Cre* line presumably allowed high enough levels of Tbx6 expression in the PS and tailbud to generate a phenotype.

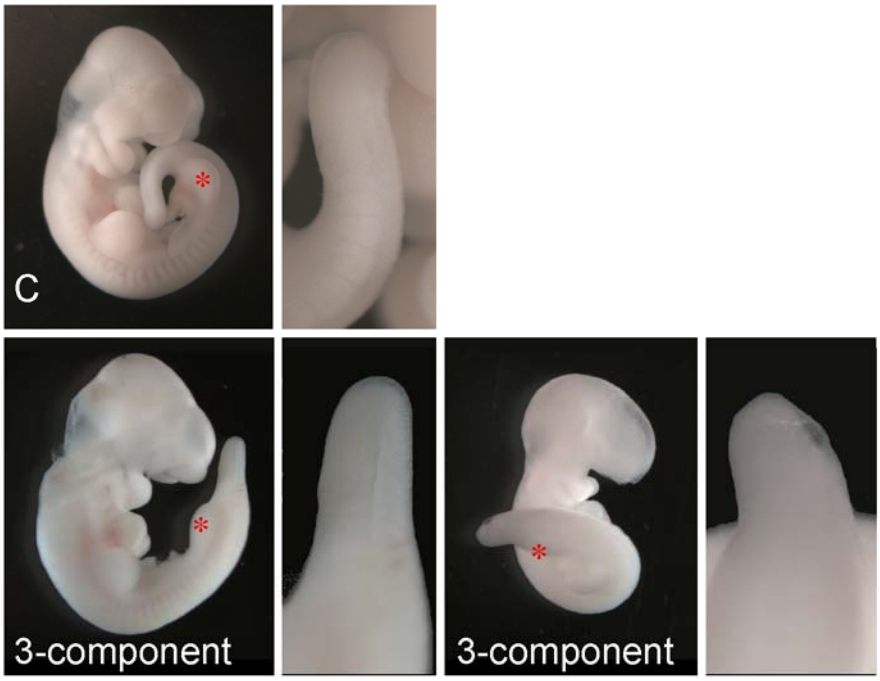

Figure 29: Gross morphology of e10.5 *Sox2-Cre* 3-component embryos. e10.5 3-component embryos were characterized by a shortened, flat tail and smaller tailbud as compared to control (C) littermates. Red asterisk marks the hindlimb bud to allow a comparison of tail size from the hindlimb caudally between 3-component and control embryos.

I further characterized the 3-component embryos by visualizing Tbx6 mRNA and protein expression. These experiments revealed that at e10.5 *Tbx6* mRNA was expressed at low levels throughout the embryo with higher expression in the jaw, heart, neural tube and forelimb as compared to control embryos (Fig. 30A). Compared to the *T-Cre* 3-components, little variability was found in the *Sox2-Cre* 3-component litters examined thus far (n=33). Tbx6 protein expression recapitulated the patterns observed in *Tbx6* mRNA expression in 3-component embryos. Higher Tbx6 protein levels were found in the jaw, heart, limb buds, PSM and tailbud,

with low levels found throughout the embryo (Fig. 30B). The small tailbuds of 3-component embryos was evident by staining for Tbx6 mRNA and protein.

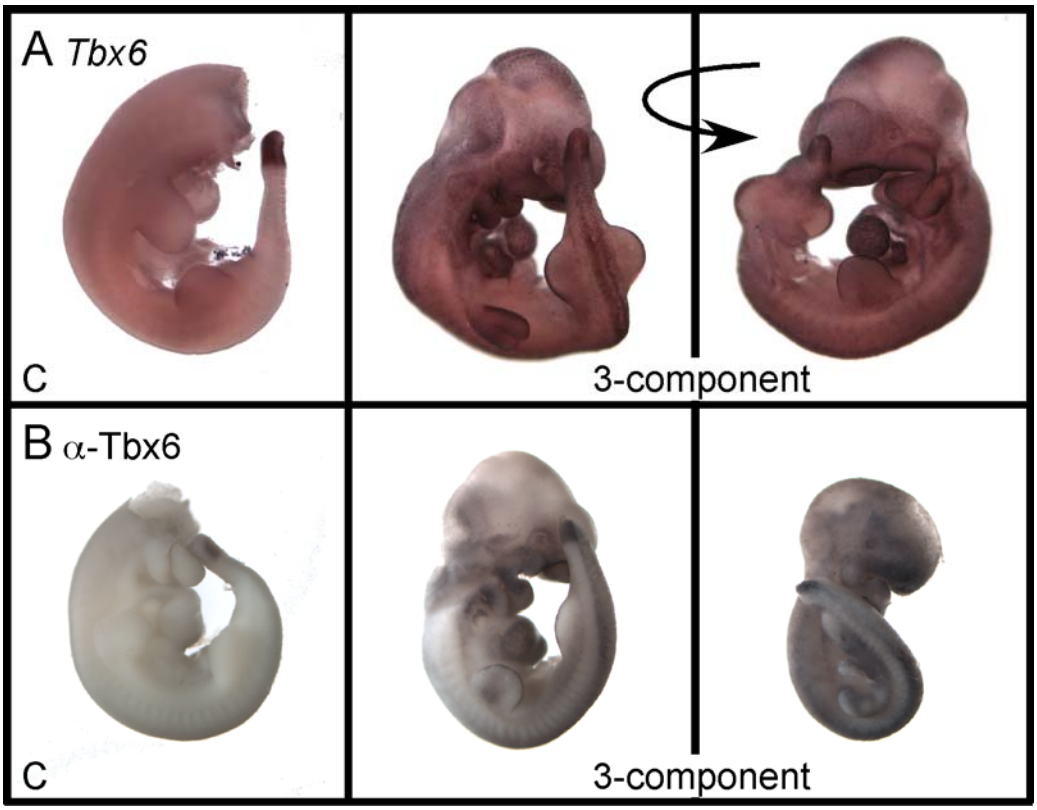

Figure 30: Tbx6 mRNA and protein expression in *Sox2-Cre* 3-component embryos. (A) Control (C) and 3-component e10.5 littermates were examined for *Tbx6* mRNA expression. In addition to the endogenous expression domain of *Tbx6* within the PSM and tailbud, 3-component embryos also expressed a low level of *Tbx6* throughout the embryo with higher expression in the jaw, heart, neural tube and limb buds. Curved arrow represents rotated orientation of the same embryo to present different expression domains (*Tbx6* panel). (B) 3-component embryos expressed ubiquitously low levels of ectopic Tbx6 protein, with higher expression in the jaw, heart, limb buds, PSM and tailbud as compared to control embryos (α-Tbx6 panel).

Altogether, misexpression of myc-Tbx6 in the *Sox2-Cre* expression domain resulted in high enough levels of Tbx6 protein and mRNA to generate a tailbud phenotype. The small tailbud and axial shortening observed phenocopies the *T* heterozygous phenotype, supporting our hypothesis that Tbx6 can compete with T in their overlapping expression domain, the tailbud. Further analysis of the *Sox2-Cre* 3-component line will be limited due to embryonic lethality. However it will reveal the importance of maintaining the proper levels of Tbx6 protein for normal development.

3.4 DISCUSSION

The above studies examined Tbx6 protein stability both *in vitro* through steady state, cycloheximide, and pulse-chase assays and *in vivo* through analysis of the *Tbx6*^{rv}, *Tg46*, and 3-component lines. *In vitro*, Tbx6 appeared to be a relatively stable protein with a half-life of approximately 6 hours. Tbx6 protein turnover appears to be partially regulated by the proteasome, as proteasomal inhibition with MG132 resulted in the accumulation of Tbx6 protein in a steady state analysis and modest extension of its half-life in pulse-chase assays. Previous studies also showed that Tbx6 protein is likely degraded by the proteasome (Oginuma et al., 2008; Chen et al., 2009). However, in addition to its role as a proteasome inhibitor, MG132 may also activate a stress response. When the cell is stressed due to the abnormal accumulation of proteins from proteasome inhibition, heat shock proteins that are normally induced during stress response also accumulate (Bush et al., 1997). These induced heat shock proteins may be functioning to stabilize Tbx6 or target it for proteasome-mediated degradation, thus in the presence of MG132 it would appear as if Tbx6 protein was accumulating. However, this

accumulation may be an artifact of the induced stress response, rather than a direct result of proteasome inhibition due to MG132. Therefore, the accumulation of Tbx6 protein that I observed in my *in vitro* studies may be a direct result of proteasome inhibition or it may be a combinatorial effect of both proteasome inhibition and a stress response, making it difficult to definitively conclude that Tbx6 degradation is regulated directly by the proteasome. However, a known target of proteasome-mediated degradation, NICD (Oberg et al., 2001; Wu et al., 2001), accumulated in my system, suggesting that the proteasome was being appropriately inhibited (Fig. 17A). Another caveat to these *in vitro* assays is the possibility that the observed protein accumulation in the presence of MG132 was an artifact of protein over-expression that occurred during transient transfections. Pulse-chase analysis revealed that the half-life of Tbx6 was extended in the presence of MG132, however I expected a greater stabilization than observed based on previous studies of other mammalian proteins regulated by the proteasome (Steinhilb et al., 2001). It is possible that another mechanism such as the lysosomal system is utilized to ensure efficient Tbx6 degradation. In this scenario, MG132 would only block the proteasome leaving lysosomal degradation of Tbx6 intact. *In vivo* maintenance of proper Tbx6 levels is essential for normal embryonic development therefore it is conceivable that multiple mechanisms exist to maintain the levels of Tbx6 protein.

Treatment of cells with MG132 resulted in the accumulation of Tbx6 protein. I used luciferase transcriptional assays to show that this accumulated protein is functionally active with MG132-treated cells inducing higher levels of luciferase. Failure to degrade Tbx6 in the embryo could lead to its continued presence in the newly formed somites and/or over-expression within the PS and PSM with subsequent ectopic activation of its downstream targets that could result in severe phenotypes. Interestingly, I did not observe ectopic expression of *Dll1* or *Ripply2* in

either the *Tg46*/*Tg46* or *T-Cre* 3-component embryos. This is likely due to the fact that Tbx6 works in conjunction with other factors, which would also need to be ectopically expressed or expressed at higher levels to result in an upregulation of downstream targets. For example, both Tbx6 and β-catenin are required for *Dll1* (Hofmann et al., 2004) and Wnt and Mesp2 are required for *Ripply2* regulation (Biris et al., 2007; Morimoto et al., 2007; Dunty et al., 2008). However, without performing quantitative RT-PCR, it is difficult to determine if there is an upregulation of downstream targets that is not detected by WISH. I did note that the *Ripply2* expression domain in *Tg46*/*Tg46* embryo appeared slightly expanded compared to wildtype embryos (Fig. 23, *Ripply2* panel). However, the broad expression pattern could represent the dynamic *Ripply2* expression domain (Biris et al., 2007).

I used a 3-component transgenic system to misexpress Tbx6 *in vivo* using either *T-Cre* or *Sox2-Cre* transgenic lines. Both resulted in embryonic lethality, suggesting that the maintenance of normal Tbx6 levels both spatially and temporally is critical for proper embryonic viability (see below). I hypothesize that Tbx6 competes with T in the PS/tailbud and predicted that increased Tbx6 expression in the tailbud would generate embryos with *T* heterozygous phenotypes. However, I did not observe any tailbud phenotypes in *T-Cre* 3-component embryos (Fig. 26). This was likely due to the low and mosaic expression of Tbx6 achieved with this expression system. While *Tbx6* mRNA appeared more widely expressed than the protein, this difference may be due to the technical issues of antibody penetration within embryos of this stage. However, *Sox2-Cre* 3-component embryos were analyzed at the same stage and appeared to have more widespread expression (Fig. 30B) as compared to *T-Cre* 3-component embryos (Fig. 26). I did observe skeletal defects in the *T-Cre* 3-component embryos, including a hole in the scapula, atlas/axis fusions and limb abnormalities which phenocopied *Tbx15* and *Tbx18* null embryos

(Bussen et al., 2004; Singh et al., 2005), suggesting that Tbx6 was able to interfere with other T-box transcription factors. In an attempt to increase both the recombination efficiency and expression of Tbx6 within the tailbud I used the *Sox2-Cre* transgenic line. This transgenic line drives expression in the entire epiblast beginning at e6.5 (Hayashi et al., 2002). While I was interested in driving *myc-Tbx6* specifically within the PS/tailbud, this experiment was tricky since introducing DOX to pregnant females too early and for too long resulted in early embryonic lethality. For most litters, DOX treatment at e8.5 for approximately 48 hours allowed for the observation of tail phenotypes before lethality. Misexpression of Tbx6 within the *Sox2-Cre* domain resulted in the production of high enough levels of ectopic Tbx6 mRNA and protein within the tailbud to presumably compete with T that resulted in the observed phenotypes (Fig. 30). Unfortunately, under these experimental conditions, it is impossible to follow how the small tailbud would translate into axial truncation at later embryonic time points due to lethality.

Lethality in both 3-component transgenic lines is likely due to heart defects resulting from high expression of ectopic Tbx6 in the heart (Fig. 26 and Fig. 30) where it may be competing with at least six other T-box family members that are normally expressed there (Naiche et al., 2005). In this scenario, ectopic Tbx6 would prevent the endogenous T-box factors from activating/repressing their respective downstream targets, which would prevent proper heart development and lethality. While *Sox2-Cre* 3-component embryos displayed milder heart defects as compared to those found in *T-Cre* 3-component embryos, possibly due to the duration of DOX treatment, I did observe a shortened, stubby tail prior to embryonic lethality.

3.5 CONCLUSIONS AND FUTURE PROSPECTUS

In conclusion, *in vitro* analyses revealed that Tbx6 is a relatively stable protein, with a half-life of approximately 6 hours and its degradation is controlled at least in part by the proteasome. *In vivo* analyses revealed that misexpression of Tbx6 within ectopic domains resulted in skeletal defects and embryonic lethality. These phenotypes suggested that not only is the maintenance of proper Tbx6 levels both spatially and temporally essential for normal development, but also that ectopic Tbx6 may be able to compete with other T-box transcription factors resulting in detrimental phenotypes. Importantly, use of the *Sox2-Cre* transgenic line allowed me to observe shortened, stubby tails that provided further confirmation to other data collected within the Chapman laboratory, that Tbx6 can compete with T to generate these phenotypes.

3.5.1 *In vitro* analyses

While my *in vitro* analyses gave me a basic understanding about Tbx6 protein regulation, there are many other biochemical assays that could be performed to further clarify Tbx6 protein turnover. It is important to note that both the steady state and cycloheximide chase analyses were missing essential time points between 6 and 24 hours, during which large changes in protein levels occurred. While it would be ideal to repeat these experiments with a more refined time course, the definitive pulse-chase experiment utilized a more refined time course and ultimately allowed me to conclude that Tbx6 is being partially degraded by the proteasome by approximately 6 hours. Pulse-chase analyses were only performed twice and a nearly significant difference ($p=0.07$, Student's t-test) was found between DMSO and MG132-treated samples. Repeating the pulse-chase experiment for significance would be ideal. In addition the modest

extension of Tbx6 protein half-life with MG132 treatment was not as dramatic as expected. It is possible that another mechanism exists to regulate Tbx6 protein turnover, such as a lysosomal-dependent mechanism. To address this hypothesis, a preliminary pulse-chase analysis was performed in the presence of both MG132 and leupeptin, a known lysosomal inhibitor. However an increased half-life was not observed. This experiment was performed using 20 μM leupeptin (Barriere et al., 2007), but this may not have been an optimal concentration for this system. This experiment should be repeated once optimal leupeptin concentrations and functionality are determined and in the presence of a positive control, such as EGFR, which is known to be degraded in a lysosomal-dependent manner (Authier et al., 1999).

In vitro studies of Tbx6 stability and turnover utilized transiently transfected cells. Expression of Tbx6 was driven by the CMV promoter and resulted in high levels of myc-Tbx6. There is the possibility that protein over-expression might cause an artificial proteasome response (Ma and Lindquist, 2001). To verify Tbx6 protein accumulation observed in the steady state assays was not due to an artifact of over-expression, these assays could be performed using a protein that is not regulated by the proteasome. The loading control was endogenous tubulin and this did not appear to accumulate in the presence of MG132 (Fig. 17A). Therefore, it would be interesting to over-express tubulin in cells treated with MG132 to test if general protein over-expression initiates a proteasome response. However, it would be necessary to verify that tubulin over-expression does not adversely affect COS-7 cell viability. Since, α-Tubulin has been over-expressed in CHO cells without any adverse effects on growth (Gonzalez-Garay and Cabral, 1995), concerns of adverse tubulin effects may not be warranted. Finally, it would be interesting to determine if proteasome regulation of Tbx6 occurs via the PEST domain, a potential signal sequence for protein degradation. Pulse-chase analyses in which the PEST

domain of Tbx6 (Tbx6ΔPEST) is deleted could be performed with the prediction that Tbx6 protein half-life would be stabilized if the PEST domain plays a role in its degradation.

3.5.2 *In vivo* analyses

I took two approaches to manipulate Tbx6 expression *in vivo*. One approach was the analysis of existing mouse lines that either under- or over-expressed *Tbx6* in its endogenous domain, for protein expression via Western blot and immunohistochemistry. These studies revealed that as predicted from mRNA analysis, *Tbx6*$^{rv/rv}$ embryos expressed approximately half as much Tbx6 protein as wildtype embryos, while *Tg46*/*Tg46* embryos expressed greater than wildtype amounts of Tbx6 protein. These results allowed me to conclude that varying Tbx6 levels within its endogenous domain resulted in rib, vertebrae and axial defects. While these analyses all supported one another, the Western blot of total Tbx6 protein across all of the genotypes was only performed once in entirety. Partial experiments, for example using only *Tbx6*$^{rv/rv}$ and *Tbx6*+/- samples, were performed at separate times and these revealed the same trends. Based on the extremely low levels of actin that the Tbx6 protein levels of *Tg46*/*Tg46* and their respective wildtype background strain were normalized to, it is difficult to make an accurate conclusion about the total Tbx6 protein levels found in that genotype. It will be necessary to repeat the Western analysis using another loading control, possibly tubulin. In addition, to make accurate comparisons between *Tbx6*^{rv} and *Tg46*, one would have to perform the immunohistochemistry experiment with e10.5 *Tbx6*$^{rv/rv}$, *Tbx6*+/-, *Tg46*/*Tg46* and their respective wildtype littermates in the same tube. In the presented data e9.5 *Tg46*/*Tg46* and e10.5 *Tbx6*$^{rv/rv}$, *Tbx6*+/-, and their respective wildtype littermates were tested in the same tube. However, the e10.5 *Tg46*/*Tg46* with its wildtype littermate experiment was performed on a separate date (Fig.

22). While this is not ideal, e9.5 *Tg46*/*Tg46* embryos appeared to express similar amounts of Tbx6 protein as e10.5 *Tg46*/*Tg46* embryos that were tested on a different day. This observation made the comparison across genotypes more palatable.

It is possible that the tailbud phenotypes of *Tbx6*$^{rv/rv}$ (enlarged) and *Tg46*/*Tg46* (diminished) were biasing the Western blot and immunohistochemistry data interpretation. For example, if the *Tbx6*$^{rv/rv}$ and the *Tg46*/*Tg46* tailbuds expressed the same amount of Tbx6 protein, but the *Tbx6*$^{rv/rv}$ tailbud is enlarged compared to the *Tg46*/*Tg46* tailbud, then the *Tbx6*$^{rv/rv}$ Tbx6 protein levels would effectively be diluted by the extra tailbud tissue, making the total Tbx6 protein levels per cell appear lower than they actually are. The converse would be true of the *Tg46*/*Tg46* tailbuds, effectively concentrating the amount of Tbx6 protein within the tailbud resulting in the appearance of greater amounts than they actually are. To address this possibility, I will examine Tbx6 protein expression within sections of *Tbx6*$^{rv/rv}$, wildtype, and *Tg46*/*Tg46* tailbuds by immunohistochemistry. Analysis of these data would allow me to determine if the overall levels within the tailbuds are affected by the genotype or whether there are regions of the tailbud that express Tbx6 protein differentially.

An unexpected result of Tbx6 protein analysis studies in *Tbx6*$^{rv/rv}$, *Tbx6*+/- and *Tg46*/*Tg46* embryos was the varying levels of Tbx6 found in the different wildtype background strains. This observation generates a prediction that there may be strain-dependent effects on the phenotypes. For example, the *Tbx6*$^{rv/rv}$ embryos are on a C57Bl/6 background that expressed relatively low levels of Tbx6. If the *Tbx6*$^{rv/rv}$ embryos were on a FVB/N background (*Tg46*) that expressed relatively high Tbx6 levels, then perhaps the *Tbx6*$^{rv/rv}$ phenotype might not be as severe. Backcrossing the different mouse lines onto C57Bl6/J, mixed or FVB/N backgrounds would determine if there are strain-dependent effects.

Altogether, differential Tbx6 protein expression among the different genotypes was supported by both the Western blot and immunohistochemistry data. However, it would also be beneficial to determine if varying Tbx6 protein levels would result in differential activation of Tbx6 downstream targets. Examination of the remaining known Tbx6 downstream targets, *Msgn1* and *mesp2*, in *Tg46*/*Tg46* embryos by WISH would address this question. However, it is likely that I will not observe any differences, similar to what I observed with *Dll1* and *Ripply2*, due to the requirement of additional factors for these genes to be properly transcribed (*Msgn1* requires Wnt and *mesp2* requires Notch (Yasuhiko et al., 2006; Wittler et al., 2007)). It would also be important to perform quantitative RT-PC to more accurately assess expression levels. I should also examine the remaining Tbx6 downstream targets, *Ripply2*, *Msgn1*, and *Mesp2* in $Tbx6^{rv/rv}$ embryos by WISH and quantitative RT-PCR to determine if lower Tbx6 levels results in the downregulation of these genes, and potentially explain some of the phenotypes observed in these embryos. It has already been shown that *Dll1* is downregulated in $Tbx6^{rv/rv}$ embryos (Beckers et al., 2000).

The second approach I took to manipulate Tbx6 expression *in vivo* was via misexpression of myc-Tbx6 within the *T-Cre* domain utilizing the 3-component transgenic system. My hypothesis was that Tbx6 would compete with T to generate a reduced tailbud. However, this was unsuccessful due to the low levels of ectopic Tbx6 expressed within the tailbud. The variability of induced expression observed with the *T-Cre* line also made it difficult to draw any conclusions. In an attempt to minimize the variability, other *T-Cre* males were tested but they transmitted similarly. Since the *T-Cre* driver did not function as expected, I utilized a *Sox2-Cre* 3-component line. Misexpression of myc-Tbx6 in this line resulted in shortened stubby tails, suggesting that Tbx6 could compete with T to phenocopy a *T* heterozygote. Further analysis of

the *Sox2-Cre* 3-component line would involve verifying the tailbud phenotype through WISH of tailbud markers *T* and *Fgf8*. It is also important to quantitate the tailbud phenotype observed in *Sox2-Cre* 3-component embryos. Measurement of the hindlimb to tailbud distance as a ratio of total body length would provide an accurate description of the tailbud phenotypes that were obtained in these embryos. It would also be interesting to determine how much ectopic Tbx6 is being produced in the tailbud to generate phenotypes. I have observed that the embryo is sensitive to the levels of Tbx6. It would be informative to quantitate the level of over-expression required to generate a phenotype by using Western blot analysis of tailbud lysates of *Sox2-Cre* 3-component embryos as was performed for *T-Cre* embryos (Fig. 28). I should also investigate if any of the Tbx6 downstream targets are affected in *Sox2-Cre* 3-component embryos via WISH. Finally, I should examine the skeletal phenotype associated with *Sox2-Cre* driven misexpression of Tbx6. These experiments are not possible using DOX administered at e8.5 since 48 hours of DOX treatment is the maximum amount possible before lethality is observed. The timing of DOX administration and dissection would have to be optimized for accurate results to be obtained. In addition to these misexpression techniques, it would also be interesting to examine the phenotypic consequences of deleting the PEST domain that would presumably prevent Tbx6 protein regulation via proteasome-mediated degradation. Therefore, pending *in vitro* verification that Tbx6ΔPEST was not degraded by the proteasome, it would be ideal to generate a knock-in transgenic line that would express Tbx6ΔPEST in the *Tbx6* endogenous domain and observe the resulting phenotypes. If Tbx6 protein is degraded by the proteasome as the new somite forms, then in *Tbx6ΔPEST* embryos, Tbx6 protein but not mRNA may be expanded in the region of the newly forming somite. In addition, it is possible that Tbx6 is degraded within the PSM and tailbud to maintain proper levels. In that scenario *Tbx6ΔPEST* embryos may accumulate Tbx6

protein within those domains and this increased level of Tbx6 would generate axial truncations or tailbud phenotypes similar to *T* heterozygotes.

3.5.3 Implications

Results from these studies revealed the importance of regulating Tbx6 levels and expression domains for an embryo to develop into a fully functioning adult. Interestingly, mice with approximately half the amount of Tbx6 protein as compared to wildtype have no phenotypic consequences as seen in normal *Tbx6*+/- mice. However, any modulations of Tbx6 protein expression below heterozygous or above wildtype levels results in skeletal defects. This suggests that Tbx6 protein levels are tightly regulated to prevent these situations from occurring, as they have adverse consequences to the embryo. Since many T-box transcription factors are expressed in overlapping domains and they can compete with one another when co-expressed, a situation is set-up such that even slight modulations of T-box protein levels can have downstream effects. Not surprisingly, there are many human disorders associated with mutations in T-box genes. Some examples include: DiGeorge Syndrome (*TBX1*) which is characterized by congenital heart defects, Ulnar-mammary syndrome (*TBX3*) which is characterized by limb defects including a loss of the hand and forearm, and Holt-Oram syndrome (*TBX5*) which is characterized by cardiac and limb abnormalities (Packham and Brook, 2003). Each of these results from haploinsufficiency, thus confirming the need to regulate T-box transcription factor levels properly, especially when other T-box transcription factors are co-expressed. While no human disorders have been mapped to mutations in *TBX6*, recently a link was found between hemivertebrae, rib abnormalities and *TBX6* haploinsufficiency (Shimojima et al., 2009). Examination of how Tbx6 is regulated and more generally, how T-box transcription factors

interact to regulate gene expression in their co-expression domains, would contribute significantly to the understanding of the etiology of skeletal disorders.

4.0 CONCLUSIONS OF THESIS WORK

Characterization of a spontaneous mutation began with the observation of a kinky tail phenotype in adult mice and led to the investigation of cellular adhesion, migration and axial elongation in the embryo. The analysis of *kinked tail* homozygotes revealed that early embryonic lethality results from the failure to establish an A-P axis during gastrulation. This failure was likely due to defective DVE migration. *Knk* heterozygous embryos and mice exhibited axial truncations and a variety of kinky tail phenotypes that are most likely caused by a primary notochord defect that may be due to defective notochord precursor cell migration or adhesion.

Understanding the consequences of Tbx6 modulation *in vivo* began with two main observations: 1) less than heterozygous levels of *Tbx6* mRNA generated rib and vertebral phenotypes, axial truncations and enlarged tailbuds and 2) greater that wildtype levels of *Tbx6* resulted in axial truncation and small tailbuds. I hypothesize that the levels of Tbx6 relative to T have been modulated, causing a cell fate change between PAM and PS, resulting in axial elongation defects. Similar to our observations of *Tbx6* mRNA, Tbx6 protein levels in transgenic lines that under- and over-express *Tbx6*, directly correlated with Tbx6 protein levels. Over-expression of Tbx6 in the tailbud results in a small tailbud and eventually a short tail phenotype supporting the hypothesis that, in this situation, Tbx6 protein competes with T in the tailbud. This Tbx6 over-expression phenotype was further supported by the 3-component transgenic system that generated ectopic Tbx6 within the PS/PSM and resulted in axial

truncations and small tailbuds. Under-expression of Tbx6 leads to an enlarged tailbud and supports the hypothesis, that in this situation, the increased levels of T relative to Tbx6 may result in the accumulation of PS cells and enlarged tailbuds.

My thesis work has afforded me the opportunity to examine developmental processes using a wide variety of embryological and biochemical techniques. I have been able to approach two important developmental questions from two different angles. The first question asked what the molecular mechanism was that generated altered vertebral morphology in heterozygotes and the second question asked what effect manipulating Tbx6 protein levels would have on the embryonic phenotype. Being able to approach these questions, from phenotype to genotype and genotype to phenotype has been a very exciting and rewarding undertaking. Ultimately, both projects examined the mechanisms underlying axial elongation in the mouse.

5.0 MATERIALS AND METHODS

5.1 MAPPING AND MOUSE LINES

5.1.1 Mapping *knk*

The FVB.B6-knk *kinked tail (knk*) (marker accession number MGI:3834125; allele accession number MGI:3834126) mouse line arose as a spontaneous mutation on a mixed C57Bl6/J FVB/N genetic background. *knk* heterozygous mice are maintained on an FVB/N background. *knk/+* mice (FVB/N Backcross-1) were crossed to FVB/N mice for two generations. e14.5 embryos (embryonic day 0.5 corresponding to noon of the day the vaginal plug was found) resulting from the third backcross were examined for abnormal tail morphology and DNA from affected individuals was used for initial mapping studies by single nucleotide polymorphisms (Harvard Partners Center for Genomics and Genetics). A second mapping set was performed using *knk/+* mice (C57Bl/6J FVB/N) that were backcrossed one generation onto a C57Bl/6J background. Affected embryos from the second backcross were isolated and DNA was used for mapping. Further refined mapping utilized both affected and unaffected embryos isolated from the backcross of *knk/+* mice (C57Bl/6J FVB/N) one generation onto a DBA background.

5.1.2 Transgenic lines

The *Tbx6* mice were maintained on a mixed C57Bl6/J/129Sv/Ev background (Chapman and Papaioannou, 1998). *Tbx6*^{rv} mice were obtained from Jackson Laboratories and maintained on a C57Bl6/J background (Beckers et al., 2000). *Tg46* mice were maintained on a FVB/N background (White et al., 2003). *T-Cre* mice were a kind gift from Mark Lewandowski and were maintained on a mixed background (Perantoni et al., 2005). *Sox2-Cre* mice were obtained from Jackson Laboratories and were maintained on a C57Bl6/J background (Hayashi et al., 2002). *ROSA26* mice were obtained from Jackson Laboratories and maintained on a mixed background (Soriano, 1999). *rtTA* mice were obtained from Jackson Laboratories and maintained on a mixed background (Belteki et al., 2005).

5.1.3 Breeding schemes

T-Cre three component embryos were generated by crossing *T-Cre*/*T-Cre* mice to *Tre-Tbx6*/*Tre-Tbx6* (or *Tre-Tbx6+/-*); *rtTA*/*rtTA* mice. *Sox2-Cre* three component embryos were generated by crossing *Sox2-Cre*/+ mice to *Tre-Tbx6*/*Tre-Tbx6* (or *Tre-Tbx6+/-*); *rtTA*/*rtTA* mice. Doxycycline was added to the pregnant females drinking water at a concentration of 1.6 mg/mL at e7.5 or e8.5 for *TCre* and *Sox2-Cre* mice respectively, and timed dissections were performed from e8.5-e13.5 where the day of vaginal plug detection was e0.5. Dissected embryos were genotyped by PCR for the presence of the TRE,Cre and rtTA transgenes and fixed according to the specific assay being performed. Genotyping primers are listed below from 5'-3':

TRE for: GCC ATC CAC GCT GTT TTG AC

TRE rev: CCA GAG AGG AAG CAA TCC AGT TTA G

CRE for: GGA CAT GTT CAG GGA TCG CCA GGC

CRE rev: CGA CGA TGA AGC ATG TTT AGC TG

rtTA for: CGT GAT CTG CAA CTC CAG TC

rtTA rev: GGA GCG GGA GAA ATG GAT ATG

Sox2-Cre for: GCG GTC TGG CAG TAA AAA CTA TC

Sox2-Cre rev: GTG AAA CAG CAT TGC TGT CAC TT

5.2 RT-PCR PRIMERS

RT-PCR was performed on e7.5 SW embryos using standard procedures. Briefly, RNA was isolated from e7.5 SW whole embryos, adult brain or intestines using TRI reagent (Sigma). cDNA synthesis was performed using 2 μg of RNA, random hexamer primers, and SuperScript II (Invitrogen). PCR amplification was performed on undiluted, 1:2 and 1:3 diluted cDNA using primers that were designed to span consecutive introns of the candidate genes within the *knk* region.

Gene	**Primer sequence 5'-3'**
1500015010Rik for	TCA AGA AGA TGC TCC AGA AAC GAG
1500015010Rik rev	CGT GAC CAT CAG GCT AAA GGA A
83430432A02Rik for	TTG AGA AAC TGC TAA AGA GGT GGC
83430432A02Rik rev	CAC AAA TAA CAG CCC CCT TTA GG
Aff3 for	CCA CAC CAG AGG ACA AAC AGT TAG C
Aff3 rev	ACA CCC CAG AGA AAC ATC GTT G
AI597479 for	TTG CCA AAG AAT AGA TGG GGG
AI597479 rev	CCC TGT TGG AAC TAC TCC TGT GAA
Chst10 for	TGA CCC CTG CTT TTG TCT TCG
Chst10 rev	TAG CCC TTT GCT GCT GGT TG
Creg2 for	TGG GAT GGG AGG TAG TCT TTG C
Creg2 rev	TTC CGT TGG ATG GGT TCT CAG C
D1Bwgo212e for	CTC GCC AGA TTG CCT TGA TG

D1Bwgo212e rev	GTG AAG AAT AGC ACT GGT GTG GAG A
Eif5b for	CAT CTT CCC CTA TTC AGG AGG TCT C
Eif5b rev	AAG TTT GTG CCG CTC AGC AG
Fhl2 for	AAG GCT GCT TCC ATT GCT CC
Fhl2 rev	CAA AAA GCC TAT CAC CAC AGG AGG
Gpr45 for	TGG TAG AGA AAG GCT GGA TGG C
Gpr45 rev	CAA TCC TAT GCC TCT CTC AGT GCC
IL18r1 for	TTG GGG GTT TCA CCA CAG TG
IL18r1 rev	CTT CGC TTT GTT CTT CTA TCA GCC
IL18rap for	TTG TTT GCT TTG CCC AGA ACT C
IL18rap rev	CAA AAA GGC TCT GCG GGT TC
Il1r1 for	TTG CCT GAG GTC TTG GAG GG
Il1r1 rev	GCA ACA CAC TTA CCA CTC GGC T
IL1r2 for	CCA TTG TGT GGT GGT TGG CTA AC
IL1r2 rev	GAC AAC CAG GAC TTC CCT TCC A
IL1rl1 for	GCA AAG GCT CTC ACT TCT TGG C
IL1rl1 rev	GCA TTT ATG GGA GAG ACC TGT TAC C
IL1rl2 for	TGT CCG CAG CCT ACA TCA TTC
IL1rl2 rev	GAG GCT GAT GGT CTT TGT GGC A
Lonrf2 for	CAG TAT CCT CTG GAA GAA GCA GGC
Lonrf2 rev	CAA ATG CCT TGA GCG TTG CC
Map4k4 for	TCC AGA GGT TGA GAA GAA GCA GGG
Map4k4 rev	CAC CAT CCA AGT GAC CAG TTT CC
Mfsd9 for	TGT AGG CTT CTT GGA CCT GTT TG
Mfsd9 rev	CAA GCC TCA ACA TCC CAG ACA A
Mrps9 for	TCC AAA ACA AAG AGC AAC CCA G
Mrps9 rev	GCT ATT GAC ATT GCC GTG CG
Nck2 for	GCT CCA AAA CTG TGC GGA TAG C
Nck2 rev	GTA GGA ATG TGC CAT CTC AAG ACT C
Nms for	CGG GAA ATG CTC ATC ACC TCT C
Nms rev	TGC TGT CTA CTG GAA GTT GTT GTC G
Npas2 for	AGC CCT CAG AAG TCA GCA GAA CTG
Npas2 rev	GCC AAC CCC GTT TTC CAT TG
Pdc13 for	TGC TTT CAG CCC AGT CTT CCA G
Pdc13 rev	CCT TAT TCC CCC AAA CCA ACT C
Pou3f3 for	AGC ATC CTC CGC AGT AAA CTT G
Pou3f3 rev	ATC ACA TCC GCA GCA CCC ATT C
Rev1 for	AGA GGA CAC TAC TCA TCA GCA GCC
Rev1 rev	TGT TCC ATA CAG ACT CCA CCG AC
Rnf149 for	TGT ATG TGG AGG GGT TGT TTC TG
Rnf149 rev	CAC GGC AAG ATT TCT CAT TTC C
Rpl29 for	AAC CAC ACC ACA CAC AAC CAG TC
Rpl29 rev	CCC ATA GAA ATG ACT CCT GCC A

Rpl31 for	CCT TGA ACT CAG AAA TCC ACC TGC
Rpl31 rev	GCT ACT GGT TGG CAA AGA TGG C
Slc9a2 for	AGT CAA GCC ACT GAT TCC CAG G
Slc9a2 rev	CAG AAA TGG ACC AAG AGC AGC C
Slc9a4 for	TTG TCA AAA AGG CTC TGC GG
Slc9a4 rev	ACT TGG GAA CTC TCA GGG AAA TG
Tbcdl8 for	TGG AAA GGC AGA GTT GAT GTC C
Tbcdl8 rev	AGG ATT GTG GAT TTG GGT TGG
Tgfbrap1 for	GGA AGG GAG CAG GAA TGT TCA G
Tgfbrap1 rev	CAT CTT GTG GAT TTG GGA CTC G
Tmem182 for	GGG TTT GAT GTC TGT GAG GCA C
Tmem182 rev	AGG CTC CTG CTA CCT TTC CAA G
Uxs1 for	GTT GGG GAC AGA TGA AAG GAC TC
Uxs1 rev	CAA GTG TTC TTC TCA GCC ACC AC

5.3 HISTOLOGY AND SKELETAL PREPARATIONS

knk heterozygous mice were intercrossed and resulting embryos were dissected beginning at e5.5. Dissected embryos or decidua were fixed in Bouin's fixative, embedded in paraffin wax and sectioned by standard methods. Sections were stained with Mason's trichrome. Skeletons from adult tails and e13.5 embryos were stained with alizarin red and alcian blue, as described (Nagy, 2003), except that the staining was performed at 37°C.

5.4 WHOLE MOUNT *IN SITU* HYBRIDIZATION, IMMUNOFLUORESENCE, AND IMMUNOHISTOCHEMISTRY

Whole-mount in situ hybridization was performed as previously described (Wilkinson, 1992) using antisense riboprobes for *myogenin*, *shh*, *Oct3/4*, *Brachyury*, *Foxa2*, *mCer1*, *Otx2*, *Hex*,

Nodal, *Fgf8*, *Ripply2*, *Uncx4.1*, *BMP4*, *Tbx6*, *Lefty1*, *Chst10*, *NIK* and *Dll1*. Hybridizations and washes were performed at 63°C. Whole-mount immunofluoresence was performed as described (Nagy, 2003). The following antibodies and stains were used at the specified dilutions: rabbit anti-laminin (Sigma; 1:100), mouse anti-E-cadherin (Sigma; 1:200), rabbit anti-phospho-Histone H3 (Upstate 1:100), and TO-PRO-3 (Molecular Probes; 1:3000). Images were acquired on a BioRad scanning laser confocal microscope at 2 or 8 μm optical sections. Whole mount immunohistochemistry was performed as described (Nagy, 2003) using 1:500 dilution of rabbit anti-Tbx6 and 1:500 dilution of HRP-anti-rabbit followed by a color reaction in DAB, $NiCl_2$ and H_2O_2.

5.5 CELL CULTURE

COS-7 monkey cells (ATCC) were maintained in DMEM supplemented with 10% FBS, pen/strep, and L-glutamine (rich media) at 37ºC and 5% CO_2. Transient transfections were performed with 2μg of pCS3-myc-Tbx6 and Lipofectamine 2000 according to manufacturer's instructions (Invitrogen). For Tbx6 stability assays, 24 hours post-transfection COS-7 cells were treated with DMSO (vehicle), 50μm MG132 (SIGMA), or 250μg/mL cycloheximide (SIGMA) incubated for 0.5, 2, 4, 6, or 24 hours post-treatment at 37ºC. For pulse-chase analysis, 24 hours post-transfection, COS-7 cells were incubated with DMSO or 50μm MG132 for 4 hours in rich media, followed by a one-hour pulse with Expre^{35}S^{35}S Protein labeling mix (NEN) in RPMI-1640 media (methionine and cysteine free) supplemented with 10% dialyzed FBS and L-glutamine, the label was chased with DMEM supplemented with 10% FBS, L-glut and 1000-fold excess of cold methionine and cysteine for 0, 2, 4, 6 or 8 hours post-chase at 37ºC and 5% CO_2.

5.6 LYSATES, IMMUNOPRECIPITATIONS, AND WESTERN BLOTTING

Cell were harvested on ice and lysed in RIPA buffer (150mM NaCl, 1% NP-40, 0.5% sodium deoxycholate, 0.1% SDS, 50 mM Tris [pH8.0]) or IP buffer (40mM Tris [pH 8.0], 5 mM EGTA [pH 8.0], 10mM EDTA [pH 8.0], 100mM NaCl, 0.5% NP-40) supplemented with 0.01% protease inhibitor cocktail (PIC). Lysates were cleared by centrifugation and stored at -80º C. e10.5 tailbuds, somites or limb buds were isolated, pooled, mechanically homogenized and resuspended in RIPA buffer supplemented with PIC. Lysates for immunoprecipitations during the pulse-chase analyses were precleared with Protein-A Sepharose (Amersham), incubated overnight with 1µg anti-Tbx6, and then incubated with Protein-A Sepharose for 1 hour. Bead/protein complexes were then washed 3 times in NETN (20mM Tris [pH 8.0], 5mM EDTA [pH 8.0], 75mM NaCl, 0.5% NP-40, 0.1% SDS), and resuspended in 2x sample buffer. The protein concentrations of the lysates for Western blot analysis were determined using Bio-Rad Protein reagent and equal amounts of protein were loaded and resolved on 7.5% SDS-PAGE gels, followed by transfer to nitrocellulose membrane. Endogenous and exogenous Tbx6 proteins were detected by affinity purified rabbit anti-Tbx6 (White and Chapman, 2005), rabbit anti-actin (Sigma), or mouse anti-tubulin (Sigma) at a dilution of 1:500 in TBST + 4% NFDM (nonfat dry milk). Primary antibodies were detected using HRP-conjugated secondary goat anti-rabbit or goat anti-mouse antibodies (Amersham) at a dilution of 1:2500 in TBST + 4% milk, followed by ECL (Amersham) and/or Kodak Image Station quantification. Pulse-chase assays were quantified using Fugi Fluroimager analysis.

5.7 LUCIFERASE ASSAYS

COS-7 cells were transiently transfected with 2.5ng of pCMV-Renilla (Promega), which serves as an internal control, 50ng pGL4-Dll1 which contains a 200 basepair region of the *Dll1-msd* enhancer element cloned upstream of the β-globin minimal promoter in pGL4 vector (Promega), where one potential T-box binding site within the vector was changed, 2.5-50ng pCS3-myc-Tbx6 which contains full-length Tbx6 with an N-terminal myc-tag, pCS2-NICD (kind gift from R. Kopan) which contains the full-length Notch Intracellular Domain (NICD) with an N-terminal myc-tag and varying amounts of pCS3 empty vector to maintain a constant amount of DNA, in 96-well format in triplicate. 24 hours post-transfection, cells were treated with DMSO or 50μm MG132 for 4 hours. Firefly luciferase activity was measured using the Dual-Glo™ Luciferase Reagent (Promega) according to manufacturer's recommendations and analyzed using the Berthold XS^3 LB960, followed by measurement and analysis of *Renilla* luciferase activity. Firefly luciferase data were normalized to *Renilla* luciferase data and plotted using Excel.

BIBLIOGRAPHY

Abdelkhalek HB, Beckers A, Schuster-Gossler K, Pavlova MN, Burkhardt H, Lickert H, Rossant J, Reinhardt R, Schalkwyk LC, Muller I, Herrmann BG, Ceolin M, Rivera-Pomar R, Gossler A. 2004. The mouse homeobox gene Not is required for caudal notochord development and affected by the truncate mutation. Genes Dev 18:1725-1736.

Acampora D, Mazan S, Lallemand Y, Avantaggiato V, Maury M, Simeone A, Brulet P. 1995. Forebrain and midbrain regions are deleted in Otx2-/- mutants due to a defective anterior neuroectoderm specification during gastrulation. Development 121:3279-3290.

Anderson C, Thorsteinsdottir S, Borycki AG. 2009. Sonic hedgehog-dependent synthesis of laminin alpha1 controls basement membrane assembly in the myotome. Development 136:3495-3504.

Ang SL, Conlon RA, Jin O, Rossant J. 1994. Positive and negative signals from mesoderm regulate the expression of mouse Otx2 in ectoderm explants. Development 120:2979-2989.

Ang SL, Jin O, Rhinn M, Daigle N, Stevenson L, Rossant J. 1996. A targeted mouse Otx2 mutation leads to severe defects in gastrulation and formation of axial mesoderm and to deletion of rostral brain. Development 122:243-252.

Ang SL, Rossant J. 1994. HNF-3 beta is essential for node and notochord formation in mouse development. Cell 78:561-574.

Aszodi A, Chan D, Hunziker E, Bateman JF, Fassler R. 1998. Collagen II is essential for the removal of the notochord and the formation of intervertebral discs. J Cell Biol 143:1399-1412.

Authier F, Metioui M, Bell AW, Mort JS. 1999. Negative regulation of epidermal growth factor signaling by selective proteolytic mechanisms in the endosome mediated by cathepsin B. J Biol Chem 274:33723-33731.

Barriere H, Nemes C, Du K, Lukacs GL. 2007. Plasticity of polyubiquitin recognition as lysosomal targeting signals by the endosomal sorting machinery. Mol Biol Cell 18:3952-3965.

Beckers J, Schlautmann N, Gossler A. 2000. The mouse rib-vertebrae mutation disrupts anterior-posterior somite patterning and genetically interacts with a Delta1 null allele. Mech Dev 95:35-46.

Belo JA, Bachiller D, Agius E, Kemp C, Borges AC, Marques S, Piccolo S, De Robertis EM. 2000. Cerberus-like is a secreted BMP and nodal antagonist not essential for mouse development. Genesis 26:265-270.

Belo JA, Bouwmeester T, Leyns L, Kertesz N, Gallo M, Follettie M, De Robertis EM. 1997. Cerberus-like is a secreted factor with neutralizing activity expressed in the anterior primitive endoderm of the mouse gastrula. Mech Dev 68:45-57.

Belteki G, Haigh J, Kabacs N, Haigh K, Sison K, Costantini F, Whitsett J, Quaggin SE, Nagy A. 2005. Conditional and inducible transgene expression in mice through the combinatorial use of Cre-mediated recombination and tetracycline induction. Nucleic Acids Res 33:e51.

Bettenhausen B, Hrabe de Angelis M, Simon D, Guenet JL, Gossler A. 1995. Transient and restricted expression during mouse embryogenesis of Dll1, a murine gene closely related to Drosophila Delta. Development 121:2407-2418.

Bielinska M, Narita N, Wilson DB. 1999. Distinct roles for visceral endoderm during embryonic mouse development. Int J Dev Biol 43:183-205.

Biris KK, Dunty WC, Jr., Yamaguchi TP. 2007. Mouse Ripply2 is downstream of Wnt3a and is dynamically expressed during somitogenesis. Dev Dyn 236:3167-3172.

Bladt F, Aippersbach E, Gelkop S, Strasser GA, Nash P, Tafuri A, Gertler FB, Pawson T. 2003. The murine Nck SH2/SH3 adaptors are important for the development of mesoderm-derived embryonic structures and for regulating the cellular actin network. Mol Cell Biol 23:4586-4597.

Brennan J, Lu CC, Norris DP, Rodriguez TA, Beddington RS, Robertson EJ. 2001. Nodal signalling in the epiblast patterns the early mouse embryo. Nature 411:965-969.

Bush KT, Goldberg AL, Nigam SK. 1997. Proteasome inhibition leads to a heat-shock response, induction of endoplasmic reticulum chaperones, and thermotolerance. J Biol Chem 272:9086-9092.

Bussen M, Petry M, Schuster-Gossler K, Leitges M, Gossler A, Kispert A. 2004. The T-box transcription factor Tbx18 maintains the separation of anterior and posterior somite compartments. Genes Dev 18:1209-1221.

Chapman DL, Agulnik I, Hancock S, Silver LM, Papaioannou VE. 1996. Tbx6, a mouse T-Box gene implicated in paraxial mesoderm formation at gastrulation. Dev Biol 180:534-542.

Chapman DL, Cooper-Morgan A, Harrelson Z, Papaioannou VE. 2003. Critical role for Tbx6 in mesoderm specification in the mouse embryo. Mech Dev 120:837-847.

Chapman DL, Papaioannou VE. 1998. Three neural tubes in mouse embryos with mutations in the T-box gene Tbx6. Nature 391:695-697.

Chen YL, Liu B, Zhou ZN, Hu RY, Fei C, Xie ZH, Ding X. 2009. Smad6 inhibits the transcriptional activity of tbx6 by mediating its degradation. J Biol Chem 284:23481-23490.

Christ B, Huang R, Scaal M. 2007. Amniote somite derivatives. Dev Dyn 236:2382-2396.

Christ B, Wilting J. 1992. From somites to vertebral column. Ann Anat 174:23-32.

Conlon FL, Lyons KM, Takaesu N, Barth KS, Kispert A, Herrmann B, Robertson EJ. 1994. A primary requirement for nodal in the formation and maintenance of the primitive streak in the mouse. Development 120:1919-1928.

Conlon FL, Smith JC. 1999. Interference with brachyury function inhibits convergent extension, causes apoptosis, and reveals separate requirements in the FGF and activin signalling pathways. Dev Biol 213:85-100.

Costello I, Biondi CA, Taylor JM, Bikoff EK, Robertson EJ. 2009. Smad4-dependent pathways control basement membrane deposition and endodermal cell migration at early stages of mouse development. BMC Dev Biol 9:54.

Coucouvanis E, Martin GR. 1999. BMP signaling plays a role in visceral endoderm differentiation and cavitation in the early mouse embryo. Development 126:535-546.

Crossley PH, Martin GR. 1995. The mouse Fgf8 gene encodes a family of polypeptides and is expressed in regions that direct outgrowth and patterning in the developing embryo. Development 121:439-451.

Damsky C, Sutherland A, Fisher S. 1993. Extracellular matrix 5: adhesive interactions in early mammalian embryogenesis, implantation, and placentation. Faseb J 7:1320-1329.

Dubrovolskaia-Zavadskaia N. 1927. Sur la mortification spontanee de la queue chez la souris nouveau-nee et sur l'existence d'un charactere heriditaire "non-viable". C R Soc Biol 97:114-116.

Dubrulle J, Pourquie O. 2004. Coupling segmentation to axis formation. Development 131:5783-5793.

Dunty WC, Jr., Biris KK, Chalamalasetty RB, Taketo MM, Lewandoski M, Yamaguchi TP. 2008. Wnt3a/beta-catenin signaling controls posterior body development by coordinating mesoderm formation and segmentation. Development 135:85-94.

Fan CM, Tessier-Lavigne M. 1994. Patterning of mammalian somites by surface ectoderm and notochord: evidence for sclerotome induction by a hedgehog homolog. Cell 79:1175-1186.

Farkas DR, Chapman DL. 2009. Kinked tail mutation results in notochord defects in heterozygotes and distal visceral endoderm defects in homozygotes. Dev Dyn 238:3237-3247.

Farley FA, Hall J, Goldstein SA. 2006. Characteristics of congenital scoliosis in a mouse model. J Pediatr Orthop 26:341-346.

Fassler R, Meyer M. 1995. Consequences of lack of beta 1 integrin gene expression in mice. Genes Dev 9:1896-1908.

Freitas C, Rodrigues S, Saude L, Palmeirim I. 2005. Running after the clock. Int J Dev Biol 49:317-324.

Giampietro PF, Blank RD, Raggio CL, Merchant S, Jacobsen FS, Faciszewski T, Shukla SK, Greenlee AR, Reynolds C, Schowalter DB. 2003. Congenital and idiopathic scoliosis: clinical and genetic aspects. Clin Med Res 1:125-136.

Giudicelli F, Lewis J. 2004. The vertebrate segmentation clock. Curr Opin Genet Dev 14:407-414.

Gluecksohn-Schoenheimer S. 1938. The Development of Two Tailless Mutants in the House Mouse. Genetics 23:573-584.

Gluecksohn-Schoenheimer S. 1944. The Development of Normal and Homozygous Brachy (T/T) Mouse Embryos in the Extraembryonic Coelom of the Chick. Proc Natl Acad Sci U S A 30:134-140.

Gonzalez-Garay ML, Cabral F. 1995. Overexpression of an epitope-tagged beta-tubulin in Chinese hamster ovary cells causes an increase in endogenous alpha-tubulin synthesis. Cell Motil Cytoskeleton 31:259-272.

Hall H, Carbonetto S, Schachner M. 1997. L1/HNK-1 carbohydrate- and beta 1 integrin-dependent neural cell adhesion to laminin-1. J Neurochem 68:544-553.

Hall H, Vorherr T, Schachner M. 1995. Characterization of a 21 amino acid peptide sequence of the laminin G2 domain that is involved in HNK-1 carbohydrate binding and cell adhesion. Glycobiology 5:435-441.

Hamill KJ, Kligys K, Hopkinson SB, Jones JC. 2009. Laminin deposition in the extracellular matrix: a complex picture emerges. J Cell Sci 122:4409-4417.

Hayashi S, Lewis P, Pevny L, McMahon AP. 2002. Efficient gene modulation in mouse epiblast using a Sox2Cre transgenic mouse strain. Mech Dev 119 Suppl 1:S97-S101.

Hendzel MJ, Wei Y, Mancini MA, Van Hooser A, Ranalli T, Brinkley BR, Bazett-Jones DP, Allis CD. 1997. Mitosis-specific phosphorylation of histone H3 initiates primarily within pericentromeric heterochromatin during G2 and spreads in an ordered fashion coincident with mitotic chromosome condensation. Chromosoma 106:348-360.

Herrmann BG. 1991. Expression pattern of the Brachyury gene in whole-mount TWis/TWis mutant embryos. Development 113:913-917.

Hofmann M, Schuster-Gossler K, Watabe-Rudolph M, Aulehla A, Herrmann BG, Gossler A. 2004. WNT signaling, in synergy with T/TBX6, controls Notch signaling by regulating Dll1 expression in the presomitic mesoderm of mouse embryos. Genes Dev 18:2712-2717.

Ikeya M, Takada S. 1998. Wnt signaling from the dorsal neural tube is required for the formation of the medial dermomyotome. Development 125:4969-4976.

Kinder SJ, Tsang TE, Wakamiya M, Sasaki H, Behringer RR, Nagy A, Tam PP. 2001. The organizer of the mouse gastrula is composed of a dynamic population of progenitor cells for the axial mesoderm. Development 128:3623-3634.

Kispert A, Herrmann BG. 1994. Immunohistochemical analysis of the Brachyury protein in wild-type and mutant mouse embryos. Dev Biol 161:179-193.

Kraus F, Haenig B, Kispert A. 2001. Cloning and expression analysis of the mouse T-box gene Tbx18. Mech Dev 100:83-86.

Lehmann JM, Riethmuller G, Johnson JP. 1990. Nck, a melanoma cDNA encoding a cytoplasmic protein consisting of the src homology units SH2 and SH3. Nucleic Acids Res 18:1048.

Leitges M, Neidhardt L, Haenig B, Herrmann BG, Kispert A. 2000. The paired homeobox gene Uncx4.1 specifies pedicles, transverse processes and proximal ribs of the vertebral column. Development 127:2259-2267.

Li L, Arman E, Ekblom P, Edgar D, Murray P, Lonai P. 2004. Distinct GATA6- and laminin-dependent mechanisms regulate endodermal and ectodermal embryonic stem cell fates. Development 131:5277-5286.

Li S, Edgar D, Fassler R, Wadsworth W, Yurchenco PD. 2003. The role of laminin in embryonic cell polarization and tissue organization. Dev Cell 4:613-624.

Liu J, He X, Corbett SA, Lowry SF, Graham AM, Fassler R, Li S. 2009. Integrins are required for the differentiation of visceral endoderm. J Cell Sci 122:233-242.

Liu P, Wakamiya M, Shea MJ, Albrecht U, Behringer RR, Bradley A. 1999. Requirement for Wnt3 in vertebrate axis formation. Nat Genet 22:361-365.

Lu CC, Brennan J, Robertson EJ. 2001. From fertilization to gastrulation: axis formation in the mouse embryo. Curr Opin Genet Dev 11:384-392.

Ma J, Lindquist S. 2001. Wild-type PrP and a mutant associated with prion disease are subject to retrograde transport and proteasome degradation. Proc Natl Acad Sci U S A 98:14955-14960.

Mansouri A, Voss AK, Thomas T, Yokota Y, Gruss P. 2000. Uncx4.1 is required for the formation of the pedicles and proximal ribs and acts upstream of Pax9. Development 127:2251-2258.

Martinez Barbera JP, Clements M, Thomas P, Rodriguez T, Meloy D, Kioussis D, Beddington RS. 2000. The homeobox gene Hex is required in definitive endodermal tissues for normal forebrain, liver and thyroid formation. Development 127:2433-2445.

Meno C, Gritsman K, Ohishi S, Ohfuji Y, Heckscher E, Mochida K, Shimono A, Kondoh H, Talbot WS, Robertson EJ, Schier AF, Hamada H. 1999. Mouse Lefty2 and zebrafish antivin are feedback inhibitors of nodal signaling during vertebrate gastrulation. Mol Cell 4:287-298.

Meno C, Saijoh Y, Fujii H, Ikeda M, Yokoyama T, Yokoyama M, Toyoda Y, Hamada H. 1996. Left-right asymmetric expression of the TGF beta-family member lefty in mouse embryos. Nature 381:151-155.

Meno C, Shimono A, Saijoh Y, Yashiro K, Mochida K, Ohishi S, Noji S, Kondoh H, Hamada H. 1998. lefty-1 is required for left-right determination as a regulator of lefty-2 and nodal. Cell 94:287-297.

Mesnard D, Guzman-Ayala M, Constam DB. 2006. Nodal specifies embryonic visceral endoderm and sustains pluripotent cells in the epiblast before overt axial patterning. Development 133:2497-2505.

Miner JH, Li C, Mudd JL, Go G, Sutherland AE. 2004. Compositional and structural requirements for laminin and basement membranes during mouse embryo implantation and gastrulation. Development 131:2247-2256.

Monsoro-Burq AH, Bontoux M, Teillet MA, Le Douarin NM. 1994. Heterogeneity in the development of the vertebra. Proc Natl Acad Sci U S A 91:10435-10439.

Morimoto M, Sasaki N, Oginuma M, Kiso M, Igarashi K, Aizaki K, Kanno J, Saga Y. 2007. The negative regulation of Mesp2 by mouse Ripply2 is required to establish the rostro-caudal patterning within a somite. Development 134:1561-1569.

Nacke S, Schafer R, Habre de Angelis M, Mundlos S. 2000. Mouse mutant "rib-vertebrae" (rv): a defect in somite polarity. Dev Dyn 219:192-200.

Nagy A, Gertenstein, M., Vinterstein K, Behringer R. 2003. Manipulating the Mouse Embryo: A Laboratory Maual. Cold Spring Harbor Press.

Naiche LA, Harrelson Z, Kelly RG, Papaioannou VE. 2005. T-box genes in vertebrate development. Annu Rev Genet 39:219-239.

O'Shea KS. 1987. Differential deposition of basement membrane components during formation of the caudal neural tube in the mouse embryo. Development 99:509-519.

Oberg C, Li J, Pauley A, Wolf E, Gurney M, Lendahl U. 2001. The Notch intracellular domain is ubiquitinated and negatively regulated by the mammalian Sel-10 homolog. J Biol Chem 276:35847-35853.

Oginuma M, Niwa Y, Chapman DL, Saga Y. 2008. Mesp2 and Tbx6 cooperatively create periodic patterns coupled with the clock machinery during mouse somitogenesis. Development 135:2555-2562.

Ong E, Yeh JC, Ding Y, Hindsgaul O, Fukuda M. 1998. Expression cloning of a human sulfotransferase that directs the synthesis of the HNK-1 glycan on the neural cell adhesion molecule and glycolipids. J Biol Chem 273:5190-5195.

Paavola LG, Wilson DB, Center EM. 1980. Histochemistry of the developing notochord, perichordal sheath and vertebrae in Danforth's short-tail (sd) and normal C57BL/6 mice. J Embryol Exp Morphol 55:227-245.

Packham EA, Brook JD. 2003. T-box genes in human disorders. Hum Mol Genet 12 Spec No 1:R37-44.

Parsons MJ, Pollard SM, Saude L, Feldman B, Coutinho P, Hirst EM, Stemple DL. 2002. Zebrafish mutants identify an essential role for laminins in notochord formation. Development 129:3137-3146.

Perantoni AO, Timofeeva O, Naillat F, Richman C, Pajni-Underwood S, Wilson C, Vainio S, Dove LF, Lewandoski M. 2005. Inactivation of FGF8 in early mesoderm reveals an essential role in kidney development. Development 132:3859-3871.

Perea-Gomez A, Lawson KA, Rhinn M, Zakin L, Brulet P, Mazan S, Ang SL. 2001a. Otx2 is required for visceral endoderm movement and for the restriction of posterior signals in the epiblast of the mouse embryo. Development 128:753-765.

Perea-Gomez A, Rhinn M, Ang SL. 2001b. Role of the anterior visceral endoderm in restricting posterior signals in the mouse embryo. Int J Dev Biol 45:311-320.

Perea-Gomez A, Shawlot W, Sasaki H, Behringer RR, Ang S. 1999. HNF3beta and Lim1 interact in the visceral endoderm to regulate primitive streak formation and anterior-posterior polarity in the mouse embryo. Development 126:4499-4511.

Perea-Gomez A, Vella FD, Shawlot W, Oulad-Abdelghani M, Chazaud C, Meno C, Pfister V, Chen L, Robertson E, Hamada H, Behringer RR, Ang SL. 2002. Nodal antagonists in the anterior visceral endoderm prevent the formation of multiple primitive streaks. Dev Cell 3:745-756.

Placzek M, Jessell TM, Dodd J. 1993. Induction of floor plate differentiation by contact-dependent, homeogenetic signals. Development 117:205-218.

Pourquie O, Coltey M, Teillet MA, Ordahl C, Le Douarin NM. 1993. Control of dorsoventral patterning of somitic derivatives by notochord and floor plate. Proc Natl Acad Sci U S A 90:5242-5246.

Rakeman AS, Anderson KV. 2006. Axis specification and morphogenesis in the mouse embryo require Nap1, a regulator of WAVE-mediated actin branching. Development 133:3075-3083.

Rivera-Perez JA, Mager J, Magnuson T. 2003. Dynamic morphogenetic events characterize the mouse visceral endoderm. Dev Biol 261:470-487.

Rodriguez TA, Srinivas S, Clements MP, Smith JC, Beddington RS. 2005. Induction and migration of the anterior visceral endoderm is regulated by the extra-embryonic ectoderm. Development 132:2513-2520.

Rogers S, Wells R, Rechsteiner M. 1986. Amino acid sequences common to rapidly degraded proteins: the PEST hypothesis. Science 234:364-368.

Ruan W, Pang P, Rao Y. 1999. The SH2/SH3 adaptor protein dock interacts with the Ste20-like kinase misshapen in controlling growth cone motility. Neuron 24:595-605.

Saga Y, Takeda H. 2001. The making of the somite: molecular events in vertebrate segmentation. Nat Rev Genet 2:835-845.

Sakamoto A, Murata K, Suzuki H, Yatabe M, Kikuchi M. 2008. Immunohistochemical observation of co-expression of E- and N-cadherins in rat organogenesis. Acta Histochem Cytochem 41:143-147.

Semba K, Araki K, Li Z, Matsumoto K, Suzuki M, Nakagata N, Takagi K, Takeya M, Yoshinobu K, Araki M, Imai K, Abe K, Yamamura K. 2006. A novel murine gene, Sickle tail, linked to the Danforth's short tail locus, is required for normal development of the intervertebral disc. Genetics 172:445-456.

Senn C, Kutsche M, Saghatelyan A, Bosl MR, Lohler J, Bartsch U, Morellini F, Schachner M. 2002. Mice deficient for the HNK-1 sulfotransferase show alterations in synaptic efficacy and spatial learning and memory. Mol Cell Neurosci 20:712-729.

Sewell W, Kusumi K. 2007. Genetic analysis of molecular oscillators in mammalian somitogenesis: clues for studies of human vertebral disorders. Birth Defects Res C Embryo Today 81:111-120.

Shawlot W, Behringer RR. 1995. Requirement for Lim1 in head-organizer function. Nature 374:425-430.

Shawlot W, Deng JM, Behringer RR. 1998. Expression of the mouse cerberus-related gene, Cerr1, suggests a role in anterior neural induction and somitogenesis. Proc Natl Acad Sci U S A 95:6198-6203.

Shimojima K, Inoue T, Fujii Y, Ohno K, Yamamoto T. 2009. A familial 593-kb microdeletion of 16p11.2 associated with mental retardation and hemivertebrae. Eur J Med Genet 52:433-435.

Shum AS, Poon LL, Tang WW, Koide T, Chan BW, Leung YC, Shiroishi T, Copp AJ. 1999. Retinoic acid induces down-regulation of Wnt-3a, apoptosis and diversion of tail bud cells to a neural fate in the mouse embryo. Mech Dev 84:17-30.

Simeone A, Acampora D. 2001. The role of Otx2 in organizing the anterior patterning in mouse. Int J Dev Biol 45:337-345.

Simeone A, Acampora D, Mallamaci A, Stornaiuolo A, D'Apice MR, Nigro V, Boncinelli E. 1993. A vertebrate gene related to orthodenticle contains a homeodomain of the bicoid class and demarcates anterior neuroectoderm in the gastrulating mouse embryo. Embo J 12:2735-2747.

Singh MK, Petry M, Haenig B, Lescher B, Leitges M, Kispert A. 2005. The T-box transcription factor Tbx15 is required for skeletal development. Mech Dev 122:131-144.

Smyth N, Vatansever HS, Murray P, Meyer M, Frie C, Paulsson M, Edgar D. 1999. Absence of basement membranes after targeting the LAMC1 gene results in embryonic lethality due to failure of endoderm differentiation. J Cell Biol 144:151-160.

Soriano P. 1999. Generalized lacZ expression with the ROSA26 Cre reporter strain. Nat Genet 21:70-71.

Srinivas S. 2006. The anterior visceral endoderm-turning heads. Genesis 44:565-572.

Srinivas S, Rodriguez T, Clements M, Smith JC, Beddington RS. 2004. Active cell migration drives the unilateral movements of the anterior visceral endoderm. Development 131:1157-1164.

Steinhilb ML, Turner RS, Gaut JR. 2001. The protease inhibitor, MG132, blocks maturation of the amyloid precursor protein Swedish mutant preventing cleavage by beta-Secretase. J Biol Chem 276:4476-4484.

Su YC, Han J, Xu S, Cobb M, Skolnik EY. 1997. NIK is a new Ste20-related kinase that binds NCK and MEKK1 and activates the SAPK/JNK cascade via a conserved regulatory domain. Embo J 16:1279-1290.

Takito J, Al-Awqati Q. 2004. Conversion of ES cells to columnar epithelia by hensin and to squamous epithelia by laminin. J Cell Biol 166:1093-1102.

Tam PP, Beddington RS. 1987. The formation of mesodermal tissues in the mouse embryo during gastrulation and early organogenesis. Development 99:109-126.

Tam PP, Behringer RR. 1997. Mouse gastrulation: the formation of a mammalian body plan. Mech Dev 68:3-25.

Tarone G, Hirsch E, Brancaccio M, De Acetis M, Barberis L, Balzac F, Retta SF, Botta C, Altruda F, Silengo L. 2000. Integrin function and regulation in development. Int J Dev Biol 44:725-731.

Theiler K, Varnum DS. 1985. Development of rib-vertebrae: a new mutation in the house mouse with accessory caudal duplications. Anat Embryol (Berl) 173:111-116.

Thomas PQ, Brown A, Beddington RS. 1998. Hex: a homeobox gene revealing peri-implantation asymmetry in the mouse embryo and an early transient marker of endothelial cell precursors. Development 125:85-94.

Timpl R. 1996. Macromolecular organization of basement membranes. Curr Opin Cell Biol 8:618-624.

Torres-Padilla ME, Richardson L, Kolasinska P, Meilhac SM, Luetke-Eversloh MV, Zernicka-Goetz M. 2007. The anterior visceral endoderm of the mouse embryo is established from both preimplantation precursor cells and by de novo gene expression after implantation. Dev Biol 309:97-112.

Tu Y, Li F, Wu C. 1998. Nck-2, a novel Src homology2/3-containing adaptor protein that interacts with the LIM-only protein PINCH and components of growth factor receptor kinase-signaling pathways. Mol Biol Cell 9:3367-3382.

Wallin J, Wilting J, Koseki H, Fritsch R, Christ B, Balling R. 1994. The role of Pax-1 in axial skeleton development. Development 120:1109-1121.

Watabe-Rudolph M, Schlautmann N, Papaioannou VE, Gossler A. 2002. The mouse rib-vertebrae mutation is a hypomorphic Tbx6 allele. Mech Dev 119:251-256.

Weinstein DC, Ruiz i Altaba A, Chen WS, Hoodless P, Prezioso VR, Jessell TM, Darnell JE, Jr. 1994. The winged-helix transcription factor HNF-3 beta is required for notochord development in the mouse embryo. Cell 78:575-588.

White PH, Chapman DL. 2005. Dll1 is a downstream target of Tbx6 in the paraxial mesoderm. Genesis 42:193-202.

White PH, Farkas DR, Chapman DL. 2005. Regulation of Tbx6 expression by Notch signaling. Genesis 42:61-70.

White PH, Farkas DR, McFadden EE, Chapman DL. 2003. Defective somite patterning in mouse embryos with reduced levels of Tbx6. Development 130:1681-1690.

Wilkinson DG. 1992. Whole mount in situ hybridization of vertebrate embryos. Oxford: IRL Press. pp. 75-83 pp.

Wilkinson DG, Bhatt S, Herrmann BG. 1990. Expression pattern of the mouse T gene and its role in mesoderm formation. Nature 343:657-659.

Wilson V, Manson L, Skarnes WC, Beddington RS. 1995. The T gene is necessary for normal mesodermal morphogenetic cell movements during gastrulation. Development 121:877-886.

Wittler L, Shin EH, Grote P, Kispert A, Beckers A, Gossler A, Werber M, Herrmann BG. 2007. Expression of Msgn1 in the presomitic mesoderm is controlled by synergism of WNT signalling and Tbx6. EMBO Rep 8:784-789.

Wolpert L, Rosa Beddington, Thomas Jessell, Peter Lawrence, Elliot Meyerowitz, Jim Smith. 2002. Principles of Development. Oxford University Press.

Wu G, Lyapina S, Das I, Li J, Gurney M, Pauley A, Chui I, Deshaies RJ, Kitajewski J. 2001. SEL-10 is an inhibitor of notch signaling that targets notch for ubiquitin-mediated protein degradation. Mol Cell Biol 21:7403-7415.

Xue Y, Wang X, Li Z, Gotoh N, Chapman D, Skolnik EY. 2001. Mesodermal patterning defect in mice lacking the Ste20 NCK interacting kinase (NIK). Development 128:1559-1572.

Yamamoto M, Saijoh Y, Perea-Gomez A, Shawlot W, Behringer RR, Ang SL, Hamada H, Meno C. 2004. Nodal antagonists regulate formation of the anteroposterior axis of the mouse embryo. Nature 428:387-392.

Yamanaka Y, Tamplin OJ, Beckers A, Gossler A, Rossant J. 2007. Live imaging and genetic analysis of mouse notochord formation reveals regional morphogenetic mechanisms. Dev Cell 13:884-896.

Yasuhiko Y, Haraguchi S, Kitajima S, Takahashi Y, Kanno J, Saga Y. 2006. Tbx6-mediated Notch signaling controls somite-specific Mesp2 expression. Proc Natl Acad Sci U S A 103:3651-3656.

Zohn IE, Li Y, Skolnik EY, Anderson KV, Han J, Niswander L. 2006. p38 and a p38-interacting protein are critical for downregulation of E-cadherin during mouse gastrulation. Cell 125:957-969.